From the Department of Nutritional Science
Biochemistry and Molecular Biology

JUSTUS-LIEBIG-
UNIVERSITÄT
GIESSEN

Genetically-encoded fluorescent ATP sensors for mode of action analyses of antiparasitic compounds in *Plasmodium falciparum*

CUMULATIVE DISSERTATION

for the award of the doctoral degree (**Dr. rer. nat.**) in the Faculty of Agricultural Sciences, Nutritional Sciences and Environmental Management at the Justus Liebig University of Giessen

submitted by

Eric Springer

from Wiesbaden

Giessen, November 12, 2025

With the permission of the Faculty of Agricultural Sciences, Nutritional Sciences and Environmental Management of the Justus Liebig University Giessen.

1st reviewer: **Prof. Dr. Jude M. Przyborski**

Biochemistry and Molecular Biology

Department of Nutritional Science

Justus Liebig University Giessen

2nd reviewer: **Prof. Dr. Uwe Wenzel**

Molecular Nutrition Research

Department of Nutritional Science

Justus Liebig University Giessen

3rd reviewer: **Prof. Dr. Kai Thormann**

Microbiology and Molecular Biology

Department of Biology

Justus Liebig University Giessen

Declaration in accordance with the Doctoral Regulations of the Faculty 09 in the version of 29.05.2019 § 17 (2)

I declare that the doctoral thesis here submitted is entirely my own work, written without any unauthorised help by a third party and solely with the assistance referred to in the thesis. I have indicated in the text those texts that have been quoted from already published sources, either verbatim or by analogy and all statements based on verbally conveyed information. During the research carried out by me and referred to in the doctoral thesis, I have at all times followed the principles of good scholarly practice as defined in the Statute of Justus Liebig University Giessen for Ensuring of Good Academic Practice.

Erklärung getreu der Promotionsordnung des Fachbereichs 09 der Version 29.05.2019 § 17 (2)

Ich erkläre: Ich habe die vorgelegte Dissertation selbständig und ohne unerlaubte fremde Hilfe und nur mit den Hilfen angefertigt, die ich in der Dissertation angegeben habe. Alle Textstellen, die wörtlich oder sinngemäß aus veröffentlichten Schriften entnommen sind, und alle Angaben, die auf mündlichen Auskünften beruhen, sind als solche kenntlich gemacht. Bei den von mir durchgeführten und in der Dissertation erwähnten Untersuchungen habe ich die Grundsätze guter wissenschaftlicher Praxis, wie sie in der „Satzung der Justus-Liebig-Universität Gießen zur Sicherung guter wissenschaftlicher Praxis“ niedergelegt sind, eingehalten.

Giessen, _____

_____

Eric Springer

Table of Contents

List of Publications

This thesis is based on the following peer-reviewed publications:

Springer, E., Heimsch, K. C., Rahlfs, S., Becker, K., & Przyborski, J. M. (2024). Real-time measurements of ATP dynamics via ATeams in *Plasmodium falciparum* reveal drug-class-specific response patterns. *Antimicrobial Agents and Chemotherapy*, *68*(5), e0169023. https://doi.org/10.1128/aac.01690-23

Author Contributions:

ES: Conceptualization, formal analysis, investigation, writing – original draft, and writing – review and editing.

KCH: Investigation and writing – review and editing.

Investigation: Expression and purification of sfpHluorin protein, drug-sfpHluorin interaction studies.

SR: Funding acquisition, project administration, supervision, and writing – review and editing.

KB: Conceptualization, funding acquisition, project administration, supervision, and writing – review and editing.

JMP: Project administration, supervision, and writing – review and editing.

Springer, E., Heimsch, K. C., Sidiropoulos, N., Krijnse Locker, J., Przyborski J. M. (2025) Arylmethylamino steroid compound 1o interferes with *Plasmodium falciparum*'s hemoglobin metabolism. *Antimicrobial Agents and Chemotherapy*, 69(8), e0033225. https://doi.org/10.1128/aac.00332-25

Author Contributions:

ES: Conceptualization, data curation, formal analysis, investigation, methodology, visualization, writing – original draft, and writing – review and editing.

KCH: Investigation and writing – review and editing.

Investigation: Expression and purification of sfpHluorin protein, drug-sfpHluorin interaction studies.

NS: Investigation and writing – review and editing.

Investigation: Blinded classification of TEM images.

JKL: Project administration, resources, supervision.

JMP: Project administration, conceptualization, funding acquisition, resources, methodology, supervision, and writing – review and editing.

Further Publications Related to this Thesis:

Sparkes PC, Famodimu MT, Alves E, **Springer E**, Przyborski J, Delves MJ. 2024. Mitochondrial ATP synthesis is essential for efficient gametogenesis in *Plasmodium falciparu*m. *Commun Biol* 7:1525. doi:10.1038/s42003-024-07240-z

dos Santos BM, Pecenin MF, Borges-Pereira L, **Springer E**, Przyborski JM, Martins-Jr DC, Hashimoto RF, Garcia CRS. 2024. The genetically encoded calcium indicator GCaMP3 reveals spontaneous calcium oscillations at asexual stages of the human malaria parasite *Plasmodium falciparum*. *Molecular and Biochemical Parasitology* 260:111650. doi:10.1016/j.molbiopara.2024.111650

Schipper S, **Springer E**, Hahn J, Rahlfs S, Bourilhon P, Bernhagen J, Becker K, Przyborski JM. 2022. Characterization of *Plasmodium falciparum* macrophage migration inhibitory factor homologue and its cysteine deficient mutants. *Parasitol Int* 87:102513. doi:10.1016/j.parint.2021.102513

*** Shared first authorship**

ABSTRACT

This dissertation is based on publications that have established the usage of novel methods for adenosine triphosphate (ATP) and pH determinations in *Plasmodium falciparum* (*P. falciparum*). Based on these and complementary methods, mode of action (MoA) analyses of established drugs and novel antiparasitic compounds were conducted to support drug development.

The deadliest form of malaria, malaria tropica, caused by the intracellular parasite *P. falciparum*, claims more than half a million casualties annually. With resistances against each established antimalarial drug class against *P. falciparum* found in the field, the development of novel and improved antiparasitic compounds poses a matter of highest concern for global health. To this end, understanding of the underlying mechanisms is crucial. Therefore, within the scope of this work, genetically-encoded fluorescence-based ATP and pH sensors were stably integrated into the genome of *P. falciparum*. Within the adult blood stages of the parasite, this allowed an analysis of its energy metabolism, which is central for parasite survival. Based on this system, MoA analyses of a panel of antiparasitic compounds were carried out. In the case of a promising drug candidate, these were complemented with additional methods for elucidation of its mechanism.

Thereby, two different variants of ATP sensors, ATeam1.03nD/nA and ATeam1.03YEMK, as well as an improved pH sensor, sfpHluorin, were established and characterized via plate reader spectrofluorometry and epifluorescence microscopy, for the first time in *P. falciparum*. *In vitro* and *in cellulo* characterization of the sensors demonstrated their proof of principle and unveiled advantages of the ATeam1.03YEMK sensor cell line in respect to fluorescence intensity and pH stability. Based on that, the effects of a selection of antiparasitic compounds on the sensor readouts were determined. This revealed characteristic response patterns caused by 4-aminoquinolines, arylamino alcohols, redox cyclers, as well as dihydroartemisinin, doxycycline, atovaquone, and cycloheximide. In a next step, the effects of the drug candidate arylmethylamino steroid compound 1o (1o) on the sensor readouts were determined. The investigation uncovered parallels to arylamino alcohols such as mefloquine. Based on these parallels, subsequent analyses via transmission electron microscopy (TEM), the parasite-derived heme species distribution, as well as light microscopic morphology of stage-specific 1o incubations suggest that the parasite-killing activity could be based on interference with the parasite's hemoglobin uptake.

The results of this work benefit the understanding of *P. falciparum*'s parasite biology and the MoA of antiparasitic compounds to support drug development. Furthermore, the established system is now available for the malaria community to address a broad range of research questions.

ZUSAMMENFASSUNG

Grundlage dieser Dissertation sind Arbeiten, die eine neuartige Methode zur Adenosintriphosphat (ATP) und pH Bestimmung im Organismus *Plasmodium falciparum* (*P. falciparum*) etabliert haben, womit die Wirkungsweisen von bereits erprobten und zukunftsträchtigen antiparasitären Malariamedikamenten untersucht werden konnten, um so die Wirkstoffforschung nach neuen Arzneimitteln zu unterstützen.

Die schwerste Form der armutsassoziierten Erkrankung Malaria, Malaria tropica, wird durch die intrazellulären Parasiten *P. falciparum* hervorgerufen und fordert jährlich mehr als eine halbe Millionen Todesopfer. Obwohl bereits mehrere Wirkstoffklassen zur Behandlung der Krankheit entwickelt wurden, ist die Neu- und Weiterentwicklung von Wirkstoffen auf Grund der Verbreitung von resistenten Erregern von höchster Bedeutung für die Weltgesundheit. Um dieses Ziel zu erreichen, ist es entscheidend die zu Grunde liegenden Wirkmechanismen besser zu verstehen. Für diesen Zweck wurden im Rahmen dieser Arbeit genetisch-kodierte Fluoreszenz-basierte ATP und pH Sensoren stabil in das Genom des Erregers *P. falciparum* integriert, um in adulten Blutstadien dessen Energiestoffwechsel zu untersuchen. Darauf aufbauend wurden Interaktionsstudien mit antiparasitären Stoffgruppen durchgeführt, die im Falle eines potentiellen Arzneimittelkandidaten durch weitere Methoden zur Aufklärung des Wirkmechanismus unterstützt wurden.

Es wurden dabei zwei verschiedene Varianten von ATP Sensoren, ATeam1.03nD/nA und ATeam1.03YEMK, sowie der neuartige pH Sensor, sfpHluorin, erstmalig im Erreger etabliert und mittels spektrofluorometischem Plattenlesegerät und Epifluoreszenzmikroskop charakterisiert. *In vitro* und *in cellulo* Charakterisierung der Sensoren demonstrierte ihre praktische Anwendbarkeit in *P. falciparum*. Zudem zeigten sich Vorteile der ATeam1.03YEMK Zelllinie durch höhere Fluoreszenzintenstiät and pH Stabilität. Darauf aufbauend wurden die Auswirkungen von einer Auswahl an antiparasitären Stoffgruppen auf ATP Level, pH und Cytosolgröße von adulten Blutstadien bestimmt. Es konnten dabei charakteristische Reaktionsmuster durch eine Auswahl an 4-Aminochinolinen, Arylaminoalkoholen, Redox-aktiven Substanzen, sowie von Dihydroartemisinin, Doxycyclin, Atovaquon und Cycloheximid identifiziert werden. Im Weiteren wurden ATP Level, pH und Cytosolgröße in Reaktion auf Arylmethylaminosteroid 1o (1o) untersucht. Es zeigten sich dabei Parallelen zu Arylaminoalkoholen wie Mefloquin in Form von erhöhten ATP Leveln, erniedrigten pH und reduzierter Cytosolgröße. Darauffolgende Untersuchungen mittels Transmissionselektronen-mikroskopie (TEM), Analysen der parasitenstämmigen Häm Fraktionen sowie lichtmikroskopische Untersuchungen von Stadien-spezifischen 1o Inkubationen legen dabei nahe, dass die Wirkungsweise von 1o auf einer Hemmung der Hämoglobinaufnahme beruhen könnte.

Die Ergebnisse dieser Arbeit tragen dazu bei die Parasitenbiologie des Malariaerregers *P. falciparum* sowie Wirkungsweisen von antiparasitären Substanzen besser zu verstehen und so die Entwicklung von neuartigen Arzneimitteln voranzutreiben. Zudem steht das etablierte System nun der Malariaforschung zur Verfügung mit einem breiten Spektrum an Anwendungsgebieten.

List of Figures

List of Abbreviations

1o	arylmethylamino steroid compound 1o
AA	amino acids
AQ	amodiaquine
ART	artemisinin
ATM	artemether
ATP	adenosine triphosphate
ATQ	atovaquone
ATS	artesunate
CSP	circumsporozoite protein
CRT	chloroquine resistance transporter
CQ	chloroquine
DV	digestive vacuole
DHA	dihydroartemisinin
DHFR	dihydrofolate reductase
DHODH	dihydroorotate dehydrogenase
DHPS	dihydropteroate synthase
DOXY	doxycycline
ETC	electron transport chain
FP	falcipains
FV	food vacuole
G6PDH	glucose-6-phosphate dehydrogenase
GLC	glucose
GEFB	genetically-encoded fluorescent biosensors
HAL	halofantrine
Hb	hemoglobin
ICH	International Council for Harmonization
iRBC	infected red blood cell
IRS	indoor residual spraying

ITN	insecticide treated nets
LUM	lumefantrine
MAL	Malarone
MCT1	monocarboxylate transporter 1
MDA	mass drug administration
MoA	mode of action
MQ	mefloquine
NADPH	nicotinamide adenine dinucleotide phosphate
NPC	nutrient permeable channels
NPP	new permeation pathways
PfEXP2	*Plasmodium falciparum* exported protein 2
PfEMP1	*Plasmodium falciparum* erythrocyte membrane protein 1
PfFNT	*Plasmodium falciparum* formate-nitrite transporter
PfHT	*Plasmodium falciparum* hexose transporter
pfmdr1	*Plasmodium falciparum* multidrug resistance 1 gene
PG	proguanil
PM	plasmepsins
PPM	parasite plasma membrane
PPQ	piperaquine
PQ	primaquine
PSAC	plasmodial surface anion channel
PTEX	*Plasmodium* translocon of exported proteins
PV	parasitophorous vacuole
PVM	parasitophorous vacuolar membrane
PY	pyrimethamine
Pyr	pyruvate
PYR	pyronaridine
Q	ubiquinone
QN	quinine
RBC	red blood cell
RST	residual surface treatment
SP	sulfadoxine-pyrimethamine
TCA	tricarboxylic acid
THF	tetrahydrofolate
TQ	tafenoquine
WHO	World Health Organization

1. INTRODUCTION

1.1 Malaria

Malaria is a severe vector-borne infectious disease that remains to be one of the most urgent threats to global health. In 2023, there were an estimated 263 million cases worldwide, resulting in approximately 597,000 deaths, primarily among children under five years of age. Alarmingly, the estimated cases, together with the incidence rate, again increased compared to the preceding year by about 11 million cases, after a relatively stable level between the years 2000 and 2019. The disease is predominantly found in tropical and subtropical regions around the globe. Thereby, the African continent has to cope with the highest burden of the disease and accounts for about 94% of cases and 95% of deaths globally. Protozoan parasites of the *Plasmodium* (*P.*) genus, transmitted by the bite of infected *Anopheles* mosquitos, cause the disease (WHO, 2024b). The parasites undergo various life cycles until they eventually manifest in the bloodstream of the host and cause a febrile illness, and unspecific symptoms such as rigors, headache, nausea, and muscle pains. If not sufficiently controlled by the immune system, malaria can manifest in its severe and potentially deadly form with severe anemia, respiratory distress, and coma, separately or as a combination of the three symptoms (Cowman et al., 2016).

1.2.1 *Plasmodium falciparum*

The malaria causing *P.* species are single-celled eukaryotes from the Apicomplexan phylum and characterized by a complex life cycle between female mosquitos and vertebrate hosts. Six *P.* species are known to cause malaria in humans: *P. falciparum*, *P. vivax*, *P. malariae*, *P. knowlesi*, *P. ovale curtisi* and *P. ovale wallikeri* (Cowman et al., 2016), while the nomenclature of the latter two is under active dispute (Higgins et al., 2024; Šlapeta et al., 2024; Snounou et al., 2024a, 2024b). Of all, *P. falciparum* poses the highest risk to global health, causing the deadliest form of the disease, which is predominately found in sub-Saharan Africa (WHO, 2024b).

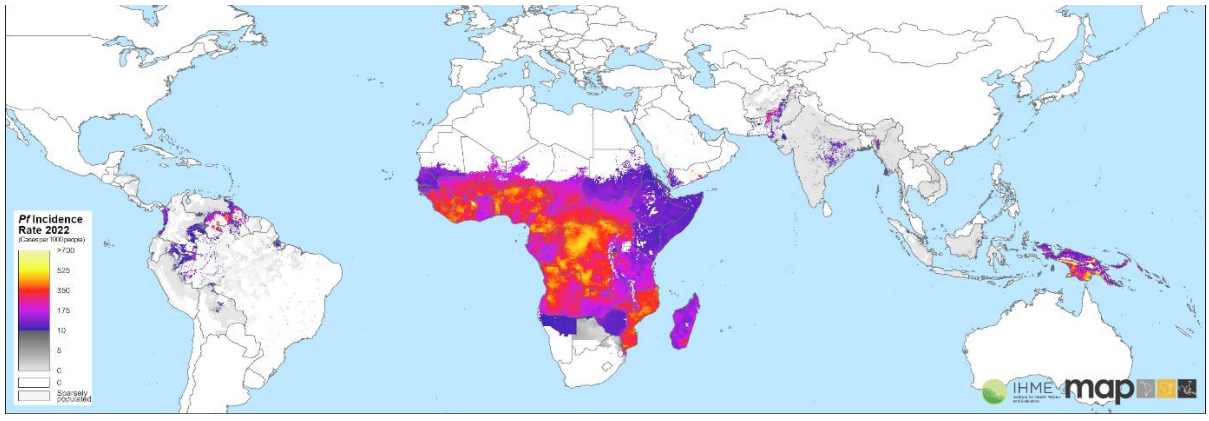

Figure 1: Predicted all-age incidence rate of *Plasmodium falciparum* malaria. Clinical cases per 1,000 population per annum in the year 2022 (The Malaria Atlas Project, 2024).

Thereby, highest case numbers of *P. falciparum* malaria, also called malaria tropica, in the top 3 affected countries, Nigeria, Democratic Republic of Congo, and Uganda, are accompanied with highest incidence rates (**Fig. 1** [WHO, 2023, 2024b]).

1.2.2 Life Cycle

The life cycle of *P. falciparum* is characterized by a complex alternation of stages within female *Anopheles* mosquitos and human hosts (Cowman et al., 2016). The human infection starts with the probing of an infected mosquito on the human skin. Sporozoite stage parasites enter the dermis via the mosquito saliva (**Fig. 2.1**), enter the bloodstream, and infect hepatocytes.

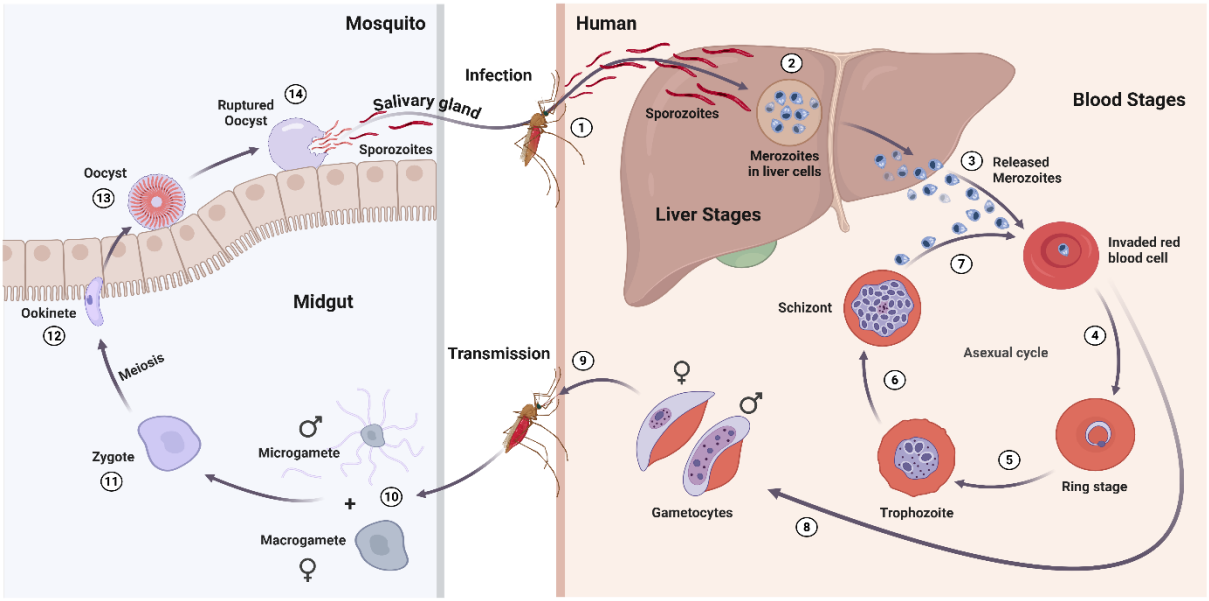

Figure 2: Life cycle of *Plasmodium falciparum.* 1: An infected *Anopheles* mosquito injects sporozoites into the dermis and initiates infection. **2:** Sporozoites migrate to the liver via the bloodstream to form merozoites. **3:** Merozoites are released from hepatocytes to infect red blood cells and to initiate the asexual cycle. **4:** Parasites develop into ring stages. **5:** Ring stages develop into trophozoites. **6:** Trophozoites undergo schizogony to schizonts which then form merozoites. **7:** Merozoites rupture from the red blood cell to start a new asexual cycle. **8:** A portion of merozoites is committed to sexual development to gametocytes. **9:** The infection is transmitted via uptake of gametocytes by a feeding mosquito. **10:** Gametocytes develop into microgametes and macrogametes within the mosquito midgut. **11:** Micro- and macrogametes form a zygote. **12:** Meiosis leads to ookinetes that invade into the midgut epithelium. **13:** Ookinetes form oocysts. **14:** Ruptured oocysts release sporozoites that infiltrate the salivary gland. Created in BioRender: https://BioRender.com/bl65c46 (based on [Cowman et al., 2016; Guttery et al., 2023; White et al., 2014]).

Within infected hepatocytes, sporozoites undergo schizogony to form tens of thousands of merozoites (**Fig. 2.2**), which takes around 10 days. Through budding off parasite-containing merosome vesicles into the bloodstream, merozoites are released and initiate the blood stage infection that provokes the characteristic malaria symptoms in humans. Free merozoites invade red blood cells (RBCs) within 2 minutes (**Fig. 2.3**), develop into ring-shaped ring stages (**Fig. 2.4**), and further to adult trophozoites (**Fig. 2.5**). Trophozoites undergo schizogony in the schizont stage to form 16-32 new merozoites (**Fig. 2.6**). When fully developed, the RBC membrane bursts, the merozoites are released, and a new cycle can be established (**Fig. 2.7**

[Cowman et al., 2016]). For *P. falciparum*, these asexual cycles take roughly 48 hours and cause inflammation in the bloodstream that is causing the febrile symptoms and anemia (White et al., 2014). Therefore, these asexual blood stages are a crucial target for antimalarial drug development. To complete the human cycle to a new transmission stage, some schizonts produce merozoites that are committed to sexual development (**Fig. 2.8**). After the invasion of RBCs, they develop into male or female gametocytes. For this, they sequester into the bone marrow and undergo five stages of gametogenesis for about 11 days. Fully-developed gametocytes migrate into the bloodstream and are taken up by a mosquito taking its blood meal (**Fig. 2.9** [Cowman et al., 2016]). Within the mosquito midgut, gametocytes develop into macro- and microgametes (**Fig. 2.10**) to form a zygote (White et al., 2014), the only diploid stage of the parasite (**Fig. 2.11** [Guttery et al., 2023]). During six developmental stages over 24 hours, the zygote initially duplicates its genome and then undergoes meiosis to form the motile ookinete with four discrete haploid genomes within a single nucleus (**Fig. 2.12**). Subsequently, the ookinete invades the gut wall to develop into an oocyst (**Fig. 2.13**). In this sporogonic stage, the oocyst produces hundreds of haploid sporozoites that migrate to the salivary gland (**Fig. 2.14**). Eventually, after injection during a new blood meal, the parasite completes its cycle (Guttery et al., 2023).

While the basic life cycle is similar in all *P*. species, it is *P. falciparum*'s ability for sequestration that makes it most distinct from the other species. Notably, *P. falciparum* erythrocyte membrane protein 1 (PfEMP1), exported to the RBC surface, mediates pronounced cytoadherence. In this way, infected RBCs (iRBCs) can compromise microcirculatory flow and ultimately lead to dysfunction of vital organs, a reason for *P. falciparum*'s high fatality rate. Sequestration of iRBCs in cerebral capillaries can lead to cerebral malaria with edema and coma. Additionally, clogged capillaries can cause increased glycolysis in affected tissues, contributing to lactic acidosis and hypoglycemia, another important cause of death. Besides, reduced microcirculatory flow is thought to promote acute kidney injury. Furthermore, pulmonary edema is a reason for high case fatality rates. Besides *P. falciparum*'s outstanding cytoadherence, it is worth noting that *P. vivax* and *P. ovale* species also have a prominent feature in their life cycle. They can form hypnozoites, dormant liver stages, which can cause relapsing of the disease after more than one year (White et al., 2014).

1.2.3 Nutrient Flux

With the invasion of RBCs, the parasite forms a parasitophorous vacuole (PV) within its host cell. This vacuole is separated towards the parasite through the parasite plasma membrane (PPM) and towards the RBC cytosol through the parasitophorous vacuolar membrane (PVM) that originates from the RBC plasma membrane. Therefore, nutrients from the serum have to pass three membranes to reach the parasite. This is facilitated via endogenous host

transporters, parasite-derived transporters in the PPM, as well as parasite-derived exported transporters in the PVM and RBC membrane (Henshall & Spielmann, 2023). Those parasite-derived host cell modifications serving the nutrient supply through the RBC plasma membrane are classified as new permeation pathways (NPP [Ginsburg et al., 1983; Ginsburg et al., 1985]), while channels through the PVM are commonly defined as PVM nutrient channels (Henshall & Spielmann, 2023), or in general, as nutrient permeable channels (NPC [Mesén-Ramírez et al., 2021a]). The latter are relatively unspecific and poorly characterized (Henshall & Spielmann, 2023) and are thought to serve as a molecular sieve for molecules up to 1.4 kDa (Desai et al., 1993; Desai & Rosenberg, 1997). Notably, one of its components *Plasmodium falciparum* exported protein 2 (PfEXP2) serves a dual role as a nutrient channel and part of the *Plasmodium* translocon of exported proteins (PTEX) that is used for protein export and host cell modifications (Garten et al., 2018). Noteworthy, PfEXP2's function and correct assembly as a nutrient channel is dependent on *Plasmodium falciparum* exported protein 1 (PfEXP1 [Mesén-Ramírez et al., 2019]). Besides, the parasite feeds on its hosts' cytosol, primarily composed of hemoglobin (Hb), which is outlined later in this work (Counihan et al., 2021).

1.2.4 Energy Metabolism

In line with their complex life cycle, *P.* species show a high degree of metabolic flexibility and adapt their energy metabolism with their changing environment (Delves et al., 2012; MacRae et al., 2013; Olszewski & Llinás, 2011; Suryavanshi et al., 2025). In the disease-promoting asexual blood stages, the parasites rely mainly on glycolysis for their adenosine triphosphate (ATP) production. In iRBCs, glucose (GLC) consumption is 10-100x higher than in non-infected cells (Roth et al., 1982; Sherman, 1979; Shivapurkar et al., 2018; van Niekerk et al., 2023). Thereby, more than 93% of internalized GLC is metabolized to lactate (MacRae et al., 2013), while inhibitors of the electron transport chain (ETC), and blockage of the tricarboxylic acid (TCA) flux (Ke et al., 2015), only have minimal effect on ATP levels (Fry et al., 1990). Furthermore, the ETC appears to be only essential for pyrimidine synthesis, which affects the parasites solely in late stages (Painter et al., 2007; Painter et al., 2010). In contrast, the rate of lactic acid fermentation of GLC decreases to around 80% in gametocytes (MacRae et al., 2013), together with upregulation of the TCA cycle (Young et al., 2005), while a fully functional TCA cycle appears to be essential for the development of mosquito stages (Ke et al., 2015).

In iRBCs, GLC is taken up from the blood mainly via the hosts' human GLC transporter 1 (GLUT1 [Preuss et al., 2012; Zhao & Keating, 2007]). The GLC is subsequently transported across the PVM, and imported into the parasite via the *Plasmodium falciparum* hexose transporter (PfHT) in the PPM (**Fig. 3** [Woodrow et al., 1999]).

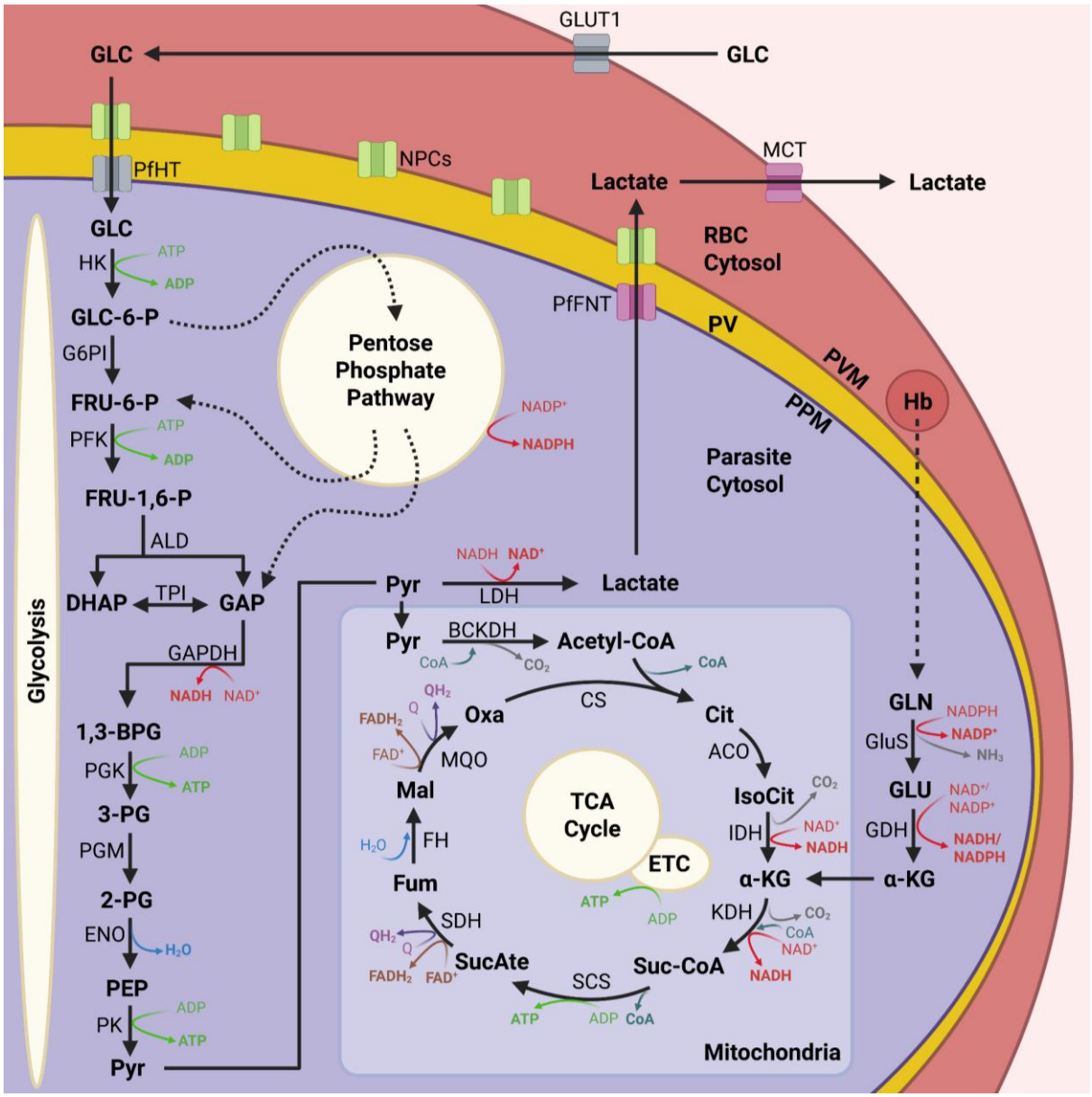

Figure 3: Energy metabolism in *Plasmodium falciparum*. Simplified scheme of the energy-generating pathways. Stoichiometric factors, protons, and anorganic phosphates are omitted. **RBC:** red blood cell; **PVM:** parasitophorous vacuolar membrane; **PV:** parasitophorous vacuole; **PPM:** parasite plasma membrane; **GLC:** glucose; **GLC-6-P:** glucose-6-phosphate; **FRU-6-P:** fructose-6-phosphate; **FRU-1,6-P:** fructose-1,6-bisphosphate; **DHAP:** dihydroxyacetone phosphate; **GAP:** glyceraldehyde-3-phosphate; **1,3-BPG:** 1,3-bisphosphoglycerate, **3-PG:** 3-phosphoglycerate; **2-PG:** 2-phosphoglycerate; **PEP:** phosphoenolpyruvate; **Pyr:** pyruvate; **CoA:** coenzyme A; **Cit:** citrate; **IsoCit:** isocitrate; **α-KG:** α-ketoglutarate; **Suc-CoA:** succinyl-CoA; **SucAte:** succinate; **Fum:** fumarate; **Mal:** malate; **Oxa:** oxaloacetate; **GLN:** glutamine; **GLU:** glutamate; **ATP:** adenosine triphosphate; **ADP:** adenosine diphosphate; **$NADP^+$/NADPH:** nicotinamide adenine dinucleotide phosphate (oxidized/reduced); **NAD^+/NADH:** nicotinamide adenine dinucleotide (oxidized/reduced); **FAD^+/$FADH_2$:** flavin adenine dinucleotide (oxidized/reduced); **Q:** ubiquinone; **QH_2:** ubiquinol; **GLUT1:** glucose transporter 1; **NPC:** nutrient permeable channel; **PfHT:** *Plasmodium falciparum* hexose transporter; **HK:** hexokinase; **G6PI:** glucose-6-phosphate isomerase; **PFK:** phosphofructokinase; **ALD:** aldolase; **TPI:** triosephosphate isomerase; **GAPDH:** glyceraldehyde-3-phosphate dehydrogenase; **PGK:** phosphoglycerate kinase; **PGM:** phosphoglycerate mutase; **ENO:** enolase; **PK:** pyruvate kinase; **LDH:** lactate dehydrogenase; **PfFNT:** *Plasmodium falciparum* formate-nitrite transporter; **MCT:** monocarboxylate transporter; **BCKDH:** branched chain ketoacid dehydrogenase; **CS:** citrate synthase; **ACO:** aconitase; **IDH:** isocitrate dehydrogenase; **KDH:** α-ketoglutarate dehydrogenase; **SCS:** succinyl-CoA synthetase; **SDH:** succinate dehydrogenase; **FH:** fumarate hydratase; **MQO:** malate quinone oxidoreductase; **GluS:** glutamate synthase; **GDH:** glutamate dehydrogenase (isoform a: NADP(H) / isoform c: NAD(H)). Created in BioRender: https://BioRender.com/60v8il6 (based on [Gemayel, 2017; Jortzik et al., 2012; Mesén-Ramírez et al., 2021b; Preuss et al., 2012; Suryavanshi et al., 2025]).

In the parasites, most of the GLC undergoes glycolysis with subsequent lactic acid fermentation as main energy-generating pathway (Preuss et al., 2012). The lactate is subsequently exported via the *Plasmodium falciparum* formate-nitrite transporter (PfFNT [Marchetti et al., 2015; Wu et al., 2015]) out of the parasite and with the monocarboxylate transporter 1 (MCT1) out of its hosts' cytosol (Kanaani & Ginsburg, 1991; Poole & Halestrap, 1994), which is contributing to the lactic acidosis that is often found in patients suffering severe malaria (Possemiers et al., 2021). In line with the increased GLC consumption, the activity of the pentose phosphate pathway is increased by about 78-fold (Atamna et al., 1994). This serves as the parasites' main source for reduced nicotinamide adenine dinucleotide phosphate (NADPH), needed to cope with the pro-oxidative environment in the RBCs (Preuss et al., 2012). While some of the pyruvate (Pyr), as well as glutamate (GLU), is fed into the TCA cycle (Ke et al., 2015), there is no evidence for β-oxidation in the parasites (Olszewski & Llinás, 2011).

1.2.5 Hemoglobin Metabolism

In its intraerythrocytic stages, *P. falciparum* feeds on its host cell's cytoplasm, composed of around 95% Hb (Krugliak et al., 2002), for its development and modifies its host to acquire all other missing nutrients (Counihan et al., 2021). The parasite consumes up to 65% of the host's Hb (Krugliak et al., 2002) and, in principle, the parasite can gather all of its amino acids (AA) from Hb digestion except for isoleucine (Liu et al., 2006). However, only around 16% of its utilized AA actually are derived from Hb digestion (Krugliak et al., 2002). Additionally, it lacks *de novo* synthesis of other essential metabolites such as pantothenate (Saliba et al., 1998) and purines (Downie et al., 2008). These, as well as AA and sugars, are partially acquired from the serum via modifications of the host membrane through NPPs, such as the plasmodial surface anion channel (PSAC [Desai et al., 2000; Lisk & Desai, 2005]).

In contrast, Hb uptake takes place in various forms of endocytosis that are relatively poorly characterized on the molecular level and appear to be clathrin-independent (Spielmann et al., 2020; Wiser, 2024). The initiation of endocytosis appears to be facilitated via non-canonical parasite-specific proteins, while endosomal transport is also facilitated by homologs of canonical proteins such as the vacuolar protein sorting 45 protein (VPS45 [Jonscher et al., 2019; Sabitzki et al., 2024]). The basic model suggests that invaginations of the PPM, filled with host cytosol as well as the PVM, are formed and transported to the digestive vacuole (DV), also known as the food vacuole (FV). During this process, the PVM and Hb are started to be digested (Spielmann et al., 2020). Commonly, four pathways of this Hb uptake are discerned. During the so-called big gulp, an initial invagination of host cytosol independent of actin polymerization, which is observed in cup-like ring stages and that is thought to represent the FV's origin. Going on from there, smaller invaginations that produce small Hb containing

vesicles are termed the cytostome. These vesicles are then trafficked actin-dependent to the FV. Furthermore, actin-dependent formation of elongated invaginations, termed cytostomal tubes, are described. Additionally, vast portions of host cytosol are incorporated similar to phagocytosis. However, this process is actin-independent and termed phagotrophy (Elliott et al., 2008).

The Hb digestion is facilitated by various proteases. These include aspartic proteases, called plasmepsins (PMs), cysteine proteases, called falcipains (FPs), metalloproteases, called falcilysins, and exopeptidases (Wiser, 2024). Among these proteases, PMs and FPs present a high degree of functional redundancy (Omara-Opyene et al., 2004). The detailed trafficking of many digestive FV proteins is still poorly understood (Mayer, 2021; Wiser, 2024). However, processes include the export via the secretory pathway to the RBC cytosol and consecutive uptake with the host cytosol, export to the PV, or targeting to the PPM (Wiser, 2024). The digestion starts with PMs that are separating the Hb into large globin fragments and heme (**Fig. 4**).

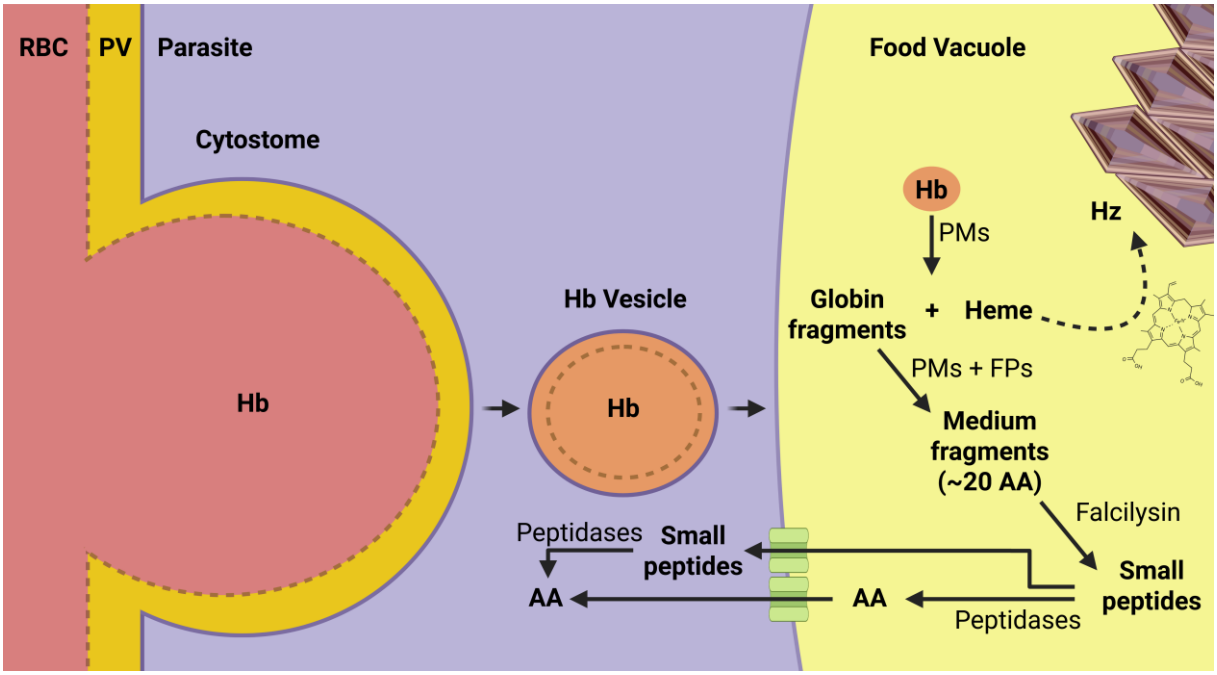

Figure 4: Hb digestion in *Plasmodium falciparum*. Hb-containing host cytosol is taken up by various forms of endocytosis, such as via the cytostome, and incorporated into the food vacuole. Hb is digested to free heme and amino acids. Free heme is detoxified to Hz crystals. RBC: red blood cell; PV: parasitophorous vacuole; Hb: hemoglobin; Hz: hemozoin; AA: amino acids; PM: plasmepsin; FP: falcipains. Created in BioRender: https://BioRender.com/wa9lvnz (based on [Omara-Opyene et al., 2004; Spielmann et al., 2020; Wiser, 2024]).

Subsequently, PMs and FPs cleave the large globin fragments into medium fragments of around 20 AA. Falcilysins then further degrade these fragments to peptides of around 6 AA that are cleaved via aminopeptidases to AA. The peptides and AA are transported to the parasite cytosol. Eventually, AA used for the parasite's biosynthesis, or are exported (Wiser, 2024). The freed heme poses a high risk for oxidative damage and membrane lysis and is

detoxified in the acidic FV via a hardly-understood biocrystallization process to hemozoin (Hz) (Wiser, 2024). Even though only a fraction of Hb-derived AA are used for the parasite's protein synthesis, the Hb digestion and heme detoxification pathway are crucial for parasite survival and target of various established drugs and drug candidates (Edgar et al., 2024; Villiers & Egan, 2021; Wiser, 2024).

1.3 Antimalarial Intervention Strategies

Intervention strategies to cope with the burden of malaria include chemotherapies, chemoprevention, vector control, mass testing, and vaccinations (WHO, 2024a).

1.3.1 Prevention

Among preventative strategies, vector control measures such as insecticide treated nets (ITN) largely contributed to the decline in disease prevalence during the last decades (Bhatt et al., 2015; WHO, 2024b). Furthermore, indoor residual spraying (IRS) and residual surface treatment (RST) with insecticides achieved the prevention of infection as well as transmission blocking of infected mosquitos (WHO, 2024a).

Malaria prevention can also be achieved using antimalarial drugs in various contexts – in individuals, high-risk groups, or as part of mass drug administration (MDA). However, resistance formation has to be considered (WHO, 2024a).

Due to the predominantly intracellular nature of the *Plasmodium* species, shielded from the immune system, vaccine development is facing various challenges. It was not until 2021, after decades of research, the World Health Organization (WHO) approved RTS,S/AS01, the first malaria vaccine in humans (WHO, 2024b). The recombinant protein vaccine is based on the circumsporozoite protein (CSP), a surface protein of the pre-liver sporozoite stage (Sallam et al., 2025). Modification of the antigen/adjuvant ratio and adjuvant composition with improved immunogenicity profile led to the R21/Matrix-M vaccine and its approval by the WHO in 2023 (Sallam et al., 2025; WHO, 2024b). However, both show limited efficacy, waning protection after a year, the requirement for annual booster vaccinations, and are indicated only for young children. Other promising vaccine concepts include whole-sporozoite vaccines using attenuated strains, or new blood and mosquito stage antigens, which could benefit to a combination of different approaches for higher efficacy (Duffy et al., 2024).

1.3.2 Chemotherapies

Acute malaria infection can be treated with suitable antimalarial drugs. Currently used antimalarial drugs can be classified according to their chemical class, or proposed mode of action (MoA). Commonly, the classification of compound classes covers amino alcohols, 4-aminoquinolines, 8-aminoquinolines, antifolates, sulfonamides, antibiotics,

naphthoquinones, and endoperoxides (Delves et al., 2012; McCarthy & Price, 2015; Patel et al., 2021). Most of them show their highest activities in the asexual blood stages, however, 8-aminoquinolines have higher activity in the liver stages (Delves et al., 2012).

Amino Alcohols

The amino alcohol quinine (QN) counts as the first antimalarial drug known to the Western world. It was discovered in the 17th century in the form of the bark of the cinchona tree of South America. Since then, it was widely used in the tropics around the globe. However, it possesses a low therapeutic index with substantial side effects (Achan et al., 2011). These include eye and auditory toxicity, cardiac effects with prolongation of the QT interval, and hypoglycemia (Taylor & White, 2004).

Mefloquine (MQ) was developed in the 1970s by the Walter Reed Army Institute of Research and was widely used as a prophylactic drug (Croft, 2007). However, high-grade resistant *P. falciparum* strains emerged in Southeast Asia in the 1990s and common gastrointestinal symptoms and neuropsychiatric effects limited its use (Alghamdi et al., 2024; McCarthy & Price, 2015; Taylor & White, 2004).

During the same research project, halofantrine (HAL) was developed (Croft, 2007). However, severe side effects were noted. HAL can cause significant QT prolongation, directly correlated with HAL serum levels, leading to potentially lethal adverse effects with sudden death (Taylor & White, 2004) and is not recommended by the WHO anymore (WHO, 2024b).

Lumefantrine (LUM) was developed in the 1970s by the Chinese research program Project 523 (Cui & Su, 2009). Despite a similar structure to QN and HAL, no cardiotoxic effects were reported and the drug appears to be well-tolerated (Taylor & White, 2004). It is still widely used in combination with artemisinin (ART) as a first line treatment (WHO, 2024b).

The amino alcohols target the asexual blood stages. Even though MQ and QN have a prominent quinoline moiety that is thought to facilitate heme binding (Ravindar et al., 2023) and they show hemozoin formation inhibition *in vitro* (Egan et al., 1994; Coy D. Fitch, 2004; Herraiz et al., 2019), their parasite-killing mechanism, as true for the other amino alcohols, is still not understood and controversially debated (Dziekan et al., 2019; C. D. Fitch, 1998; Coy D. Fitch, 2004; Hoppe et al., 2004; Sheridan et al., 2018; Wong et al., 2017). Especially, as resistance is mediated via the P-glycoprotein encoded by the *P. falciparum* multidrug resistance 1 gene (*pfmdr1*), which facilitates drug export from the cytosol into the FV, making a main mechanism via Hz inhibition unlikely (Price et al., 2004; Ward et al., 2022).

4-Aminoquiniolines

The 4-aminoquinoline chloroquine (CQ) was first synthesized in 1934 in Germany and widely used in the second half of the 20th century throughout the malaria endemic world (McCarthy & Price, 2015). CQ is generally well tolerated, except for mild side effects such as widespread itching. However, severe side effects including neuromyopathy, irreversible retinopathy, and cornea opacity after long-term use are well documented, as well (Taylor & White, 2004).

CQ and other 4-aminoquinolines are thought to kill the parasite via interference with the Hz crystallization process and increase in free heme (Abshire et al., 2017; Combrinck et al., 2013; Delves et al., 2012; Famin & Ginsburg, 2002; McCarthy & Price, 2015). Parasite resistance is mediated via the CQ resistance transport (CRT), which facilitates the export of the drugs from the FV into the parasite cytosol (Djimdé et al., 2001; Fidock et al., 2000). Due to widespread resistance in *P. falciparum*, especially in Africa, CQ is not considered first line treatment anymore (WHO, 2024b).

However, based on CQ, other 4-aminoquinoline were developed. These include hydroxychloroquine, amodiaquine (AQ), pyronaridine (PYR), or piperaquine (PPQ). They show various degrees of cross resistance to CQ (McCarthy & Price, 2015) and are used in ART combination therapies (WHO, 2024b).

8-Aminoquinolines

Notably, 8-aminoquinolines such as primaquine (PQ) and tafenoquine (TQ) possess high activity against liver stages and the dormant hypnozoite forms (McCarthy & Price, 2015), while they do not show high activity against asexual blood stages (Delves et al., 2012). However, they potentially induce hemolysis in patients with GLC-6-phosphate dehydrogenase (G6PDH) deficiency (Taylor & White, 2004). In line with this, they are thought to produce oxidative metabolites and disrupt the ETC, rather than interfering with heme polymerization (Camarda et al., 2019). Notably, even after decades of usage in the field, no clinically relevant resistances emerged (Vale et al., 2009).

Antifolates and Sulfonamides

Protozoan parasites, such as the *P.* species, lack a pyrimidine salvage pathways and rely on *de novo* synthesis. Thereby, thymidine monophosphate synthesis is mediated via tetrahydrofolate (THF) as cofactor. Thus, for THF regeneration, they need the activity of the dihydrofolate reductase (DHFR), which shows sufficient sequence variation among organisms to demonstrate a good drug target. Such drugs are classified as antifolates. Additionally, the *de novo* synthesis of folate via the dihydropteroate synthase (DHPS) is targeted by sulfonamides (McCarthy & Price, 2015).

Antifolates include pyrimethamine (PY), which is usually given in combination with the sulfonamide sulfadoxine (McCarthy & Price, 2015). However, sulfadoxine-pyrimethamine (SP) can cause severe cutaneous symptoms, such as Steven Johnson syndrome, and liver adverse effects that led to withdrawal as general prophylaxis. Fatal reactions among travelers are estimated between 1/11,000 and 1/35,000. Besides, hematological symptoms might occur in vulnerable folate-deficient groups. Additionally, the combination became largely ineffective in many places around the globe (Taylor & White, 2004).

The antifolate prodrug proguanil (PG) is usually combined with atovaquone (ATQ), marketed as Malarone (MAL) to treat uncomplicated malaria and is widely used for chemoprophylaxis (McCarthy & Price, 2015). PG's metabolite cycloguanil (CG) is known to target the DHFR, however, PG itself is found to interfere synergistically with ATQ on the ETC membrane potential (Mounkoro et al., 2021; Skinner-Adams et al., 2019).

Additionally, the sulfonamide dapsone is clinically used (McCarthy & Price, 2015). Originally synthesized 1908 in Freiburg, it was repurposed to treat malaria in the 1960s and widely used in the Vietnam War in the face of spreading CQ resistance.

However, single point mutations in the DHFR and DHPS are sufficient to cause drug resistance in this class, which is limiting their use (Alghamdi et al., 2024).

Antibiotics

The apicomplexan *Plasmodium* species harbor a plastid, termed apicoplast, that is thought to originate from secondary endosymbiosis of a red algae (Mamudu et al., 2024). The apicoplast functions include isoprenoid biosynthesis, Fe-S cluster, heme, and fatty acid synthesis (Chakraborty, 2016). However, only the isoprenoid synthesis is essential for survival of the asexual blood stage parasites (Yeh & DeRisi, 2011). Its prokaryotic origin offers several targets for established antibiotics, such as DNA replication, transcription, or the plastid-specific isoprenoid biosynthetic pathway (Mamudu et al., 2024).

Most prominently, doxycycline (DOXY) and tetracycline, targeting the apicoplast ribosome (Biddau & Sheiner, 2019), were widely used as prophylaxis (McCarthy & Price, 2015). However, as the apicoplast pathways in the asexual blood stages are only essential for development in the consecutive cycle, they cause a delayed death phenotype, limiting their use for clinical applications (Biddau & Sheiner, 2019).

Naphthoquinones

In addition, the naphthoquinone ATQ targets the cytochrome bc_1 complex, complex III of the ETC, in *Plasmodium*, which shows sufficient sequence variation to mammals. This is thought to indirectly block the dihydroorotate dehydrogenase (DHODH), which is in need of ubiquinone

(Q) for pyrimidine synthesis (Patel et al., 2021; Siregar et al., 2015). Notably, ATQ is also active against liver stages (McCarthy & Price, 2015). Compared to MQ, which was widely used for prophylaxis, ATQ is generally well-tolerated with significantly fewer neuropsychiatric symptoms than MQ (Taylor & White, 2004). However, resistant parasites rapidly appeared in the field with mutations in cytochrome b, if given alone (Korsinczky et al., 2000), and is therefore commonly combined with PG as MAL for chemoprophylaxis (McCarthy & Price, 2015).

Endoperoxides

The antimalarial endoperoxides include the first-line antimalarials ART and its derivatives (Meshnick et al., 1996). ART, characterized by a 1,2,4-trioxane endoperoxide ring system, was first isolated in 1972 from the leaves of *Artemisia annua*, which were used to treat fever in the traditional Chinese medicine for centuries (Rudrapal & Chetia, 2016). Since then, ART and ART-derivatives, such as artemether (ATM), artesunate (ATS), and dihydroartemisinin (DHA), have been widely used, well tolerated, and show a potent and rapid parasite clearance. Their molecular target is seen to be of pleiotropic nature. However, it is thought, that the main mechanism involves a heme-mediated cleavage of their endoperoxide bridges, causing free radical species. As a consequence, alkylation of heme, proteins, lipids, DNA, and other biomolecules results in multifold cellular damage. However, resistant parasites emerged, that predominantly show mutations in the Kelch13 protein, involved in Hb endocytosis, which are thought to limit heme release and thereby radical formation (Ward et al., 2022). To counter resistant parasites, ART combination therapies (ACTs) with additional different MoA and longer half-life were deployed. Of those, ATM-LUM is the one most widely used. Additionally, the WHO recommends ATS-AQ, DHA-PPQ, ATS-MQ, ATS-PYR, ATS-SP (WHO, 2024a). However, there are rising reports of resistance to various ACTs and therefore, further triple combinations are discussed (Alghamdi et al., 2024; Siqueira-Neto et al., 2023).

New Developments

Currently, a broad range of new compounds is analyzed in clinical trials. Many of them are modifications or combinations of existing compound classes. Other promising targets under investigation are found within pathways of protein synthesis, protein export, vesicle trafficking, sodium homeostasis, fatty acid synthesis, cytoadherence, or host immune modulation (Nandal et al., 2024; Siqueira-Neto et al., 2023; Umumararungu et al., 2023).

Key for the approval of new drugs is the understanding of their underlying mechanism to ensure the safety and efficacy of drugs (Aronson et al., 2018; Davis, 2020). Drug development and approval in many countries is guided by the International Council for Harmonization (ICH) that was founded by the European Union, the United States of America, and Japan (Niazi et al., 2023). While the identification of a molecular target is not a prequisite for drug approval per

se, it is a key consideration for the safety assessment, already in non clinical studies. Thereby, the necessety for understanding of the underlying mechanism is inderectly demanded by the pharmacodynamics studies. These are outlined by ICH guidelines such as ICH M3 (R2) Non-clinical safety studies for the conduct of human clinical trials for pharmaceuticals or ICH S7A Safety Pharmacology Studies for Human Pharmaceuticals (ICH, 2000; ICH, 2009).

1.4 Genetically-Encoded Fluorescent Biosensors

The analysis of biochemical metabolites can be an effective way to validate drug targets, to support target identification, or to investigate basic parasite biology and parasite-host interactions. However, metabolites might only exist in a transient state or potentially degrade before the extraction out of a specimen allows direct analysis of a compound. Furthermore, extraction processes potentially confound the interpretation of analytic results, as their native surrounding is often not accounted for. One way to circumvent such potentially confounding factors is to use genetically-encoded fluorescent biosensors (GEFBs) for their analyses. GEFBs are protein-based and gene-encoded sensors. This allows measurements of molecules, enzymatic activities, or cellular processes inside of living cells in a physiologic environment. Furthermore, they allow measurements on the single-cell level (Ovechkina et al., 2021). GEFBs usually consist of a sensing domain, which is analyzing the molecule or process of interest, and a fluorescent reporting domain, which is facilitating the information transfer to detection devices such as fluorescence microscopes, or other spectroscopic cell analysis methods outside of the cells (Frei et al., 2024). Thereby, the sensing domain can introduce a conformational change, which affects the fluorescence properties of the reporting domain (Ovechkina et al., 2021). Their possible applications are countless, and over the last decades, a broad range of sensors were designed to suit specific research questions that are reviewed extensively elsewhere (Frei et al., 2024; Kim et al., 2021; Kostyuk et al., 2020; Ovechkina et al., 2021; Terai et al., 2019). Their sensing domain can be derived from endogenous proteins that naturally interact with the analyte, or they can be modified to suit the specific need. Their underlying reporting principle can also vary to a great degree and might exploit time-resolved or bioluminescent methods (Ovechkina et al., 2021). However, generally, they can be classified as either intensiometric or ratiometric. Intensiometric sensors change their fluorescence intensity in response to the analyzed event. However, when analyzing fluorescence changes of GEFBs in cells, a change in fluorescence intensity could also be derived from changes in sensor abundance. This potentially leads to confounding of the measurement. In contrast, ratiometric sensors are characterized by an additional fluorescence peak as a reference, which is derived from the same molecule. In this way, ratiometric sensors exclude confounding factors such as sensor expression level or sample thickness (Mo et al., 2023; Thiele et al., 2024).

Various GEFBs were successfully established in *P. falciparum*. These include sensors for pH, the glutathione redox potential, H_2O_2, Ca^{2+}, heme, NADH:NAD^+, or NADPH (Abshire et al., 2017; Borges-Pereira et al., 2020; Heimsch & Justus Liebig University Giessen, 2022; Kasozi et al., 2013; Kuhn et al., 2007; Mohring et al., 2016; Pandey et al., 2016; Rahbari et al., 2017; Thiele et al., 2024). However, sensors for genetically-encoded ATP measurements were missing, so far.

1.5 Objective of this Study

As the eradication of malaria in the near future is unforeseeable, and due to the rising threat of drug-resistant parasites, the development of novel and safe antiplasmodial compounds remains critical for global health. Therefore, basic research for compounds with novel mechanisms and unique targets is essential for feed into the drug development pipeline. To achieve this, understanding of the basic, at times outlandish, parasite biology with its biochemical processes can be one of the first steps needed for rational drug design (Mandal et al., 2009). The molecular target of many existing drugs remains to be elusive or poorly defined. This leaves room for improved efficacy and options against resistance development. Furthermore, the mechanism of potential new drug candidates should be characterized as well as possible to preclude severe adverse reactions in humans. Thus, one way to serve drug development is to deepen the understanding of drugs MoAs. The MoA defines cellular reactions towards a compound and can therefore give insights into the compound's target or validate proposed mechanisms (Trapotsi et al., 2022).

Thereby, the central and vital energy metabolite ATP is an informative factor to analyze. Due to its essential role, the energy metabolism and interconnected pentose phosphate pathway are seen as promising drug targets (Jortzik et al., 2012; van Niekerk et al., 2016). ATP analysis could uncover processes that interfere with the aforementioned and other interconnected pathways. Furthermore, ATP analysis can gain insights into the complex parasite-host interaction and the dynamic parasite development. However, only cell-disruptive or intensiometric ATP assays were available, so far (Ayi et al., 2009; Cevenini et al., 2014; Frei et al., 2024; Kanaani & Ginsburg, 1989, 1992; Khan et al., 2012; Kirk et al., 1996; Lelièvre et al., 2012; Miguel-Blanco et al., 2017; Morais et al., 2022; Peatey et al., 2012; Saliba & Kirk, 1999; Shi et al., 2021; van Schalkwyk et al., 2013). When analyzing drug effects on ATP level of rapidly growing *Plasmodium* cells, an intensiometric ATP readout should be normalized to the respective parasite volume. If parasite size is not accounted for, a decreased ATP readout could potentially derive from smaller cell size, rather than decreased [ATP]. In its intraerythrocytic stages, cell size is not easily determined and prone to confounding. Additionally, single-cell data is not feasibly generated using cell disruptive methods.

To overcome the limitations of the previously available ATP analysis methods, the work presented here aimed to establish ratiometric genetically-encoded fluorescent ATP sensors of the ATeam series (Imamura et al., 2009; Kotera et al., 2010) in the cytosol of *P. falciparum*. These allow the comparison of [ATP] between different treatment groups. Moreover, they allow measurements on the single-cell level. They were already established in mammalian cells, and nematodes (Ando et al., 2012; Baeza-Lehnert et al., 2019; Conley et al., 2017; Doysabas et al., 2020; Forkink et al., 2014; Fujisawa et al., 2022; Gerkau et al., 2019; Haynes et al., 2019; Imamura et al., 2009; Iworima et al., 2016; Kahancová et al., 2020; Kishikawa et al., 2012; Köhler et al., 2020; Kotera et al., 2010; Lerchundi et al., 2020; Lerchundi et al., 2019; Toloe et al., 2014; Valdebenito et al., 2016; Wang et al., 2019), however, their applicability in *P. falciparum* was not investigated, so far. ATeam sensors are limited by a certain sensitivity range and are potentially affected by pH fluctuations (Imamura et al., 2009). As the respective ATP level was not known in *P. falciparum*, it was aimed to establish two different sensors, to cover a broad concentration range. These were meant to be characterized in detail to identify the most suitable sensor for the application in *P. falciparum*. Furthermore, it was aimed to establish the improved pH sensor sfpHluorin to control for potentially confounding pH levels (Reifenrath & Boles, 2018).

With suitable sensors at hand, the aim was to characterize the effects of a panel of established drugs and promising drug candidates on the ATP level of trophozoite stage iRBCs. The asexual blood stages were meant to be investigated, as these are responsible for the malaria symptoms. Thus, these are the main targets for antimalarial chemotherapy. Thereby, the trophozoite stages proposedly have the highest metabolic turnover and ATP demand. At the same time, this stage is targeted by most of the established antimalarial compounds. With this setup, it was amined to gain a better understanding of the MoAs of existing drugs. Moreover, it was aimed to develop MoAs of promising drug candidates that could potentially support drug development. More importantly, the system was meant to be shared with the broader malaria research community to accelerate basic research in the fight against the disease.

1.6 Synopsis

This dissertation is based on two publications that established the usage of novel methods for ATP and pH determinations via GEFBs in *P. falciparum* for MoA analyses of antiparasitic compounds to support drug development.

In the first publication, the sensor measurements were established in *P. falciparum* and the effects on the sensor readout of a selection of antiparasitic compounds was investigated in trophozoite stage parasites. Thereby, two different variants of genetically-encoded fluorescence-based ATP sensors, ATeam1.03nD/nA and ATeam1.03YEMK, as well as an improved pH sensor, sfpHluorin, were applied in *P. falciparum* for the first time. Initially, purified

sensor proteins, recombinantly expressed in *Escherichia coli*, were characterized via a spectrophotometric plate reader to validate their proposed spectroscopic properties. Additionally, direct interactions of later-used antiparasitic compounds on the recombinant proteins were investigated, to preclude potentially confounding effects on sensor measurements. Comparing the spectroscopic properties and pH responsiveness of the ATeam1.03nD/nA and ATeam1.03YEMK sensors side by side for the first time, ATeam1.03nD/nA revealed less pH stability compared to ATeam1.03YEMK. In a next step, the sensors were stably integrated into the genome of the NF54*attB* parasite strain. Within the trophozoite stage, transfected parasite lines showed sensor expression in the cytosol that was verified via western blot and fluorescence microscopy. The parasites showed a reversible and dynamic response towards a changing nutrient environment controlled by GLC and 2-desoxy-D-GLC in accordance to their spectroscopic properties. This was demonstrated via measurements of cell suspensions in the plate reader and via single-cell measurements within the fluorescence microscope. Among both ATP sensor cell lines, the ATeam1.03nD/nA sensor cell line revealed a multifold lower signal intensity. Consecutive measurements of drug effects on ATP level were exclusively conducted with the ATeam.103YEMK cell line. Based on the establishment of the sensors, the effects of a selection of antiparasitic compounds on ATP level, pH, and cytosol size were determined. This revealed characteristic sensor response patterns caused by 4-aminoquinolines, arylamino alcohols, redox cyclers, as well as dihydroartemisinin, doxycycline, atovaquone, and cycloheximide. Besides, the aylamino alcohol MQ was capable of preventing specific sensor responses caused by the 4-aminoquinoline CQ.

In the second publication, the effects of the promising drug candidate arylmethylamino steroid compound 1o (1o), with so far unknown MoA, on the previously outlined ATP, pH, and size measurements were determined. The investigation uncovered parallels to arylamino alcohols such as MQ, including elevated ATP level, lowered pH, as well as lowered parasite size. Like MQ, 1o was able to prevent CQ-specific sensor reactions. Partially, these effects already manifested in the same order of magnitude as the half-maximal growth inhibitory concentration. Subsequently, 1o's effects on the ultrastructural morphology of Hz and the FV, the parasite-derived heme species distribution, as well as the light microscopic morphology of were analyzed. Prevention of CQ effetcs, alteration of the heme species distribution, and less intereference with late parasite stages suggest, that the parasite-killing activity could be based on an interference with the parasite's Hb uptake.

2. PUBLICATIONS

2.1 Publication I

Real-time measurements of ATP dynamics via ATeams in *Plasmodium falciparum* reveal drug-class-specific response patterns

Springer, E., Heimsch, K. C., Rahlfs, S., Becker, K., & Przyborski, J. M.

Antimicrobial Agents and Chemotherapy, *68*(5), e0169023.

2024

https://doi.org/10.1128/aac.01690-23

AMERICAN SOCIETY FOR MICROBIOLOGY | Antimicrobial Agents and Chemotherapy

Real-time measurements of ATP dynamics via ATeams in *Plasmodium falciparum* reveal drug-class-specific response patterns

Eric Springer,[1] Kim C. Heimsch,[1] Stefan Rahlfs,[1] Katja Becker,[1] Jude M. Przyborski[1]

AUTHOR AFFILIATION See affiliation list on p. 25.

ABSTRACT *Malaria tropica*, caused by the parasite *Plasmodium falciparum* (*P. falciparum*), remains one of the greatest public health burdens for humankind. Due to its pivotal role in parasite survival, the energy metabolism of *P. falciparum* is an interesting target for drug design. To this end, analysis of the central metabolite adenosine triphosphate (ATP) is of great interest. So far, only cell-disruptive or intensiometric ATP assays have been available in this system, with various drawbacks for mechanistic interpretation and partly inconsistent results. To address this, we have established fluorescent probes, based on Förster resonance energy transfer (FRET) and known as ATeam, for use in blood-stage parasites. ATeams are capable of measuring $MgATP^{2-}$ levels in a ratiometric manner, thereby facilitating *in cellulo* measurements of ATP dynamics in real-time using fluorescence microscopy and plate reader detection and overcoming many of the obstacles of established ATP analysis methods. Additionally, we established a superfolder variant of the ratiometric pH sensor pHluorin (sfpHluorin) in *P. falciparum* to monitor pH homeostasis and control for pH fluctuations, which may affect ATeam measurements. We characterized recombinant ATeam and sfpHluorin protein *in vitro* and stably integrated the sensors into the genome of the *P. falciparum* NF54*attB* cell line. Using these new tools, we found distinct sensor response patterns caused by several different drug classes. Arylamino alcohols increased and redox cyclers decreased ATP; doxycycline caused first-cycle cytosol alkalization; and 4-aminoquinolines caused aberrant proteolysis. Our results open up a completely new perspective on drugs' mode of action, with possible implications for target identification and drug development.

KEYWORDS *Plasmodium falciparum*, ATP, ATeam1.03YEMK, ATeam1.03-nD/nA, sfpHluorin, 4-aminoquinolines, arylamino alcohols, chloroquine, pyronaridine, amodiaquine, quinine, mefloquine, lumefantrine, plasmodione, SBI-750, methylene blue, cycloheximide, doxycycline, cytosol alkalization, malaria

Malaria is a serious infectious disease and remains one of the greatest public health burdens for humankind. In 2022, an estimated 249 million cases occurred worldwide. Of these, around 608,000 people died, with the majority of victims being children under five. Of *Plasmodium* species, *Plasmodium falciparum* has the highest impact on global health, causing most infections as well as the deadliest form of the disease (1). With growing drug resistance, basic research for the development of new drugs remains critical for global health.

In the asexual blood stages, it was shown, using isotopic labeling (2) and extracellular flux analysis (3), that the parasites rely mainly on glycolysis for adenosine triphosphate (ATP) production and use oxidative phosphorylation to only a minimal extent. Due to this limited metabolic flexibility, glycolytic enzymes (4), as well as upstream processes such as glucose transporters (5), were proposed as potential drug targets. These data also

Editor Audrey Odom John, The Children's Hospital of Philadelphia, Philadelphia, Pennsylvania, USA

Address correspondence to Jude M. Przyborski, Jude.Przyborski@ernaehrung.uni-giessen.de.

The authors declare no conflict of interest.

See the funding table on p. 25.

Received 20 December 2023
Accepted 26 February 2024
Published 19 March 2024

further highlight the importance of ATP as the main energy source for these parasites and stimulate research into ATP metabolism.

There are various approaches for measuring ATP, which are extensively reviewed elsewhere (6). In *P. falciparum*, most ATP measurement approaches to date used luciferase-based bioluminescence assays to measure ATP (7–19) or transgenic luciferase-expressing cell lines as a surrogate for parasite viability (13, 20). However, these approaches have inherent flaws regarding their applicability for mechanistic drug-response interpretation. ATP response toward drug interventions in luciferase-based bioluminescence ATP assays is usually compared to the output of a control group and based on the parasite count, as the exact parasitic cytosolic volume at a given time is hard to define. While using estimations of average parasite volume to calculate a definite [ATP] can partially circumvent this issue, this approach is even less applicable when comparing [ATP] between a control and a drug intervention group in situations in which growth differences are expected, as many drug treatments are known to interfere with protein biosynthesis (21). If a given intervention causes growth retardation and a reduction in cell volume, the intensity of a luciferase-based bioluminescence assay reaction normalized to a certain cell count can decrease in the intervention group, even when the actual molar [ATP] is identical. Additionally, measurements cannot easily be applied to subcellular compartments and are prone to influence from sample preparation. While the intensiometric approach using luciferase-expressing cell lines can be applied to specific subcellular compartments, it also does not necessarily reflect true differences in ATP levels, as the output is responsive to other factors that are expected to change through drug interventions, such as levels of sensor expression or degradation. These difficulties were highlighted by Khan et al. (13), who used both a cell-disruptive luciferase-based bioluminescence assay and a transgenic luciferase-expressing cell line to study ATP-drug response in trophozoite stages. This study showed that while mefloquine and artemisinin caused a clear increase in the amount of ATP over 10 h, the luminescence of the transgenic cell line decreased strongly under the same conditions.

To overcome these limitations, we decided to establish genetically encoded ratiometric FRET-based $MgATP^{2-}$ sensors from the ATeam (Adenosine 5′-Triphosphate indicator based on Epsilon subunit for Analytical Measurements) family in the *P. falciparum* NF54*attB* strain. ATeams were developed by Imamura et al. (22) and offer real-time *in cellulo* measurements of ATP dynamics on a single-cell or even compartmental level. ATeams are composed of a circular permutated mVenus yellow fluorescent protein (YFP) and an mseCFP cyan fluorescent protein (CFP) connected with an ATP-binding domain, the ε-subunit of a *Bacillus subtilis* F_oF_1-ATP synthase. Upon ATP binding, this domain changes its conformation, which brings YFP and CFP into close proximity and increases the FRET interaction. Analysis of the YFP- and CFP-specific emission ratio after CFP excitation demonstrates a correlative response toward $MgATP^{2-}$. Thus, this approach should reflect $MgATP^{2-}$ levels independently of the sensor expression level. It should be noted that the physiologically relevant form of ATP is $MgATP^{2-}$; however, we shall follow convention and simply refer to this as ATP, unless otherwise required for clarity.

Modification of the ATP-binding domain led to a series of ATeams with different sensitivities toward ATP (22). Furthermore, red-shifted GO-ATeams were developed based on green fluorescent protein (GFP) and orange fluorescent protein (23). In addition, the dimerization interface of GFP-based proteins was modified to yield sensors with improved dynamic range. Kotera et al. (24) discovered that the L206A mutation yielded the highest dynamic range. We therefore chose the ATeam1.03-nD/nA sensor with an improved dynamic range and sensitivity in the low millimolar range, as well as the ATeam1.03YEMK mutant with a slightly higher sensitivity toward ATP. Despite their advantages over other ATP analysis methods, GFP-based genetically encoded sensors also have pitfalls to consider. Most importantly, the fluorescence of GFP-based proteins may exhibit sensitivity to pH, as reviewed elsewhere (25). Treatment with antiparasitic compounds might induce pH changes in *P. falciparum,* and it has previously been

shown that illumination itself can induce a pH drop (26). To control for this, we, in parallel, established a parasite line expressing a genetically encoded pH sensor to monitor possible pH changes caused by drug interventions and sample preparation. pH indicator systems, such as pHluorin (27) or Sypher (28), have already been established in *P. falciparum*. Nevertheless, we chose to establish the superfolder variant developed by Reifenrath and Boles (29). Schuh et al. (30) found that the superfolder mutations appear to cause increased fluorescence intensity in the parasites. Establishing the super folder variant of pHluorin is therefore likely to be advantageous with respect to the increased signal-to-noise ratio.

Another pitfall to consider is the possibility of drug-sensor interactions, which might lead to potential experimental artifacts. We therefore recombinantly produced ATeam and sfpHluorin proteins to analyze drug-sensor interactions *in vitro* and, thereby, control for potential confounding effects.

With these sensors, we aimed to establish a simple and robust platform to analyze ATP-drug response levels and make these tools available for the malaria community. Additionally, we analyzed the ATeam response toward exposure to a selection of different antiparasitic compound classes. These include the 4-aminoquinolines chloroquine (CQ), amodiaquine (AQ), and pyronaridine (PYRO), the arylamino alcohols quinine (QN), mefloquine (MQ), and lumefantrine (LUM), dihydroartemisinin (DHA), the redox-cycler methylene blue [MB (31)], plasmodione [PD (32)], the apicoplast-targeting doxycycline [DOXY (33)], the electron transport chain (ETC)-targeting atovaquone [ATQ (34)], the protein synthesis inhibitor cycloheximide [CHX (35)], as well as the PfGluPho-targeting drug candidate SBI-0797750 [SBI (36)]. With these, we wanted to provoke possibly distinct sensor responses to gain new insights into their mode of action.

RESULTS

Recombinant ATeam proteins show a concentration-dependent increase in emission ratio toward ATP

To measure potential direct drug-sensor interactions and to characterize ATeam1.03-nD/nA and ATeam1.03YEMK sensors side by side for the first time, we produced His-tagged ATeam proteins recombinantly expressed in *E. coli* and purified them using affinity chromatography. Titration of the ATeam1.03-nD/nA and ATeam1.03YEMK proteins with ATP caused a dose-dependent emission ratio increase, as reported by Kotera et al. (24) and Imamura et al. (22), respectively (Fig. 1). We saw a higher dynamic range for ATeam1.03-nD/nA and a higher sensitivity toward ATP for ATeam1.03YEMK. We also confirmed that neither sensor showed a response to AMP or ADP, as previously shown by De Col et al. (37) and Imamura et al. (22).

We further compared the pH sensitivity, emission spectra, and time responsiveness of both sensors. Despite small discrepancies likely due to different buffer conditions, the ratio response trend is generally in accordance with Imamura et al. (22), Kotera et al. (24), and De Col et al. (37). We saw an apparent increased dynamic range of ATeam1.03-nD/nA toward pH 6 (Fig. 2A). However, the sensor also showed varying ratios at different pH even in the absence of ATP, indicating direct pH sensitivity of the fluorophores. In contrast, the ratio of ATeam1.03YEMK without ATP substrate was consistent between pH 6 and 9 (Fig. 2B). ATeam1.03YEMK showed an apparent lower dynamic range from pH 5 to 7 (Fig. 2B), but the actual FRET response (Fig. S1D) remained consistent. We believe that the decreased ratio between pH 7 and 5 results from an actual lower distribution of $MgATP^{2-}$ species in the lower pH solution, as they are unstable at this pH (38), which was already noted by De Col et al. (37). Both sensors showed typical changes in their emission spectrum in response to increasing [ATP] in accordance with the FRET response, as expected (Fig. 2C and D). With increasing [ATP], CFP fluorescence decreased, while YFP fluorescence increased. Within seconds, both sensors showed a rapid response to changing [ATP] and equilibration within 1 minute (Fig. 2E and F).

ATeam fluorescence and FRET response are influenced by temperature and pH (22). We aimed to imitate the environment in living parasites and therefore chose 37°C and

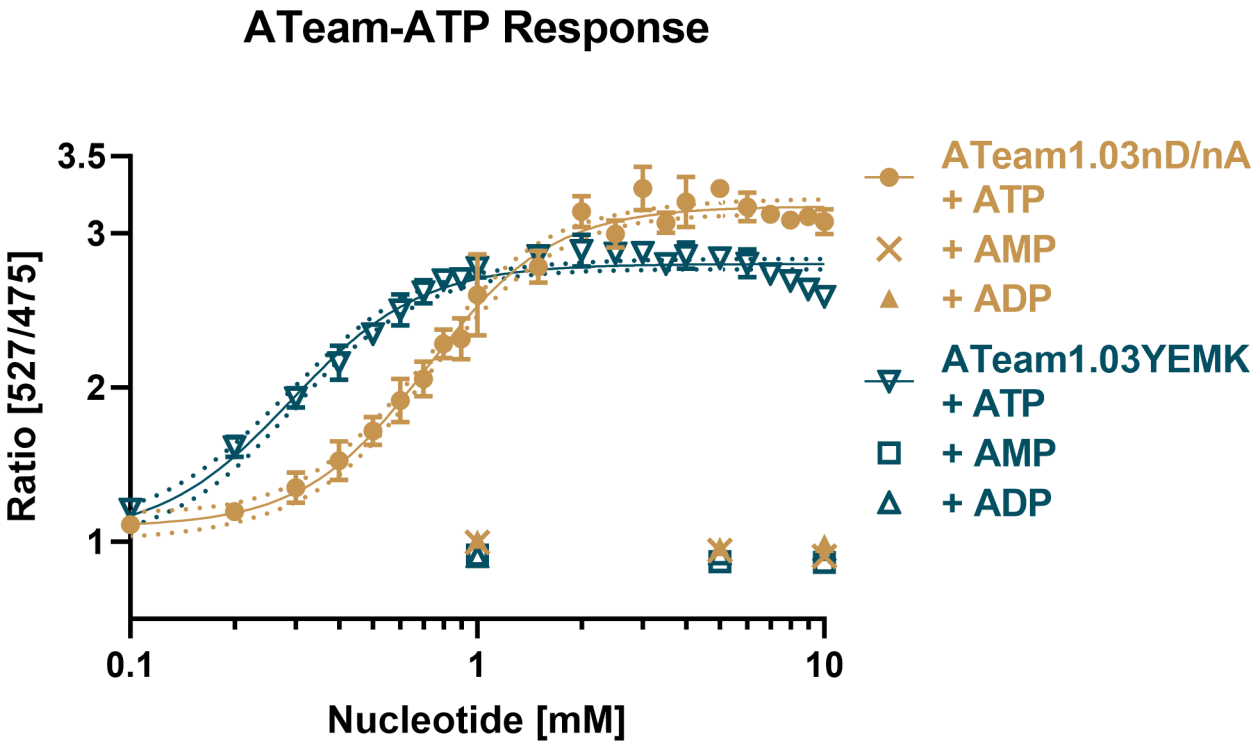

FIG 1 ATeam1.03-nD/nA and ATeam1.03YEMK show a dose-dependent ratio increase in response to ATP. Nucleotides were dissolved in an equimolar solution of $MgCl_2$. Measurements were conducted in a plate reader via excitation at 435 nm and emission sensing at 527 nm for YFP and 475 nm for CFP. Mean ratios of $n = 3$ independent experiments are shown. Error bars indicate SD.

pH 7.34 [cytosolic pH as determined in later experiments (Fig. 9B)] for all experiments with recombinant protein, if not indicated otherwise. Drug-sensor interaction studies did not find any relevant direct interaction between compounds and sensors in our desired concentration range for ATeam1.03YEMK (Fig. S2A) and ATeam1.03-nD/nA (data not shown).

ATeams can be stably expressed in *P. falciparum* NF54*attB* and are capable of measuring dynamic real-time changes of ATP level in a plate reader format

We used the NF54*attB* cell line lacking a selectable marker (39) to generate our transgenic cell lines. This allows *attB-attP* recombination within the cg6 gene using the mycobacteriophage Bxb1 integrase (40) and, thereby, facilitates rapid generation of stable transfectants. We used limiting dilution to generate clonal lines and PCR for verification (Fig. S3 and S4). NF54*attB*$^{[ATeam1.03\text{-}nD/nA]}$ and NF54*attB*$^{[ATeam1.03YEMK]}$ cell lines showed sensor-specific fluorescence in a shape resembling the cytosol of the parasites, as shown for a representative NF54*attB*$^{[ATeam1.03\text{-}nD/nA]}$ clonal line (Fig. 3A through E) with similar absolute fluorescence intensity within each cell population (data not shown). Under identical imaging conditions, NF54*attB*$^{[ATeam1.03YEMK]}$ clonal lines showed constantly higher absolute fluorescence intensity than NF54*attB*$^{[ATeam1.03\text{-}nD/nA]}$ clonal lines (data not shown). As ATeams are based on CFP and YFP proteins that are derived from GFP, we used cross-reactive anti-GFP antibodies for western blot analyses. In accordance with the lower fluorescence intensity, western blot analysis revealed a higher signal intensity of NF54*attB*$^{[ATeam1.03YEMK]}$ compared to NF54*attB*$^{[ATeam1.03\text{-}nD/nA]}$ relative to aldolase loading control, indicating higher sensor abundance in the NF54*attB*$^{[ATeam1.03YEMK]}$ parasites (Fig. 3F).

To demonstrate proof-of-principle of ATeam-expressing cell lines in a plate reader format, we analyzed their emission spectrum after glucose (GLC) starvation in response to the re-addition of GLC. GLC starvation is expected to cause ATP depletion and

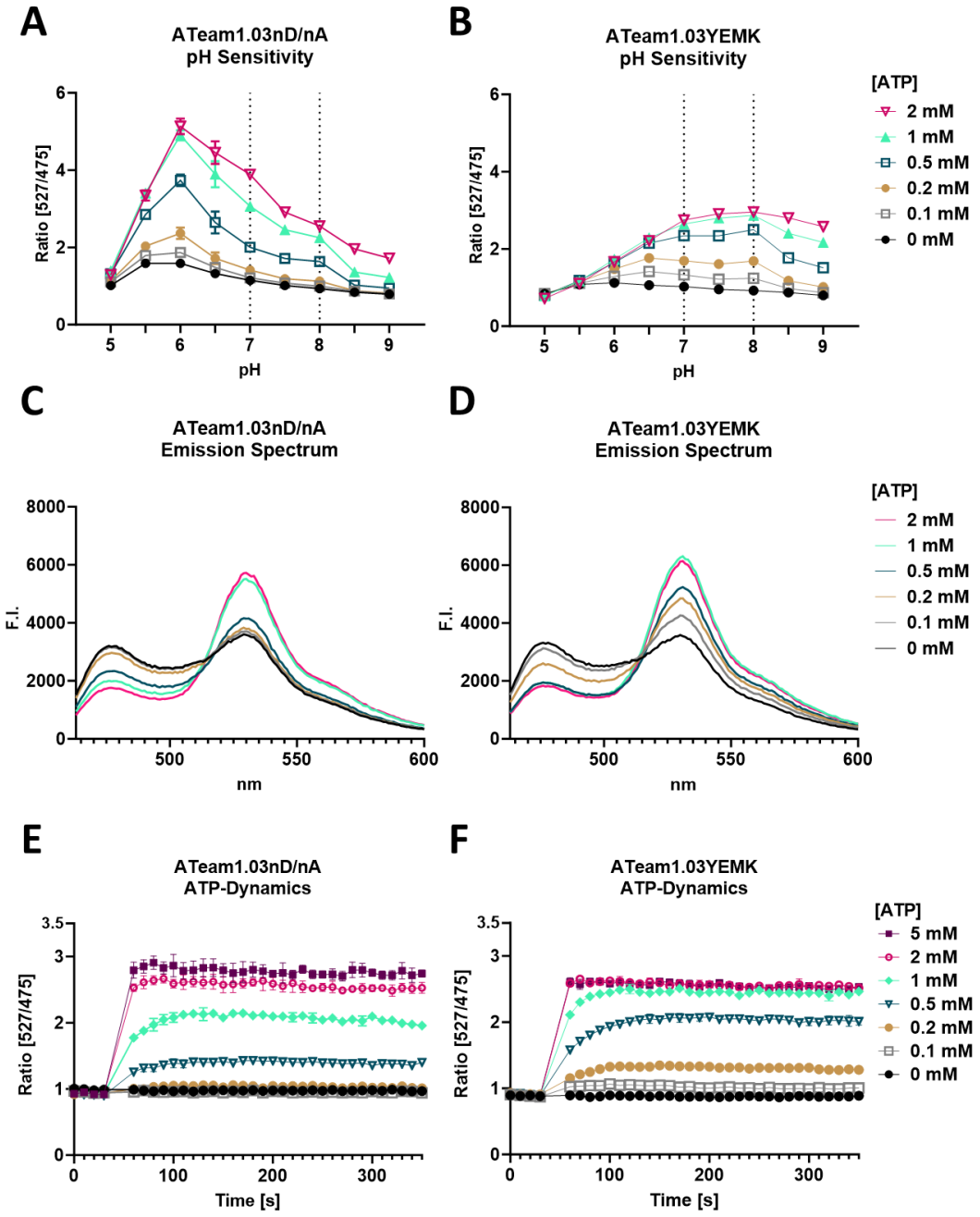

FIG 2 pH, emission spectrum, and time-response characteristics of ATeam1.03-nD/nA and ATeam1.03YEMK. (A and B) ATeam1.03-nD/nA shows a higher dynamic range but less pH stability than ATeam1.03YEMK. (C and D) Both sensors show a characteristic change in emission spectrum after excitation at 435 nm and emission detection from 463 to 600 nm in response to different [ATP] in accordance with FRET. Error bars were omitted for clarity. (E and F) Both sensors show a rapid response toward changes in [ATP]. The ratio reached a stable level approximately 1 minute after ATP addition. Measurements were conducted via excitation at 435 nm and emission sensing at 527 nm for YFP and 475 nm for CFP. Mean values of $n = 3$ independent experiments are shown. Error bars indicate SD.

an according ATeam emission spectrum in the parasites, while GLC re-addition after starvation is expected to restore ATP level, with increasing YFP and decreasing CFP emission peaks. NF54*attB*$^{[ATeam1.03\text{-}nD/nA]}$ and NF54*attB*$^{[ATeam1.03YEMK]}$ showed a change in emission spectrum with increasing [GLC] and a 10-minute incubation time, in accordance with the FRET response (Fig. 4A and B). A marked increase in YFP and decrease in

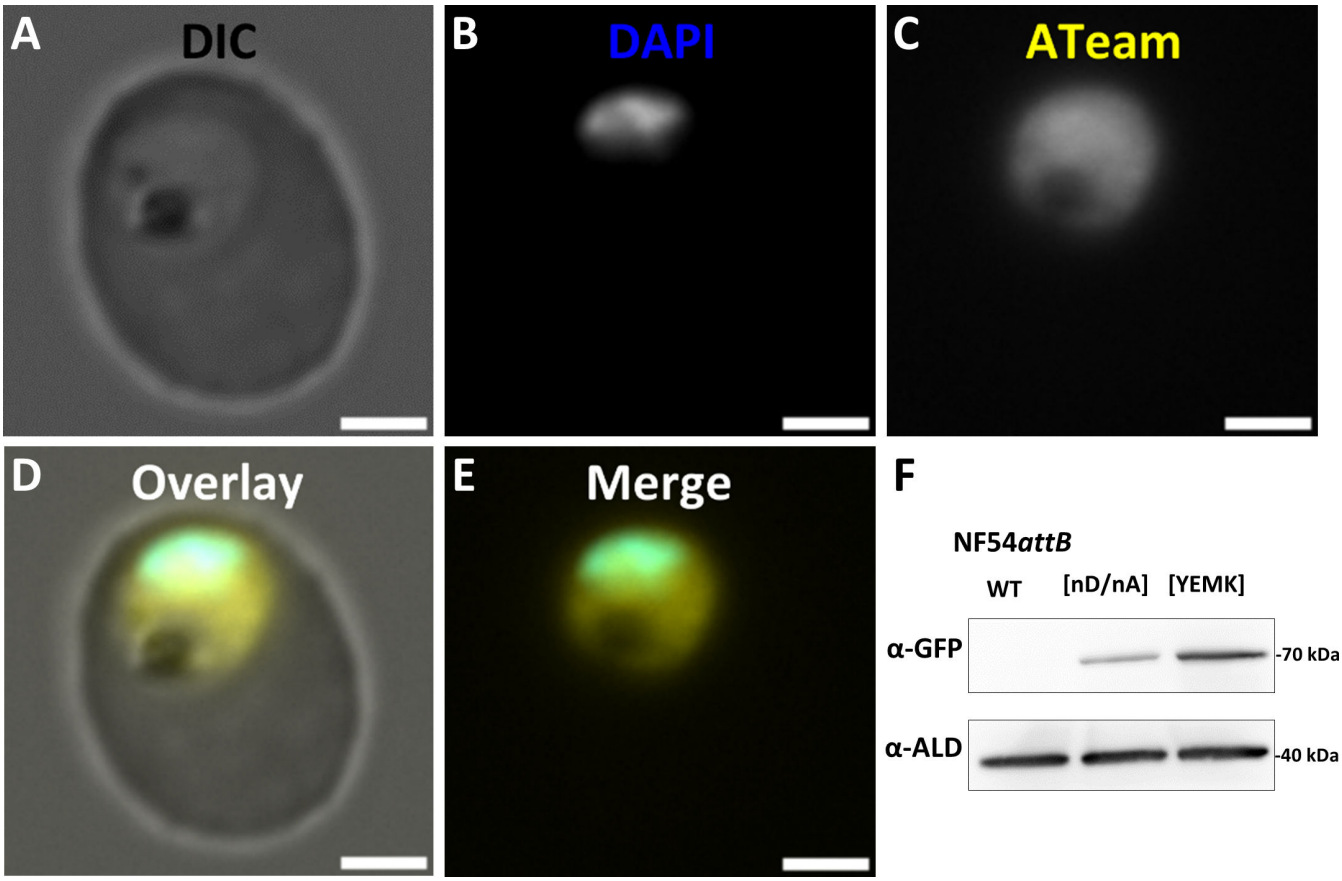

FIG 3 NF54*attB*$^{[ATeam1.03YEMK]}$ and NF54*attB*$^{[ATeam1.03-nD/nA]}$ show cytosolic ATeam fluorescence. DIC (A), DAPI (B), ATeam (C), overlay of panels A–C (D), and merge of panels B + C (E) of NF54*attB*$^{[ATeam1.03-nD/nA]}$ as representative for both ATeam cell lines. DAPI: ex 353 nm/em 465 nm and ATeam: ex 488 nm/em 509 nm. Scale bar equals 2 µm. (F) Both cell lines show α-GFP signal with the size of ATeam1.03-nD/nA and ATeam1.03YEMK protein (67.8 and 68.0 kDa, respectively). NF54*attB*$^{[ATeam1.03YEMK]}$ shows 1.96 ± 0.38 (SD) fold higher western blot signal than NF54*attB*$^{[ATeam1.03-nD/nA]}$ (n = 3) normalized to α-aldolase as loading control.

CFP peak was already observable with 150 µM GLC. There is no apparent difference between the addition of 1 and 20 mM GLC. No conditions fully replicated the emission spectrum of the control spectrum of parasites that were kept continuously in GLC-rich Ringer's solution (control). NF54*attB*$^{[ATeam1.03-nD/nA]}$ showed overall lower fluorescence intensity compared to NF54*attB*$^{[ATeam1.03YEMK]}$ under comparable conditions, leading to a lower signal-to-noise ratio.

We further demonstrated proof-of-principle of dynamic plate reader measurements over time using treatment with GLC and subsequent addition of the glycolysis inhibitor 2-deoxyglucose [2-DG (41)] after GLC starvation (Fig. 5). GLC addition is expected to restore ATP levels, while the addition of 2-DG is expected to deplete parasite ATP levels. Cells were washed in phosphate-buffered saline (PBS) for GLC depletion or GLC-rich Ringer's solution as a control. After 2 minutes, cells were treated with either PBS, Ringer's, or 1 mM GLC solution. Within 10 minutes, GLC-depleted cells treated with 1 mM GLC solution restored their emission ratio almost to that of the control group in Ringer's solution, indicating restoration of their ATP level. The ratio matched that of the control group in Ringer's solution over an additional 30 minutes within the plate reader, while both groups showed a small but steady ratio decline over time within the plate reader. In contrast, the addition of 2-DG 10 minutes after recovery of GLC-depleted cells caused a rapid ratio decrease to the baseline level in the GLC-depleted PBS solution. Under the same conditions, NF54*attB*$^{[ATeam1.03-nD/nA]}$ showed a similar response but a much lower signal-to-noise ratio (Fig. 5B). As both total sensor fluorescence and pH independence

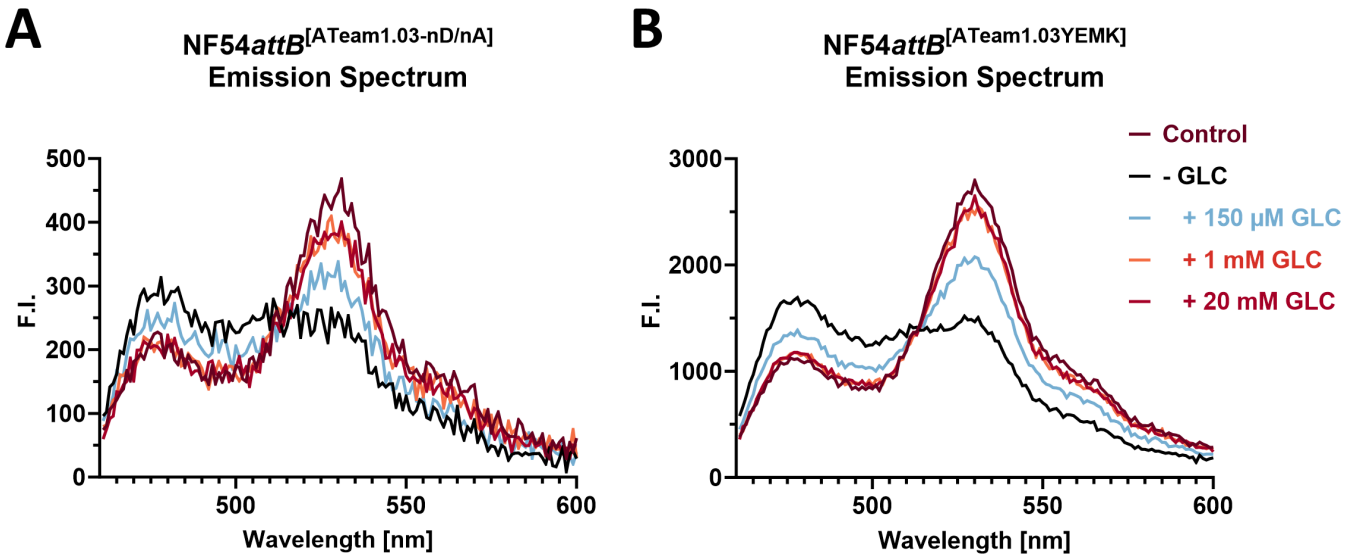

FIG 4 Emission spectrum of NF54*attB*$^{[ATeam1.03\text{-}nD/nA]}$ and NF54*attB*$^{[ATeam1.03YEMK]}$ responds to glucose titration in accordance with ATeam FRET. (A) NF54*attB*$^{[ATeam1.03\text{-}nD/nA]}$ and (B) NF54*attB*$^{[ATeam1.03YEMK]}$. Plate reader emission spectra of 2 million magnetic-activated cell sorting (MACS)-enriched trophozoite-infected red blood cells after excitation at 435 nm and emission detection from 463 to 600 nm in response to different [GLC] after 10-minute incubation time are shown. Parasites were washed in phosphate-buffered saline (PBS) for GLC depletion (–GLC) or GLC-rich Ringer's solution (control). Mean emission spectrum of n = 3 independent experiments is shown. Error bars were omitted for clarity.

were lower when using ATeam1.03-nD/nA, we decided to prioritize ATeam1.03YEMK for all further experiments.

NF54*attB*$^{[ATeam1.03YEMK]}$ can be used to monitor dynamic changes in ATP at single-cell level using fluorescence microscopy

Following on from plate reader measurements, we established NF54*attB*$^{[ATeam1.03YEMK]}$ measurements on a single-cell level using fluorescence microscopy. Similar to the plate reader experiments (Fig. 5), we treated GLC-starved parasites with GLC and subsequent addition of 2-DG. Figure 6 shows the emission ratio, overlay, YFP-, and CFP-emission channel of a representative trophozoite-infected red blood cell (iRBC) over time. The cell dynamically reacts to GLC addition with an increase and decrease of fluorescence intensities in the YFP and CFP channels, respectively, leading to an increase in emission ratio. The process is reversed via the application of 2-DG. Plotting the emission ratio of multiple single cells over time demonstrates a dynamic *in cellulo* sensor reaction in a fluorescence microscope (Fig. 7). The measurements also reveal a steady emission ratio decrease in untreated control parasites that may reflect limited photobleaching.

The pH sensor sfpHluorin allows robust measurement of cytosolic pH and is capable of measuring dynamic pH changes in a plate reader

As shown in Fig. 2, *in cellulo* ATeam measurements could be affected by pH fluctuations. To control for this, we generated parasites expressing the genetically encoded pH sensor sfpHluorin. Additionally, we produced His-tagged sfpHluorin protein to characterize the sensor's behavior *in vitro* and to control for possible direct drug-sensor interactions. pH titration and changes in emission and excitation spectra in a plate reader (Fig. S5) were in accordance with Reifenrath and Boles (29). We could not detect any direct drug-sensor interactions in our desired concentration range (Fig. S2B). We generated stable sfpHluorin-expressing cell lines and used limiting dilution to isolate clonal lines. To verify stable integration, we used PCR (Fig. S6). The NF54*attB*$^{[sfpHluorin]}$ clonal line showed sensor-specific fluorescence in a shape resembling the parasitic cytosol (Fig. 8).

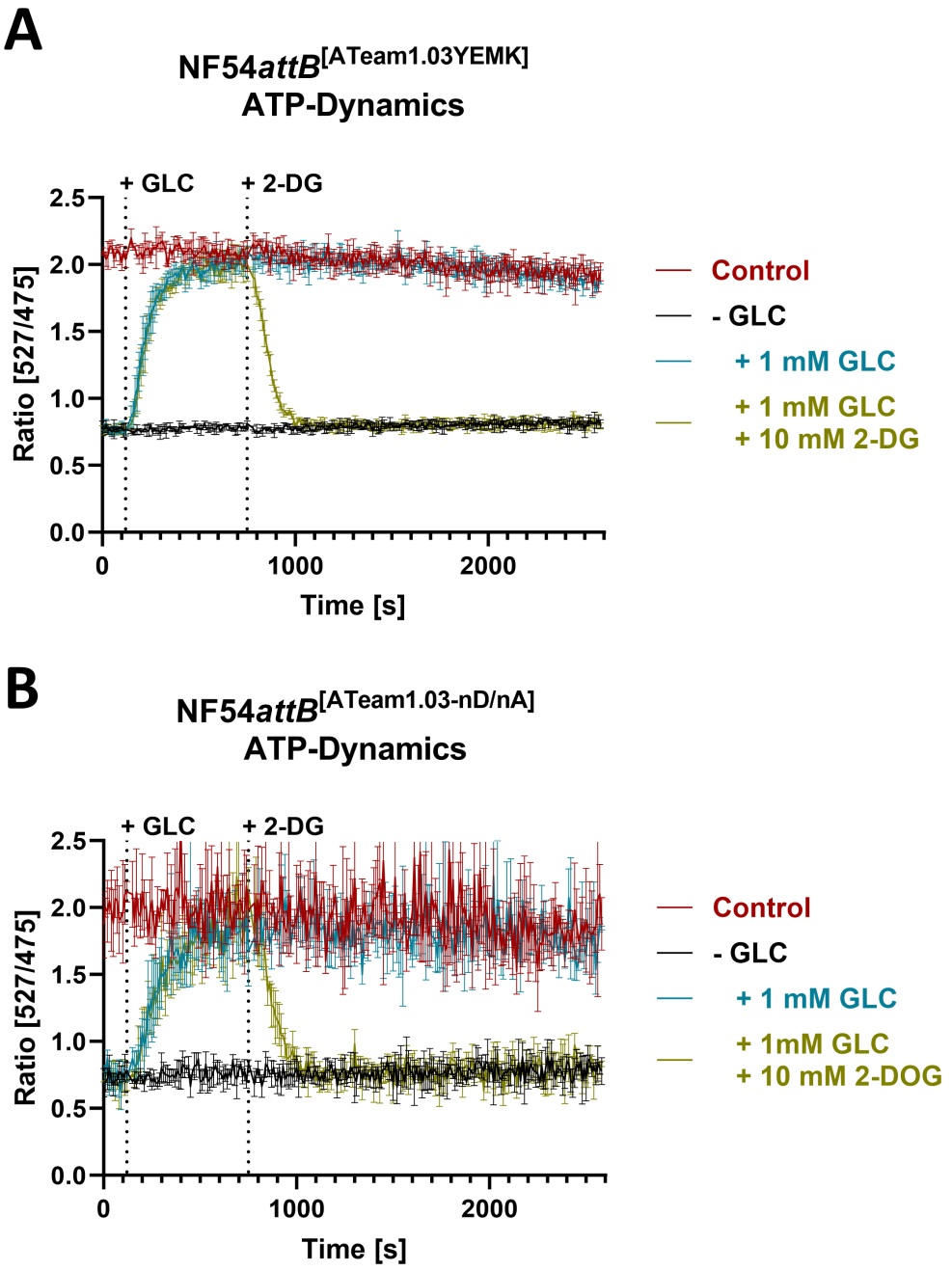

FIG 5 Monitoring of NF54*attB*$^{[ATeam1.03YEMK]}$ and NF54*attB*$^{[ATeam1.03-nD/nA]}$ emission ratio demonstrates dynamic *in cellulo* sensor response in plate reader format. Plate reader emission ratio of 2 million MACS-enriched NF54*attB*$^{[ATeam1.03YEMK]}$ (A) or NF54*attB*$^{[ATeam1.03-nD/nA]}$ (B) trophozoite-infected red blood cells after excitation at 435 nm and emission sensing at 527 nm for YFP and 475 nm for CFP. Parasites were washed in PBS for GLC depletion (−GLC) or GLC-rich Ringer's solution (control). Treatment with 1 mM GLC restored the ratio to control in Ringer's solution. Additional treatment with 10 mM 2-DG after 10 minutes reversed GLC-induced restoration to GLC-deprived baseline ratio. Mean emission ratios of n = 3 independent experiments are shown. Error bars indicate SD.

To demonstrate proof-of-principle of NF54*attB*$^{[sfpHluorin]}$ *in cellulo*, we applied nigericin pH calibration. Nigericin is an ionophore, allowing pH equilibration of the cytosol with the extracellular media (42). Spectral analysis of nigericin-permeabilized NF54*attB*$^{[sfpHluorin]}$-iRBCs reveals excitation spectra changing in response to pH in accordance with that of recombinant sfpHluorin, with pH-responding peaks around 390

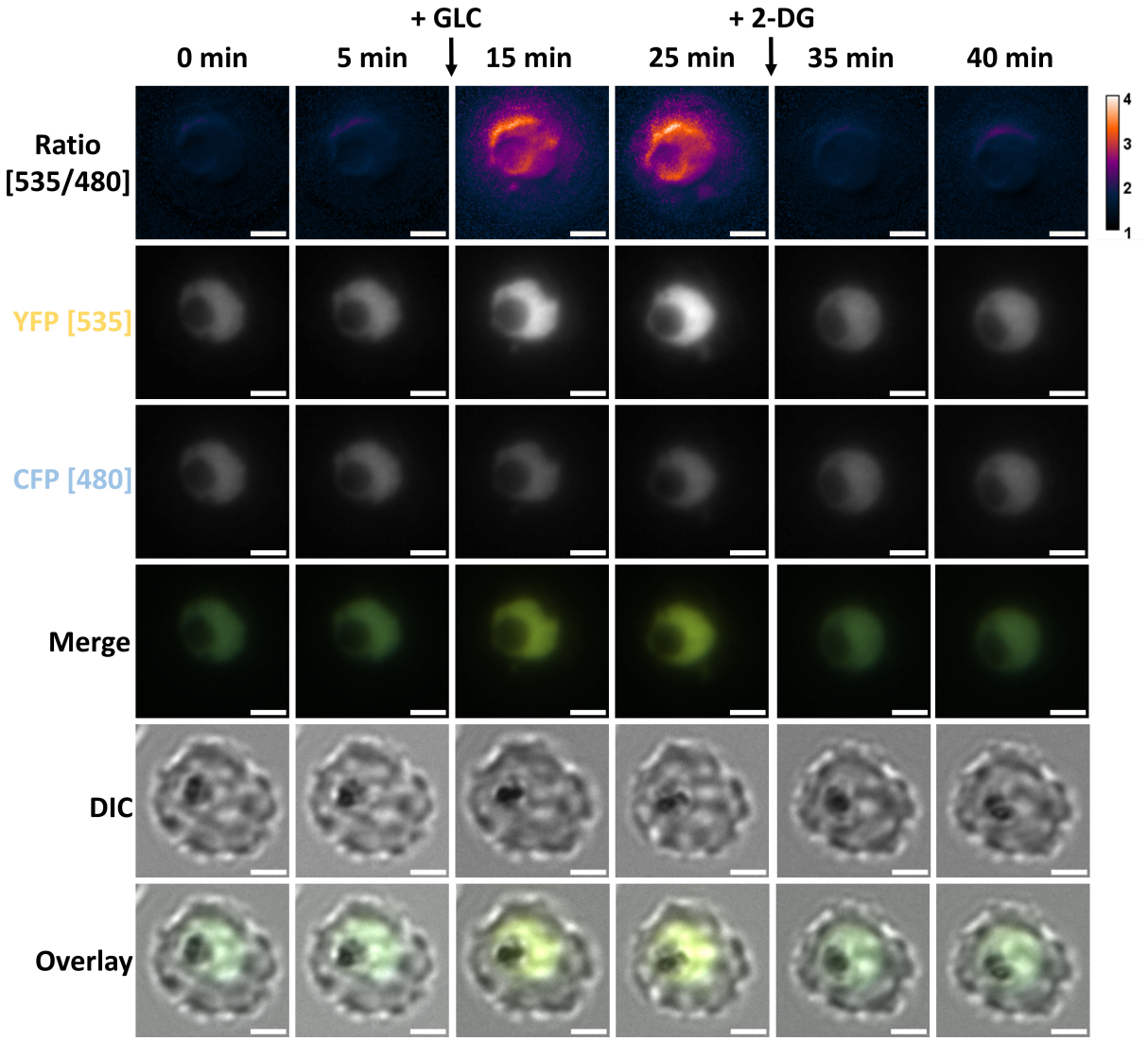

FIG 6 Fluorescence microscopy of NF54*attB*$^{[ATeam1.03YEMK]}$ allows monitoring of ATP-glucose dynamics on a single-cell level. Emission ratio of NF54*attB*$^{[ATeam1.03YEMK]}$ was measured using excitation at 430 nm and emission sensing at 535 and 480 nm for the YFP and CFP channel, respectively. GLC was added to a concentration of 2 mM after taking the 5-minute image. 2-DG was added to a concentration of 10 mM after taking the 25-minute image. Scale bar equals 2 µm.

and 482 nm (Fig. 9A). The excitation ratio of 390–482 nm plotted over pH level allows the fitting of a sigmoidal calibration curve for *in cellulo* pH measurements with a high dynamic range in the physiological relevant range of the parasitic cytosol between pH 6 and 8. Estimation of parasite resting pH in physiologic Ringer's solution determines a pH ± SD of 7.34 ± 0.07 (Fig. 9B), in large agreement with previous determinations, such as 7.29 ± 0.01 (11), 7.31 ± 0.02 (43), or 7.3 ± 0.05 (26).

To further demonstrate the suitability of NF54*attB*$^{[sfpHluorin]}$ for measuring dynamic pH changes, the cell line underwent GLC starvation, recovery, and subsequent 2-DG treatment as in previous experiments (Fig. 10). Starvation from GLC in PBS led to a lower excitation ratio compared to the control. Treatment with 1 mM GLC restored the excitation ratio to almost that of the control. Subsequent 2-DG treatment after 10 minutes rapidly reversed the GLC-induced recovery. The dynamic pH response of the parasite in response to GLC starvation and recovery shown here matches the findings of Saliba and Kirk (11), who showed that starvation from GLC causes a drop in parasite cytosolic pH and that recovery from acidification is heavily impaired under GLC starvation.

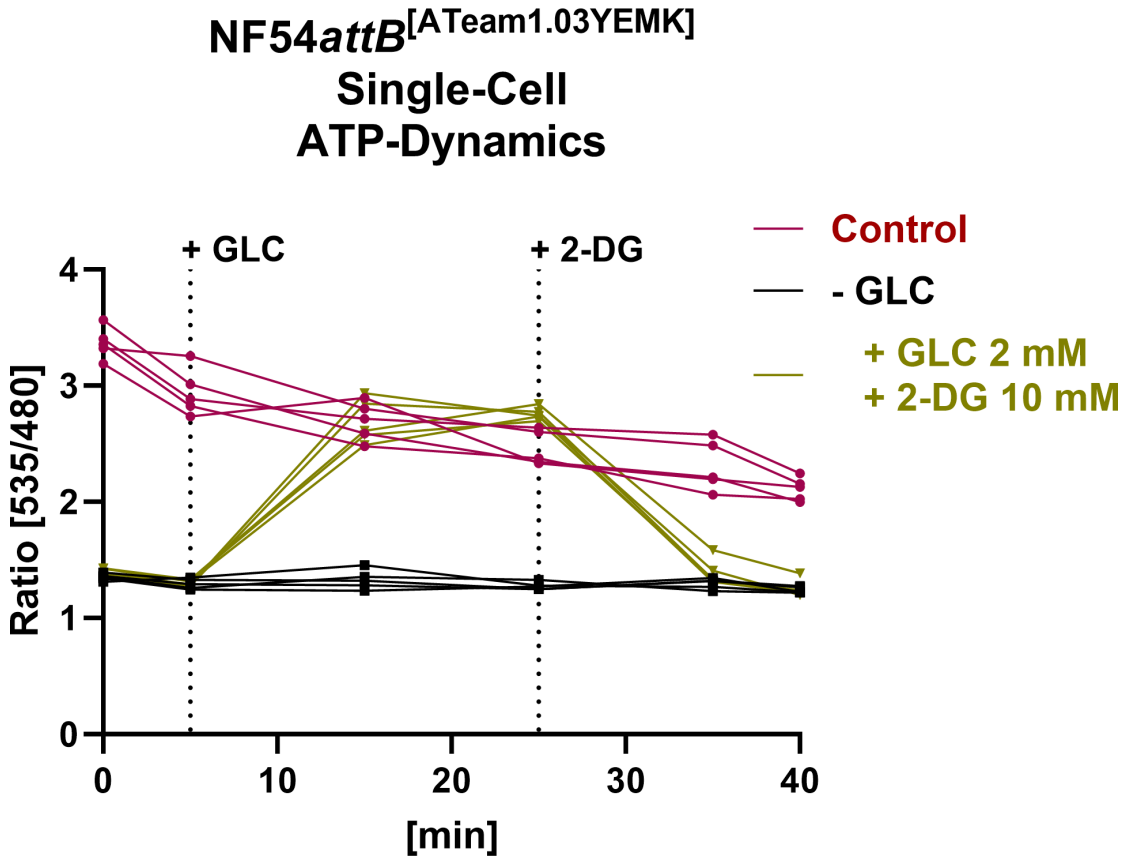

FIG 7 Fluorescence microscopy of NF54*attB*$^{[ATeam1.03YEMK]}$ demonstrates dynamic *in cellulo* sensor response on single-cell level. Emission ratio of NF54*attB*$^{[ATeam1.03YEMK]}$ was measured using excitation at 430 nm and emission sensing at 535 and 480 nm for the YFP and CFP channel, respectively. Background-corrected ratios are shown. Cells were washed and treated either with GLC-rich Ringer's solution (control) or GLC-depleted PBS (−GLC). Intervention group was treated with GLC and 2-DG after GLC starvation in PBS as indicated. GLC was added to a concentration of 2 mM after taking the 5-minute image. 2-DG was added to a concentration of 10 mM after taking the 25-minute image. Continuous measurements of $n = 5$ parasites/group are shown.

NF54*attB*$^{[sfpHluorin]}$ can be used to monitor pH changes at a single-cell level using live-cell imaging

To control pH changes that might occur during sample preparation and measurements in the single-cell microscopy setup for NF54*attB*$^{[ATeam1.03YEMK]}$, we further established NF54*attB*$^{[sfpHluorin]}$ measurements in a similar live-cell setup. We used the nigericin calibration method as described earlier. Accordingly, we observed a 385–475 nm excitation ratio increase with increasing pH and a high dynamic range between pH 6 and 8. Through interpolation of a standard curve, we could determine the resting pH (mean ± SD) of parasites in the microscopy setup in Ringer's solution to be 7.32 ± 0.12 (Fig. 11A),

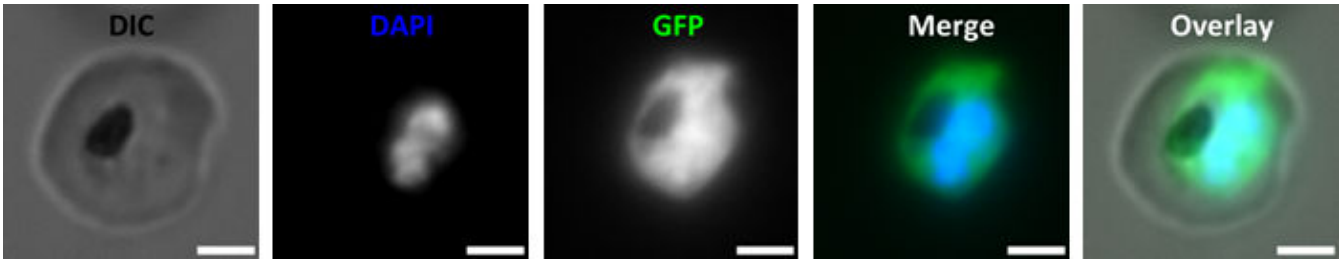

FIG 8 NF54*attB*$^{[sfpHluorin]}$ shows cytosolic GFP fluorescence. DIC, DAPI, GFP, merge, and overlay of a representative trophozoite stage parasite of NF54*attB*$^{[sfpHluorin]}$ are shown. DAPI: ex 353 nm/em 465 nm and GFP: ex 488 nm/em 509 nm. Error bar equals 2 µm.

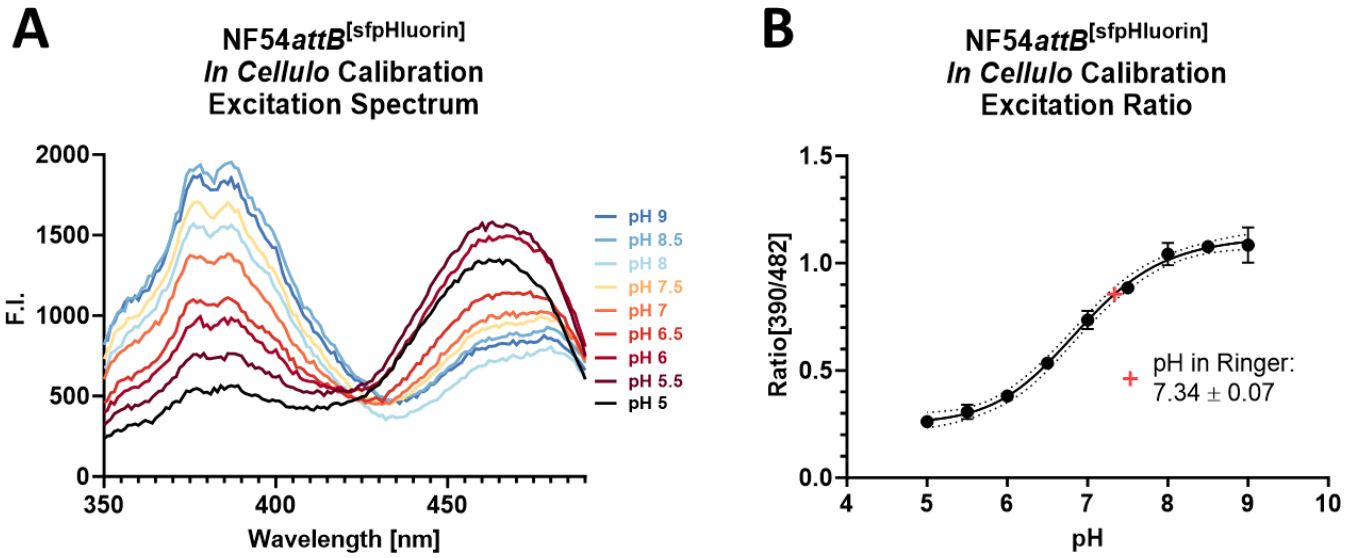

FIG 9 NF54*attB*[sfpHluorin] *in cellulo* calibration in plate reader format. A total of 1 million MACS-enriched trophozoite-iRBCs were incubated with 10 µM nigericin for 30 minutes at 37°C in 384-well plates in buffers with pH from 5 to 9. (A) Excitation spectra from 350 to 490 nm with emission sensing at 530 nm show pH-responsive peaks around 390 and 482 nm. Error bars were omitted for clarity. (B) Fitting a calibration curve using anexcitation ratio of 390–482 nm with emission sensing at 530 nm of nigericin-treated cells in pH buffers allows pH determination of untreated cells in Ringer's solution. Means of *n* = 3 independent experiments are shown. Error bars indicate SD.

in strong accordance with our measurements made using a plate reader (7.34 ± 0.07, Fig. 9B). Additionally, we demonstrate morphologic integrity and cytosolic fluorescence localization of single iRBCs after nigericin calibration (Fig. 11B).

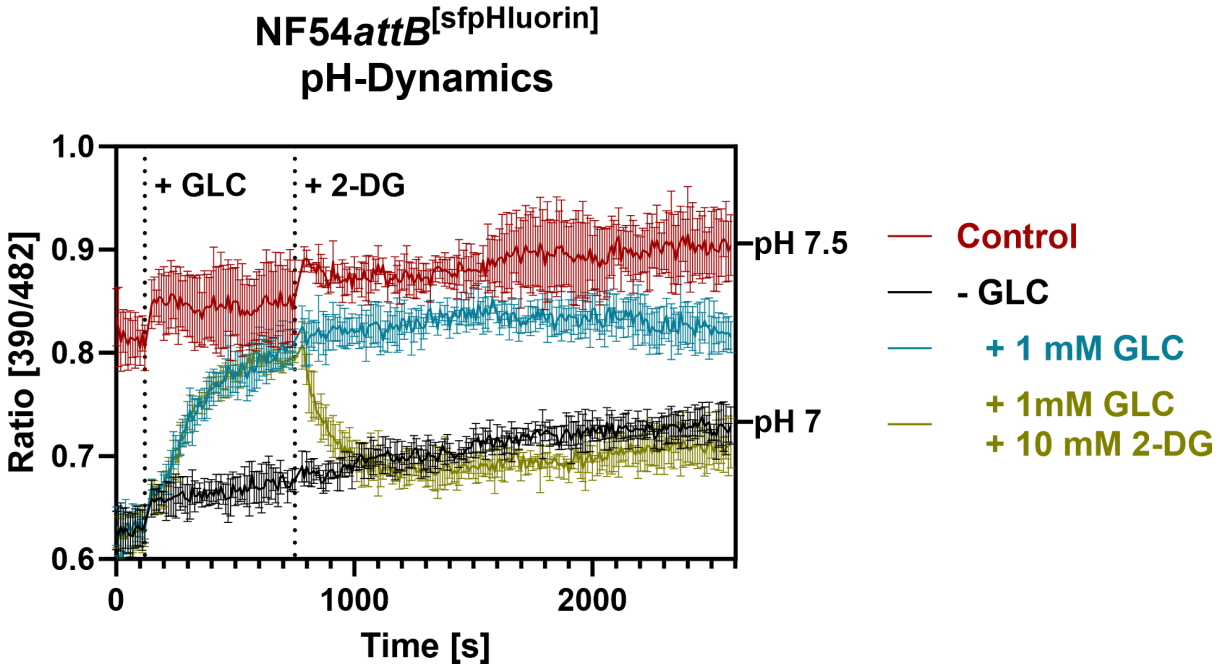

FIG 10 Monitoring of NF54*attB*[sfpHluorin] excitation ratio demonstrates dynamic *in cellulo* sensor response in plate reader format. Plate reader excitation ratio of 1 million MACS-enriched trophozoite infected-iRBCs after excitation at 390–482 nm with emission sensing at 530 nm. Parasites were washed in PBS for GLC depletion (–GLC) or GLC-rich Ringer's solution (control). Treatment with 1 mM GLC restored the ratio close to control in Ringer's solution. Additional treatment with 10 mM 2-DG after 10 minutes reversed GLC-induced restoration close to the GLC-starved baseline ratio. Mean emission ratios of *n* = 3 independent experiments are shown. Error bars indicate SD.

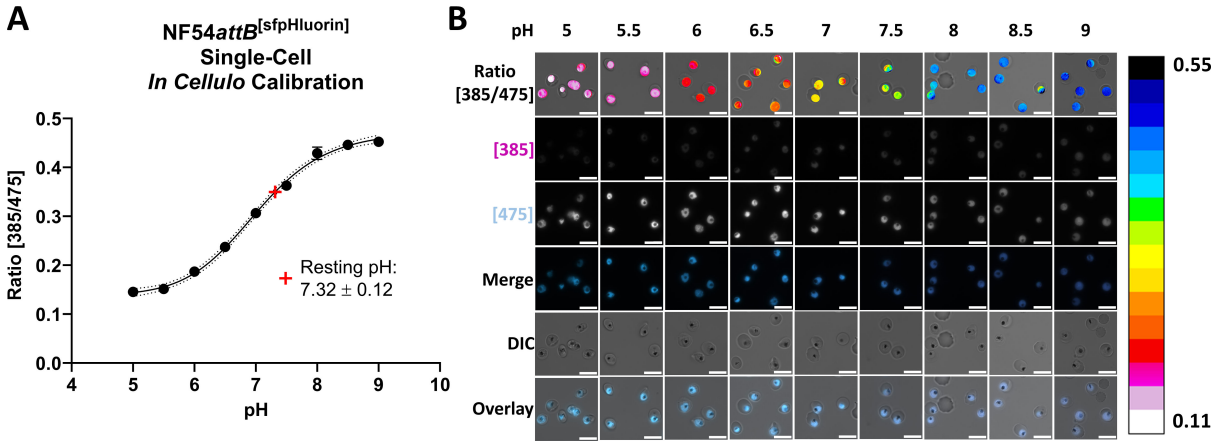

FIG 11 NF54*attB*[sfpHluorin] single-cell *in cellulo* calibration in epifluorescence microscope. MACS-enriched trophozoite-iRBCs incubated with 10 µM nigericin for 30 minutes at 37°C in buffers with pH from 5 to 9 show a pH-responsive increase in 385–475 nm excitation ratio at 525 nm. (A) Fitting a calibration curve allows resting pH determination of untreated cells in Ringer's solution. Measurements show the mean of $n = 3$ independent experiments with 100 cells ± SD. (B) Representative single-cell images of calibration experiments. Calibration bar color codes pixel by pixel 385–475 nm excitation ratio at 525 nm. Scale bar equals 10 µm.

NF54*attB*[ATeam1.03YEMK] shows distinct response patterns toward different drug classes

Having established NF54*attB*[ATeam1.03YEMK] and NF54*attB*[sfpHluorin] as ATP and pH measurement systems, we wished to use these new tools to study parasite responses to different established drug classes and promising drug candidates. We incubated the sensor cell lines with the compounds at approximately 100× and 10× of their EC_{50} concentrations (Table S1) to induce rapidly detectable effects over an incubation time of 4 and 6 h. Exceptions to this approach were DOXY and the model inhibitor of protein synthesis CHX. DOXY was used at the fixed concentrations of 5 and 1 µM to account for first- and second-cycle effects (33), and CHX was used at a single dose of 50 µg/mL to demonstrate the effect of a protein synthesis inhibitor.

To detect the ATeam response, we used the microscopic measurement approach with $n = 5$ independent experiments and calculated the mean of 100 parasites for each independent experiment with a concurrent vehicle-treated control group in each microscopic dish. We used this randomized block design to tease out parasite responses to different compound classes and used two-way ANOVA for statistical analysis. To cope with the multiple comparisons problem, we used the false discovery rate [FDR (44)], as this approach retains high power for the identification of drug response patterns. Discoveries with 5% FDR are reported with a single asterisk. Further statistical analysis can be found in Tables S2 to S7.

After 6-h incubation, we found distinct ATeam response toward different drug classes (Fig. 12). The 4-aminoquinoline compounds CQ, AQ, and PYRO caused a marked drop in ATeam emission ratio at 100× of their EC_{50} and, except for CQ, additionally at 10× EC_{50}. In contrast, the arylamino alcohols MQ and LUM caused an increase in emission ratio, both at 100× and 10× EC_{50} concentration. The structurally related QN did not show any effect on the ATeam emission ratio. DHA caused a mixed effect on the emission ratio. We could detect a decrease in emission ratio for 100× EC_{50}, while we could detect an increase for 10× EC_{50}. The redox-active compounds MB (31) and PD (32) caused an emission ratio decrease at 100× EC_{50} but not at 10× EC_{50}. The apicoplast-affecting drug (33), DOXY, the inhibitor of the mitochondrial ETC (34), ATQ, as well as the PfGluPho inhibitor, SBI-0797750 (36), did not show any effects under the given conditions. Additionally, we included the effects of GLC starvation (–GLC) and the inhibitor of protein biosynthesis CHX in our study. As expected, GLC starvation just before measurement caused a drastic drop in the emission ratio. In contrast, CHX caused an increase in ratio. Overall, we found

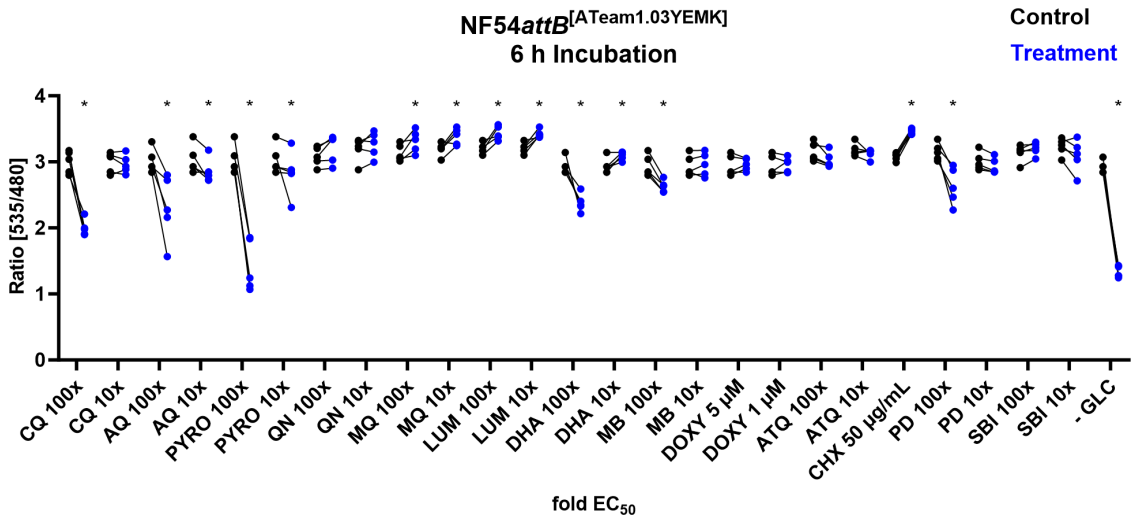

FIG 12 NF54*attB*[ATeam1.03YEMK] shows distinct ratio changes in response toward different drug classes after 6-h incubation. Fluorescence microscopic measurement of MACS-enriched trophozoite-iRBCs. Each measurement corresponds to the 535–480 nm emission ratio after excitation at 430 nm. Means of 100 single-cell analyses of compound intervention (treatment) and concurrent vehicle control (control) with n = 5 independent experiments are shown. Treatment groups included CQ, AQ, PYRO, QN, MQ, LUM, DHA, MB, DOXY, ATQ, CHX, PD, SBI, and –GLC. Cells were starved from GLC through washing in PBS just before measurement. If not indicated otherwise, compounds were applied with 100× and 10× EC_{50} concentrations. Asterisks indicate discovery with FDR = 5%.

similar results for all tested compounds already after 4-h incubation. However, the results were less pronounced and not detected as discovery according to the FDR for 10× EC_{50} of AQ, PYRO, MQ, DHA, SBI, and 100× and 10× EC_{50} of LUM (Fig. S7).

Pooling the single-cell data of the n = 5 independent experiments gives further insights into the compound-induced ATeam response. Though not suitable for statistical analysis, as the pooling and lack of concurrent control would make statistical analysis questionable, we nevertheless observed distinct ATeam response patterns toward different drug classes on a single-cell level (Fig. 13). The 4-aminoquinolines, CQ, AQ, and PYRO, caused a distinctive bimodal ratio distribution at 100× EC_{50} concentration.

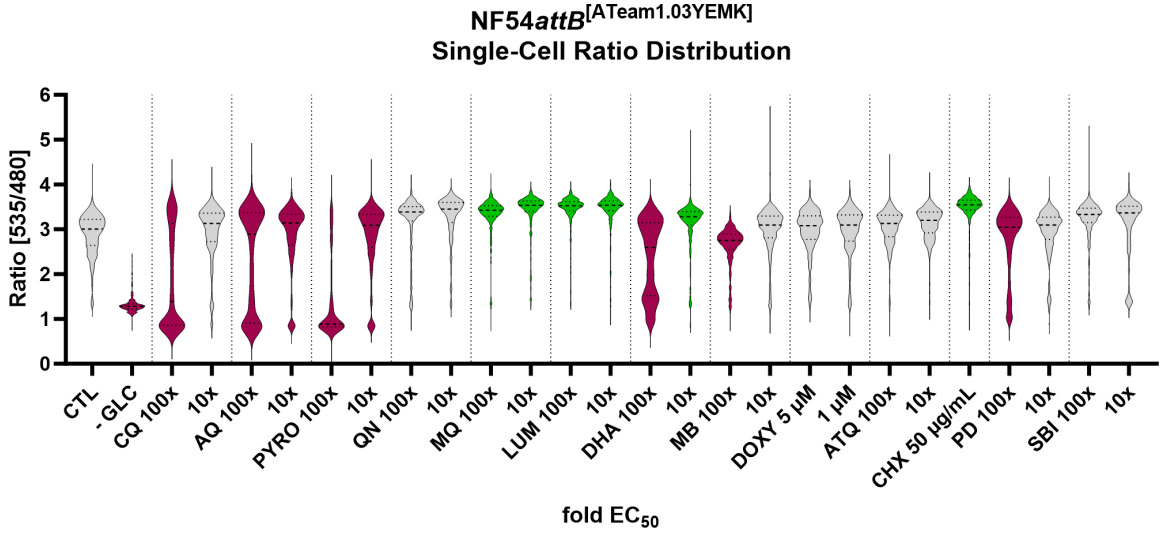

FIG 13 NF54*attB*[ATeam1.03YEMK] shows distinct single-cell emission ratio distribution in response toward different drug classes. Fluorescence microscopic measurement of MACS-enriched trophozoite-iRBCs. Each measurement corresponds to the 535–480 nm emission ratio after excitation at 430 nm. Pool of n = 5 independent experiments with each 100 single-cell analyses is shown. Treatment groups included CQ, AQ, PYRO, QN, MQ, LUM, DHA, MB, DOXY, ATQ, CHX, PD, SBI, and –GLC. Cells were starved from GLC through washing in PBS just before measurement. If not indicated otherwise, compounds were applied with 100× and 10× EC_{50} concentrations. Colors indicate up- (green) or down (magenta)-shifted discoveries according to the statistical analysis described in Fig. 12.

A notable proportion of their ratio distributions are located below 1, while even cells starved of GLC did not show such low ratios. In contrast, the distributions of the arylamino alcohols, QN, MQ, LUM, in addition to CHX, and SBI are more compressed and higher in location compared to a representative control group. DHA caused mixed effects in the ratio distribution. It showed a compressed and higher-located distribution at 10× EC_{50}, while it shows a tendency toward a bimodal and downwardly skewed distribution at 100× EC_{50}. MB showed a tendency for compression and lower ratios at 100× EC_{50}. PD showed a tendency toward a lower and bimodal distribution. DOXY and ATQ did not show any apparent change in their distributions compared to the representative control.

pH changes induced by drug interventions are generally small and unlikely to affect *in cellulo* ATeam measurements

As shown in Fig. 2B, ATeam1.03YEMK showed a stable ratio response within the pH range of 6–8. In order to investigate if pH changes might influence ATeam measurements upon treatment, all compound treatments shown in Fig. 12 were repeated with NF54*attB*$^{[sfpHluorin]}$. We used the microscopic measurement approach with n = 3 independent experiments and calculated the mean of 100 parasites for each independent experiment with a concurrent vehicle-treated control group in each microscopic dish. The pH levels were interpolated from excitation ratio measurements using the *in cellulo* calibration shown in Fig. 11. After 6-h incubation, we found distinct sfpHluorin responses toward different drug classes (Fig. 14). The 4-aminoquinoline compounds, CQ, AQ, PYRO, as well as PD at their 100× EC_{50} concentration caused a marked drop below pH 7. Among all compounds tested, only DOXY at a concentration of 5 µM caused an increased pH; however, this is still in the range classed as reliable for ATeam measurements. All other compounds caused no or only marginal sfpHluorin excitation ratio changes through the concentrations tested. In addition to that, GLC starvation just before measurement caused the strongest excitation ratio drop, indicating a mean pH ± SD of 6.71 ± 0.02. With the exception of CQ and LUM 10× EC_{50} concentrations, we could detect the same significant trends after only 4-h incubation time (Fig. S8). Mean pH with a 95% confidence interval for all treatments after 4- and 6-h incubation is listed in Tables S9 and S8, respectively.

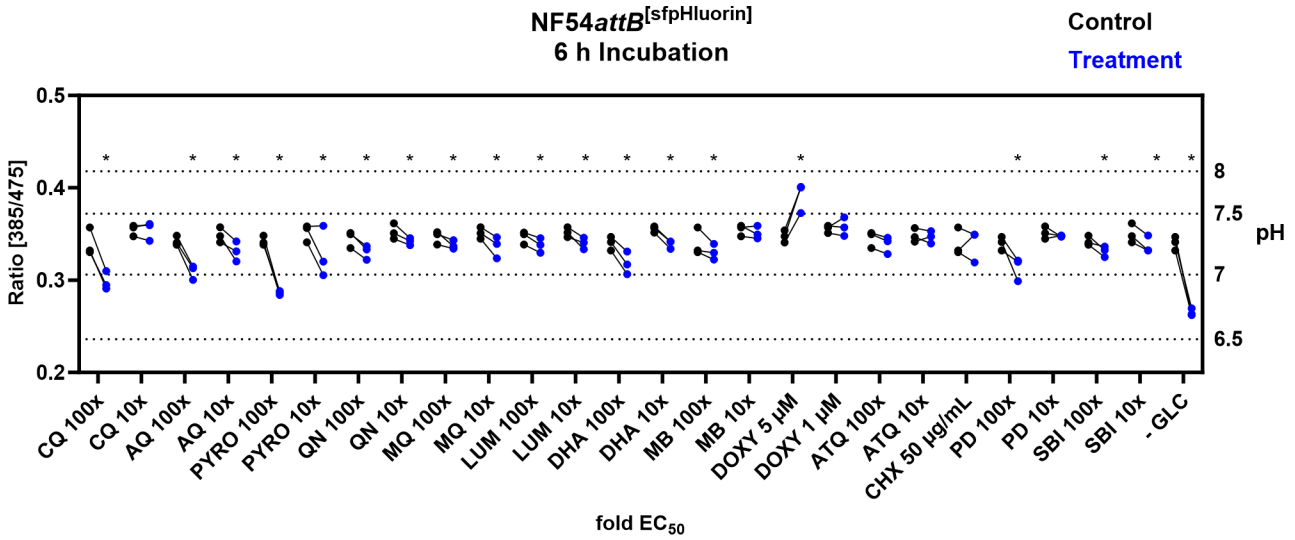

FIG 14 NF54*attB*$^{[sfpHluorin]}$ shows predominantly marginal ratio changes in response toward different drug classes after 6-h incubation time. Fluorescence microscopic measurement of MACS-enriched trophozoite-iRBCs. Each measurement corresponds to the 385–475 nm excitation ratio at 525 nm emission. Means of 100 single-cell analyses of compound intervention (treatment) and concurrent vehicle control (control) with n = 3 independent experiments are shown. Treatment groups included CQ, AQ, PYRO, QN, MQ, LUM, DHA, MB, DOXY, ATQ, CHX, PD, SBI, and −GLC. Cells were starved from GLC through washing in PBS just before measurement. If not indicated otherwise, compounds were applied with 100× and 10× EC_{50} concentrations. Asterisks indicate discovery with FDR = 5%.

As previously demonstrated, ATeam1.03YEMK protein shows a stable ratio response between pH 6 and 8, indicating the pH stability of the fluorophores in that range. Although all measured average values lie within this range, plotting the pooled ratio distribution of n = 3 independent experiments with each containing 100 single-cell analyses to the interpolated pH reveals that some proportion of cells exhibit drastic changes in pH levels, which is masked when analyzing only mean ratios (Fig. S9). For example, at the higher DOXY concentration (5 µM), a number of single-cell measurements lie outside of the calibration range.

Various compounds cause reduced parasite size

The single-cell image analysis for the NF54*attB*$^{[ATeam1.03YEMK]}$ and NF54*attB*$^{[sfpHluorin]}$ drug response measurements included the definition of region of interest (ROI) that corresponds to the area of the parasites. To gain a deeper understanding of the parasite's response to the compound interventions, we analyzed the mean sizes of these ROIs as a proxy for parasite size and compared them to the mean of the control group (Fig. 15). We found that the 4-aminoquinoline compounds, CQ, AQ, and PYRO, caused a decreased parasite size at their 100× EC_{50} concentrations. Additionally, PYRO caused decreased size already at 10× EC_{50}. The arylamino alcohols, QN, MQ, and LUM, in addition to DHA, and SBI caused a decreased cytosol size at both 100× and 10× EC_{50}. In addition, 100× EC_{50} of PD and 50 µg/mL CHX caused reduced size. MB, DOXY, and ATQ did not show an effect on parasite size with any of the concentrations tested. Most of the effects were already detected after 4-h incubation. Only AQ 10×, LUM 100×, LUM 10×, and SBI 100× EC_{50} did not show a detectable effect after this shorter incubation time (Fig. S10).

Parallel analysis of drug responses reveals common patterns

The characteristics we analyzed are not truly independent, as severe metabolic alterations that affect ATP or pH levels are likely to also cause growth effects and vice versa. Accordingly, examination of cytosol size and sensor response patterns in the synopsis shows that most of the compounds tested caused either an effect on none or all of the analyzed characteristics after 6-h incubation time (Fig. 16). CQ 10×, MB 10×, ATQ 100× and 10×, and PD 10× EC_{50}, as well as DOXY 1 µM did not show any effects classified

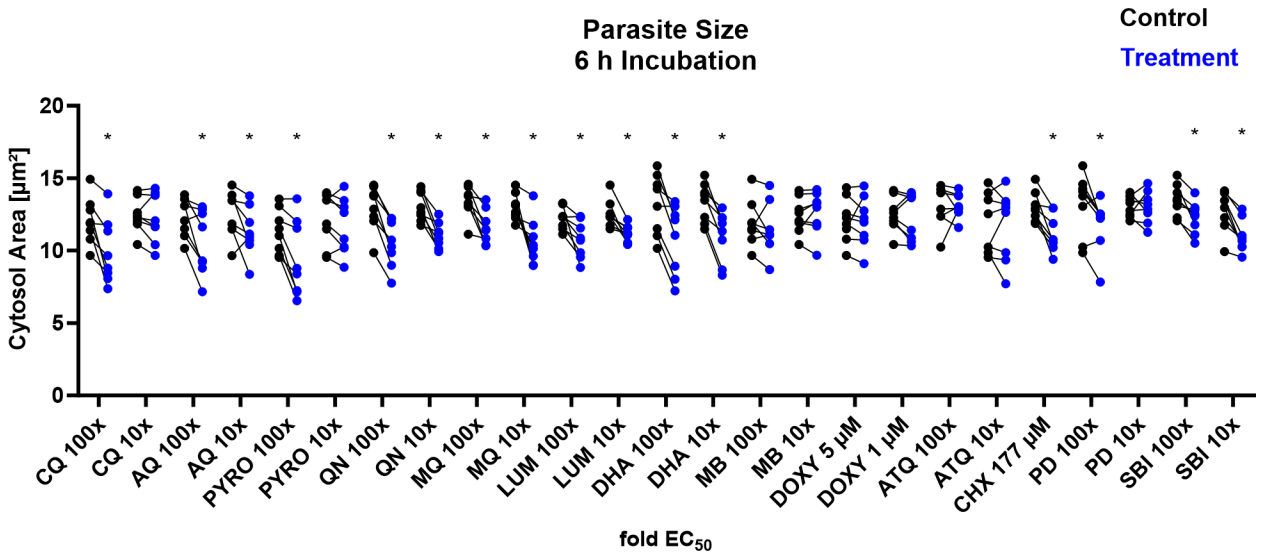

FIG 15 NF54*attB*$^{[ATeam1.03YEMK]}$ and NF54*attB*$^{[sfpHluorin]}$ show decreased parasite size in response toward different drug classes after 6-h incubation. The mean cytosol size of 100 MACS-enriched trophozoite-iRBCs derived from automated ROI definition from fluorescence microscopic measurements of NF54*attB*$^{[ATeam1.03YEMK]}$ (n = 5) and NF54*attB*$^{[sfpHluorin]}$ (n = 3) is combined. Analyses of compound intervention (treatment) and concurrent vehicle control (control) with n = 8 independent experiments are shown. Treatment groups included CQ, AQ, PYRO, QN, MQ, LUM, DHA, MB, DOXY, ATQ, CHX, PD, and SBI. If not indicated otherwise, compounds were applied with 100× and 10× EC_{50} concentrations. Asterisks indicate discovery with FDR = 5%.

6 h Incubation	Discovery? (FDR = 5 %)		
	Size	ATeam	sfpHluorin
CQ 100x	Yes	Yes	Yes
CQ 10x	No	No	No
AQ 100x	Yes	Yes	Yes
AQ 10x	Yes	Yes	Yes
PYR 100x	Yes	Yes	Yes
PYR 10x	No	Yes	Yes
QN 100x	Yes	No	Yes
QN 10x	Yes	No	Yes
MQ 100x	Yes	Yes	Yes
MQ 10x	Yes	Yes	Yes
LUM 100x	Yes	Yes	Yes
LUM 10x	Yes	Yes	Yes
DHA 100x	Yes	Yes	Yes
DHA 10x	Yes	Yes	Yes
MB 100x	No	Yes	Yes
MB 10x	No	No	No
DOXY 5 µM	No	No	Yes
DOXY 1 µM	No	No	No
ATQ 100x	No	No	No
ATQ 10x	No	No	No
CHX 50 µg/mL	Yes	Yes	No
PD 100x	Yes	Yes	Yes
PD 10x	No	No	No
SBI 100x	Yes	No	Yes
SBI 10x	Yes	No	Yes
PBS	N/A	Yes	Yes

4 h Incubation	Discovery? (FDR = 5 %)		
	Size	ATeam	sfpHluorin
CQ 100x	Yes	Yes	Yes
CQ 10x	No	No	Yes
AQ 100x	Yes	Yes	Yes
AQ 10x	No	No	Yes
PYR 100x	Yes	Yes	Yes
PYR 10x	No	No	Yes
QN 100x	Yes	No	Yes
QN 10x	Yes	No	Yes
MQ 100x	Yes	Yes	Yes
MQ 10x	Yes	No	Yes
LUM 100x	No	No	Yes
LUM 10x	No	No	No
DHA 100x	Yes	Yes	Yes
DHA 10x	Yes	No	Yes
MB 100x	No	Yes	Yes
MB 10x	No	No	Yes
DOXY 5 µM	No	No	Yes
DOXY 1 µM	No	No	No
ATQ 100x	No	No	No
ATQ 10x	No	No	No
CHX 50 µg/mL	Yes	Yes	No
PD 100x	Yes	Yes	Yes
PD 10x	No	No	No
SBI 100x	No	No	Yes
SBI 10x	Yes	Yes	Yes
PBS	N/A	Yes	Yes

FIG 16 Heatmap of sensor and parasite size drug-response patterns shows coinciding effects of compound treatments. The table shows a synopsis of the effects of different compound treatments on size, ATeam emission ratio, and sfpHluorin excitation ratio of NF54*attB*$^{[ATeam1.03YEMK]}$ and NF54*attB*$^{[sfpHluorin]}$ with concentrations in multiples of EC_{50} or otherwise indicated concentrations after 4- or 6-h treatment time. Effects are classified as discovery (Yes), or no discovery (No) with an FDR of 5%. Color indicates if treatment caused an increase (green) or decrease (magenta) in group means, in case a treatment was classified as discovery in analyses described in Fig. 12, 14, and 15; Fig. S9 to S11. Treatment groups included CQ, AQ, PYRO, QN, MQ, LUM, DHA, MB, DOXY, ATQ, CHX, PD, and SBI.

as discovery. CQ 100×, AQ 100× and 10×, PYRO 100×, MQ 100× and 10×, LUM 100× and 10×, DHA 100× and 10×, and PD 100× caused effects on all characteristics. PYRO 10× and MB 10× caused effects only on ATeam ratio and pH, while QN 100× and 10× and SBI 100× and 10× only caused effects on size and pH. CHX only caused effects on cytosol size and ATeam ratio, while DOXY 5 µM caused only an increased pH. Measurements after 4-h incubation showed similar trends, though for some characteristics less pronounced and not detected as discovery.

Mefloquine but not amodiaquine prevents chloroquine-mediated ATeam and sfpHluorin ratio depletion

We could detect a characteristic drop in ATeam ratio and pH (Fig. 16) caused by the 4-aminoquinolines, CQ, AQ, and PYRO, after incubation with 100× EC_{50} for 6 h. CQ, AQ, and PYRO are thought to kill the parasites through the inhibition of hemozoin formation with the accumulation of free heme (45). The detected effects on the sensor ratios might

therefore be heme mediated. To investigate further the specificity of these effects, we analyzed the interaction of CQ, as a representative of the 4-aminoquinoline group, with MQ or AQ. MQ is reported to inhibit CQ-mediated heme accumulation (46). Therefore, we predicted a preventative effect of MQ on the CQ-mediated ATeam ratio and pH drop. AQ, which belongs to the 4-aminoquinoline group, as does CQ, was used as a control in this setting. We found that, indeed, MQ but not AQ prevented CQ-mediated ATeam1.03YEMK (Fig. 17A) and sfpHluorin (Fig. 17B) ratio depletion at 100× and 10× of their EC_{50} concentrations. In contrast, AQ did not show such a preventative effect.

Mefloquine but not amodiaquine prevents chloroquine mediated ATeam sensor degradation

As shown in Fig. 13, we see a distinct emission ratio response of NF54*attB*$^{[ATeam1.03YEMK]}$ toward 4-aminoquinoline compounds. The single-cell ratio distributions resemble a bimodal distribution with ratio allocations way below the ratio allocations of parasites starved from GLC. As the ATeam sensors are based on intramolecular FRET, such low ratios are only expected if the sensors are degraded, or, if the cytosolic pH is heavily affected. We found only moderate effects on cytosolic pH (Fig. 14). Therefore, we were interested in whether CQ treatment led to ATeam sensor degradation and whether MQ could prevent such degradation. Thus, we carried out western blot analysis of cells treated with CQ, CQ and MQ, CQ and AQ, or vehicle control (Fig. 18). In mock-treated NF54*attB*$^{[ATeam1.03YEMK]}$ parasites, we could detect a clear band around 70 kDa, at the predicted size of ATeam1.03YEMK protein (68.0 kDa). Treatment with 100× EC_{50} CQ for 6 h caused a considerably lower band intensity at this size, but a concomitant detection of a band at around 25 kDa. This band is at the molecular weight of the protease-resistant core of GFP variants, thus likely indicating proteolytic cleavage of the ATeam sensor. Parasites treated with both CQ and MQ did not, or only to a marginal extent, show such a band; however, simultaneous treatment with both CQ and the 4-aminoquinoline AQ still resulted in the degradation product.

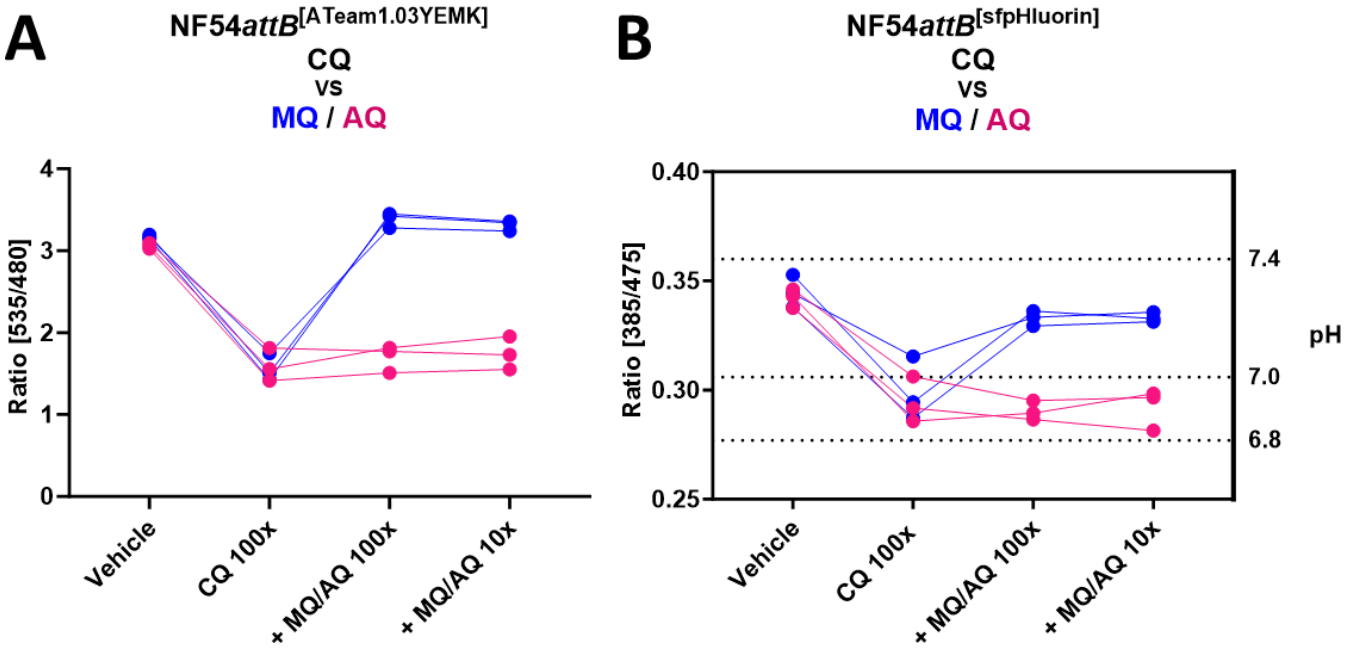

FIG 17 MQ but not AQ prevents CQ-mediated ATeam and sfpHluorin ratio depletion. Fluorescence microscopic measurement of MACS-enriched NF54*attB*$^{[ATeam1.03YEMK]}$ (A) and NF54*attB*$^{[sfpHluorin]}$ (B) trophozoite-iRBCs. Each measurement corresponds to the 535–480 nm emission ratio after excitation at 430 nm, or 385–475 nm excitation ratio with emission sensing at 525 nm, as indicated. Means of 100 single-cell analyses after incubation with multiples of EC_{50} with n = 3 independent experiments are shown. NF54*attB*$^{[ATeam1.03YEMK]}$ and NF54*attB*$^{[sfpHluorin]}$ were treated either with vehicle control, 100× CQ, 100× CQ and 100× MQ, 100× CQ and 10× MQ (blue) or with vehicle, 100× CQ, 100× CQ and 100× AG, and 100× CQ and 10× AQ (magenta) of their EC_{50} concentration for 6 h.

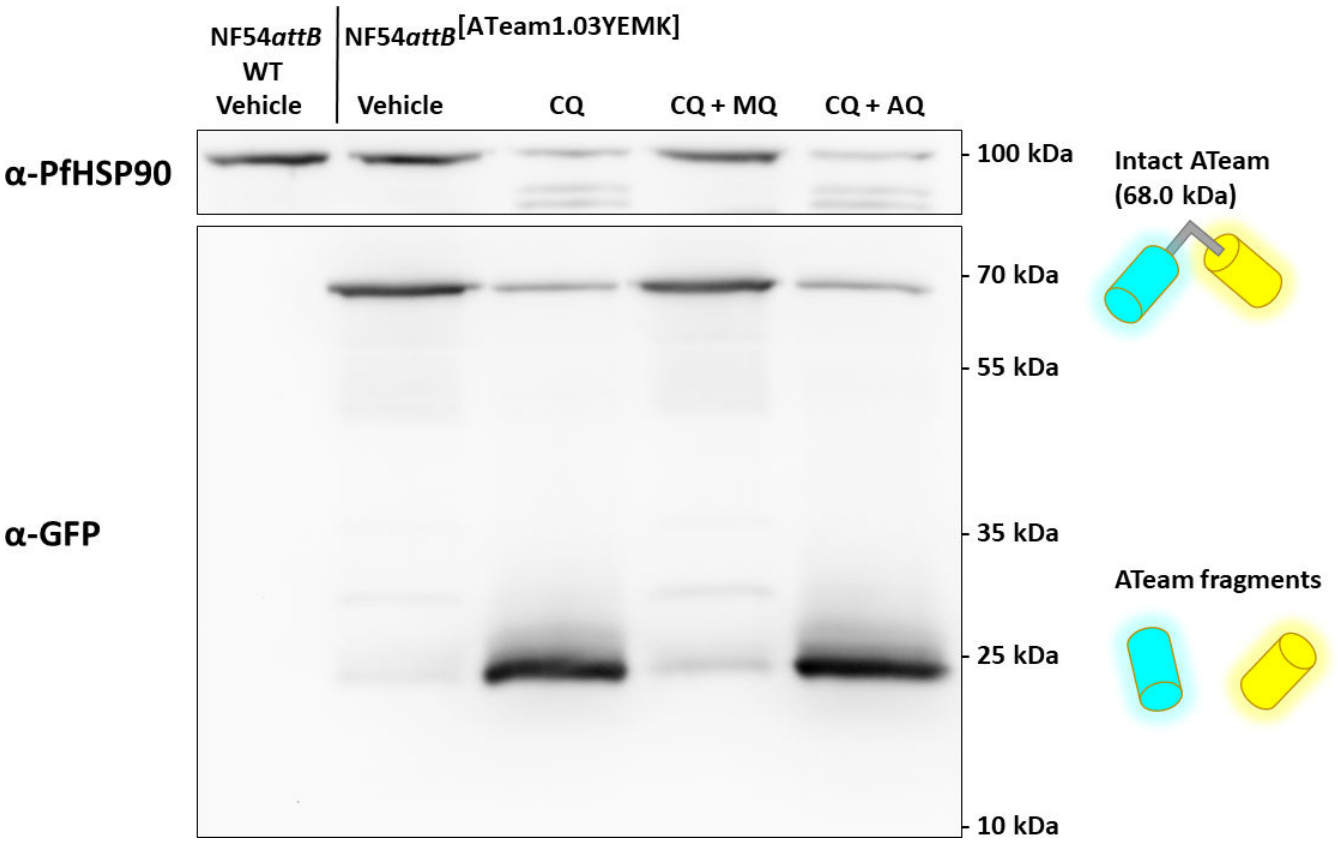

FIG 18 α-GFP western blot of NF54*attB*$^{[ATeam1.03YEMK]}$ demonstrates CQ-induced sensor degradation and the protective effect of MQ. α-GFP western blot of 5 million NF54*attB* (WT) or NF54*attB*$^{[ATeam1.03YEMK]}$ trophozoite-iRBCs treated with CQ, CQ and MQ, CQ and AQ, or vehicle control at 100× EC_{50} for 6 h each.

We detected PfHSP90 as a loading control. We could detect a similar PfHSP90 signal around the 100-kDa marker band in the CQ + MQ group and in the untreated control group. In the CQ and CQ + AQ-treated group, we could only detect a faint signal at this molecular mass and two additional bands between 70 and 100 kDa, indicating HSP90 degradation products. As housekeeping genes, such as HSP90, can be up- or downregulated as a stress response or degraded under proteolytic stress, we demonstrate via Ponceau S total protein staining that the western blot signal distribution is unlikely to be explained only by unequal sample loading (Fig. S11).

DISCUSSION

In this report, we largely verified previous *in vitro* data for ATeam proteins (22, 24, 37), with small variations likely being due to slightly different experimental conditions, such as temperature or buffer composition. Overall, all sensors exhibited spectral properties as expected and were assessed by us as functional. We further excluded direct compound-sensor interactions as a cause of ratio changes, under the conditions studied. Our analyses did, however, identify a pH dependence for ATeam1.03-nD/nA under specific conditions, which must be considered when applying such sensors, especially under conditions, such as drug treatments, which may cause pH shifts. Following this, we established ATeam1.03YEMK and ATeam1.03-nD/nA measurements in *P. falciparum*. We could successfully demonstrate dynamic changes in ATP levels, both in a plate reader, as well as in live single-cell fluorescence microscopy. Both sensor cell lines exhibit spectral properties as expected and changed their emission ratio in response to GLC starvation, recovery, and subsequent 2-DG treatment in accordance with the expected corresponding ATP levels. We therefore assess our measurement systems as validated. NF54*attB*$^{[ATeam1.03\text{-}nD/nA]}$ showed a marked lower fluorescence intensity in the parasites and

an unstable pH response of the recombinant protein and was thus excluded from further analyses.

For our ATP-drug-response analyses, we are interested in qualitative changes in ATP level, not absolute quantitative measurements of [ATP]. Instead, we present the ATeam system as a reliable semi-quantitative tool for measuring ATP responses in *P. falciparum*. Based on our *in vitro* and *in cellulo* characterization, we are certain about NF54*attB*$^{[ATeam1.03YEMK]}$'s capabilities to measure exact cytosolic $MgATP^{2-}$ level, even though it is difficult or impossible to extrapolate absolute molar [ATP] from our data. While it might be tempting to use *in vitro* characterization of the recombinant sensor protein for calibration to deduce to quantitative *in cellulo* [ATP], we think that the deduction from ratios of recombinant sensor protein to intracellular [ATP] is neither viable nor, in our case, necessary. We cannot exclude that the exact intracellular milieu has an effect on quantitative ATP measurements using our sensor, and our calibration experiments, while attempting to mirror the most important conditions, cannot account for many other (unknown) factors. To avoid this issue, various *in situ* calibration protocols have been attempted in different cell systems; however, these revealed discrepancies between the values obtained using different methods, making it impossible to define a "gold standard" (47, 48). We wish to note that both parasites and the host cell generate ATP from GLC, and ATP starvation is likely to also block ATP production in the host cell. The exchange (and direction) of ATP between parasite and host cell is a complex and poorly understood topic (7, 49, 50). We cannot formally exclude an extra-parasite source for some cytosolic ATP but believe that this is not relevant to our current measurements.

As we observed the pH dependence of the sensor under certain conditions, we established the genetically encoded pH sensor sfpHlourin to monitor pH changes under the experimental conditions we applied. Our determinations for the resting pH ± SD of 7.34 ± 0.07 and 7.32 ± 0.12 in our plate reader and live single-cell measurement setup, respectively, are in large agreement with previously reported methods (11, 26, 43) with larger discrepancies likely due to the differences in experimental conditions (26, 27, 51, 52). We, therefore, assess our sfpHluorin measurement system and our interpolated pH determinations as validated.

Having established our experimental system, we then analyzed parasite responses to compounds from varying chemical classes. For our experimental setup, we used 100× and 10× EC_{50} compound concentrations to induce rapid effects in a relatively short time frame, which have been determined in previous studies to largely reflect at least the peak concentration of most of the drugs *in vivo* (53–61). For setting up our drug-response assays, we used starvation from GLC as a control for total ATP depletion. Thus, ratios observed below this level would be indicative of other non-specific effects such as sensor degradation. We observed the highest ratios when treating parasites with CHX. CHX is an inhibitor of protein synthesis, and as protein synthesis is the major ATP-consuming process in rapidly proliferating microorganisms (62), its inhibition has been observed to lead to increases in cytosolic ATP concentration in other systems (63). Our data suggest that, following CHX treatment, ATP concentrations approach sensor saturation, indicated by the compression of ratio distribution values.

Taken individually, each parameter we measured does not allow strong conclusions to be drawn about differing modes of action. However, taken as a whole and encompassing measurement of ATP, pH, and cell size, our results reveal distinct response patterns to 4-aminoquinolines, arylamino alcohols, artemisinins, a selection of redox cyclers, as well as of DOXY, ATQ, and CHX.

Like the 4-aminoquinolines presented in this study, the arylamino alcohols QN, MQ, and LUM all inhibit the formation of hemozoin *in cellulo* and increase free heme to a limited extent (64). However, they also show distinct differences in their cellular effects and resistance mechanisms, as reviewed before (65). As resistances against CQ and MQ are inversely correlated, it is now consensus that the mode of action of arylamino alcohols, such as MQ, is distinct to that of 4-aminoquinolines and that their target most likely lies in the parasite cytosol rather than in the food vacuole (66). In line with this,

MQ counteracts many effects of CQ such as Hb accumulation (46), and QN inhibits CQ-induced heme accumulation (67). Aside from this, and even after decades of research, the exact mechanism of action of MQ and QN is still uncertain and hotly debated (21, 68, 69), and for LUM, the situation is even less clear. QN, MQ, and LUM all seem to share a downstream inhibitory effect at 10× EC_{50} on protein synthesis (21) although the exact point at which they exert their influence is unknown. Our study found increasing ATeam ratios after MQ and LUM treatment with 100× and 10× EC_{50}. We found a similar trend for QN regarding its single-cell ratio distribution. These findings support Khan et al. (13), who detected increased ATP levels in response to 5× EC_{50} MQ. Additionally, for all three drugs, we measured a reduced parasite size that could be indicative of translation inhibition. As already described for CHX, inhibition of protein synthesis seems to elevate the ATP level in *P. falciparum*. Thus, the increased ATP level following MQ or LUM treatment might be the consequence of such translational arrest.

For artemisinin (ART)-based drugs, their modes of action are thought to be even more pleiotropic in nature than for the other compound classes. Recently, Ward et al. (66) reviewed artemisinin's mode of action. Upon activation via heme iron, ART is activated to a free radical leading to the alkylation of heme, proteins, lipids, DNA, and other biomolecules and thereby, among others, interfering with Hb metabolism and inducing proteotoxic stress. In our study, we found that 10× EC_{50} of the artemisinin derivative DHA leads to an increased ATP level, while 100× EC_{50} leads to a decreased ATP level. Considering the large number of potential targets and biochemical pathways influenced by DHA treatment, we do not believe that it is possible to draw strong conclusions as to the exact mechanism leading to these ATP responses.

In our selection of compounds, we included two redox cyclers, PD and MB. PD is a 1,4-naphthoquinone derivative, active against all asexual stages, and a promising lead compound (32). In contrast, MB is the first synthetic chemotherapeutic that was developed. The history, redox-cycling activity, and other pleiotropic targets of MB were reviewed extensively by Schirmer et al. (31). In our study, we found that both compounds exert quite similar effects, causing a moderate drop in ATeam ratio and only a slight drop in cytosolic pH. PD treatment of parasites under similar conditions to those we applied has been shown to lead to a significant shift in the cytosolic redox potential toward oxidation (70). Kehr et al. (71) showed that the proteome of *P. falciparum* is highly redox regulated, including glycolytic enzymes such as PfGAPDH. One explanation of our results is that, faced with oxidative stress, the parasites upregulate the activity of the pentose phosphate pathway at the cost of glycolysis.

DOXY and other tetracyclines are known to target the apicoplast's ribosomal translation and kill the parasites with a delayed death phenotype (33) resulting largely from the inhibition of isoprenoid synthesis and subsequent loss in the second cycle of the apicoplast itself (72). At higher concentrations (up to 10 µM), the first cycle effect was also noted, which could be negated by supplementation with either the isoprenoid precursor IPP or iron, suggesting that this effect is apicoplast dependent (73). Interestingly, we find that 5 µM DOXY causes an increase in cytosolic pH, while this did not occur upon the addition of 1 µM, indicating that first cycle effects include misregulation of cytosolic pH by a mechanism as yet unknown.

SBI-0797750 is a promising drug candidate with nanomolar activity targeting PfGluPho, the bi-functional fusion protein of glucose 6-phosphate dehydrogenase and 6-phosphogluconolactonase, and treatment of parasites at 1× EC_{50} led to a significant shift in the cytosolic redox potential toward oxidation after 4 h (36). As PfGluPho redirects glucose-6-phosphate from glycolysis to the oxidative pentose phosphate pathway, inhibition of this enzyme may be expected to allow a higher rate of glycolysis and thus higher rate of ATP production. However, we could not detect dramatic effects on the ATeam ratio, even though the single-cell ratio distribution does appear to be more compressed and elevated compared to control parasites. One explanation is that the more oxidative environment generated upon SBI treatment leads, in parallel, to

downregulation of glycolytic activity as noted above. Alternatively, changes in ATP levels over the course of the experiment may be too small to be evident.

ATQ is an inhibitor of the ETC (34). Malaria parasites rely, during the blood stages, largely on energy production via glycolysis (2, 3), and the only essential function of the ETC during these stages appears to be regeneration of ubiquinone for pyrimidine synthesis (74). In accordance with this, mitochondrial inhibitors are reported to cause only slight alterations in cellular ATP levels over a short time frame (9). In our experimental setup, ATQ was the only compound that did not show any effects on the trophozoite stages after 4 or 6 h at any of the concentrations tested. Our data fit the observations of Wilson et al. (75) that ATQ asserts its effects only on later-stage parasites.

It is a general consensus that the 4-aminoquinolines CQ, AQ, and PYRO kill the parasites through inhibition of hemozoin formation and the induction of similar metabolomics effects (76). However, they also show differences regarding the size of their effect on the distribution of heme species (46, 64, 77). In our study, we found that all of the 4-aminoquinolines included in our study show similar distinct sensor responses. High concentrations of 100× EC_{50} led to reduced parasite size, a moderate drop in pH to 7 or slightly below 7, as well as ATeam ratio depletion, which was indicative of a drop in [ATP]. Unusually, the single-cell ATeam ratio distribution dropped below the expected minimum ratio defined by parasites starved from GLC. One explanation for this behavior would be sensor degradation. To investigate this phenomenon, we used CQ as a representative of the compound class and monitored sensor integrity via western blot. Indeed, treatment of parasites with CQ led to sensor degradation. In addition to effects on ATeam sensor integrity, we also observed degradation of the PfHSP90 loading control under 100× EC_{50} CQ. Interestingly, co-treatment with MQ, which is known to block endocytosis and thus uptake of hemoglobin (78), as well as CQ-mediated Hb accumulation (46), prevented both effects. We therefore believe that the sensor degradation observed is, likely indirectly, heme-mediated, by mechanisms, which will require further investigation. Although we did not carry out western blot on parasites treated with AQ or PYRO, given the similar distinct ATeam ratio depletion, we believe the latter is highly likely to cause similar sensor degradation.

Conclusion and future outlook

Here, we have established ATeam and sfpHluorin measurements in *P. falciparum* and demonstrated their feasibility to dynamically monitor changes in ATP and pH levels in either a plate reader or single-cell microscopy format. We show that, despite some limitations, ATeams and sfpHluorin are valuable tools for studying ATP and pH metabolism in *P. falciparum*. Using these new tools, we uncover distinct response patterns toward different compound classes, adding new momentum for mode of action studies. We believe that this system shows great potential to support mode of action studies of current and future anti-malaria compounds, and thus accelerate drug development, and these tools are available on request to the malaria community. Although not herein demonstrated, we wish to note that these sensors, by virtue of their genetically encoded nature, can easily be targeted to specific subcellular compartments, and thus can be used to elucidate compartment-specific effects that may have otherwise been overlooked using conventional methods.

MATERIALS AND METHODS

Cloning of expression and integration plasmids

For cloning, ATeam1.03-nD/nA, ATeam1.03YEMK, and sfpHluorin template sequences were amplified via forward primer conferring BamHI and AvrII, as well as reverse primer conferring XhoI and HindIII restriction sites. In the case of ATeam sequences, the primer had multiple binding sites within the template sequence leading to multiple amplification products. Amplification products were separated and extracted from agarose gel

electrophoresis for further cloning of the desired product. The sequences were cloned into the pQE-30 vector via BamHI and HindIII, while cloning into the pDC2-CAM-[X]-BSD-*attP* vector was facilitated via the AvrII and XhoI restriction sites.

Expression and purification of recombinant ATeam and sfpHluorin protein

E. coli strain M15 carrying pQE-30[ATeam1.03-nD/nA] or pQE-30[ATeam1.03YEMK] were grown in lysogeny broth (LB), as described in reference (79) (1 g/L NaCl, 5 g/L yeast extract, and 1 g/L tryptone), at 37°C overnight to inoculate 1 L LB to an OD_{600} of 0.2 with subsequent incubation to OD_{600} of 0.6 at 37°C. Protein expression was induced via isopropyl β-D-1-thiogalactopyranoside to a final concentration of 0.2 mM overnight at 24°C. Cells were collected via centrifugation at 11,448 *g* for 15 minutes at 4°C and stored at −20°C until purification. Cells were thawed in lysis buffer (100 mM Tris-HCl, 200 mM NaCl, and 10 mM imidazole, pH 8.0) enriched with 150 nM pepstatin, 4 nM cystatin, and 100 µM phenylmethylsulfonylfluoride. Cells were lysed using lysozyme and DNaseI for 30 minutes on ice, disrupted by sonication, and collected via centrifugation at 38,000 *g* for 30 minutes. The supernatant was loaded onto a nickel nitrilotriacetic acid (Ni-NTA) column equilibrated in lysis buffer for affinity chromatography. After washing, proteins were eluted with increasing concentrations of imidazole (20–500 mM). Fractions containing predominantly ATeam protein were pooled and applied to a HiLoad 16/600 Superdex 200 column (GE Healthcare) equilibrated with 20 mM Tris-HCl and 150 mM NaCl, pH 8.0 for size-exclusion chromatography. Fractions containing ATeam protein were pooled and concentrated in a 30 kDa cutoff Vivaspin tube, supplemented with 20% (vol/vol) glycerol, and stored at −80°C in single-use aliquots. sfpHluorin in pQE-30 was expressed and purified in *E. coli* M15 in the same way as ATeam protein with the following exceptions: protein expression was induced at 37°C; lysis was conducted in HEPES buffer (50 mM HEPES and 300 mM NaCl, pH 7.5); elution from Ni-NTA was conducted with 10–500 mM imidazole; size-exclusion chromatography was conducted in HEPES buffer; protein was concentrated using 10 kDa cutoff Vivaspin tubes; protein was stored at −20°C in HEPES buffer. The concentration of proteins was either determined according to reference (80) or using the mVenus extinction coefficient as described by Imamura et al. (22).

Plate reader measurements of purified ATeam protein

Purified ATeam protein was mixed to a final concentration of 1 µM in ATeam buffer (100 mM HEPES, 50 mM KCl, and 0.5 mM $MgCl_2$, pH 7.34), except for pH response analyses, in which buffers contained 50 mM KCl, 0.5 mM $MgCl_2$, and 100 mM of either MES (pH 5–6.5), HEPES (pH 7–8), or CHES (pH 8.5–9). Measurements were performed on a Clariostar plate reader (BMG Labtech, Ortenberg, Germany) preheated to 37°C. Emission ratios were calculated after background subtraction of emission at 527/10 nm and emission at 475/10 nm after excitation at 435/10 nm, respectively. Dynamic measurements over time were collected every 10 s, accordingly. Spectral scans were collected from 463 to 600 nm for each nanometer after excitation at 435/10 nm. Mean values of $n = 3$ experiments with independently produced proteins are shown.

Plate reader measurements of purified sfpHluorin protein

Purified sfpHluorin protein was equilibrated in buffers to a final concentration of 1 µM with pH varying from 5.0 to 9.0 (pH 5.0–6.5: 10 mM MES-KOH, 100 mM NaCl, and 5 mM EDTA; pH 7.0–8.0: 100 mM HEPES-KOH, 100 mM NaCl, and 5 mM EDTA; pH 8.5–9.0: 100 mM Tris-HCl, 100 mM NaCl, and 5 mM EDTA) at 37°C before use. Measurements were performed on a Clariostar plate reader (BMG Labtech, Ortenberg, Germany) preheated to 37°C. Excitation scan was recorded in the range from 340 to 490 nm with emission sensing at 530/40 nm. Mean values of $n = 3$ experiments with independently produced proteins are shown.

Drug-sensor interaction studies

Purified sensor proteins were equilibrated in ATeam (100 mM HEPES, 50 mM KCl, and 0.5 mM $MgCl_2$, pH 7.34) or sfpHlourin (100 mM potassium phosphate, 100 mM NaCl, and 0.5 mM Na_2-EDTA, pH 7.0) buffer at 37°C to a final concentration of 1 µM together with 10× stock solutions ranging from 100 to 10 µM of compound, before use. Measurements were performed on a Clariostar plate reader (BMG Labtech, Ortenberg, Germany). ATeam emission ratio was calculated after background subtraction of emission at 527/10 nm and emission at 475/10 nm after excitation at 435/10 nm, respectively. sfpHluorin excitation ratio was calculated from 390/15 and 482/16 nm excitation and 530/20 nm emission, respectively. Mean values of $n = 3$ experiments with independently produced proteins are shown.

Stable integration of sensors into NF54*attB*

We used the NF54*attB* strain lacking a selectable marker (39) for *attB-attP* recombination of *attP* plasmids, containing the sensor sequences, within the cg6 gene using the mycobacteriophage Bxb1 integrase as described elsewhere (40). Briefly, 200 µL of 5% iRBCs were transfected with 50 µg pDC2*attP* plasmids, including blasticidin S deaminase selectable marker, conferring resistance to blasticidin S, calmodulin promotor, and the respective sensor sequence, in addition to 50 µg of the integrase-encoding pINT plasmid, including neomycin selectable marker, conferring resistance to Geneticin (G418). For transfection, cells were mixed with plasmids and cytomix (120 mM KCl, 0.15 mM $CaCl_2$, 2 mM EGTA, 5 mM $MgCl_2$, 10 mM K_2HPO_4/KH_2PO_4, and 25 mM HEPES, pH 7.6), transferred to a 2 mm electroporation cuvette and electroporated (310 V, 950 µF, and capacitance ∞). Transfectants were selected with 2.5 µg/mL blasticidin (until clonal selection) and 125 µg/mL G418 (5 days). Clonal parasite lines were generated using limiting dilution. Stable integration was verified using PCR as described by Schuh et al. (30), binding inside the genomic cg6 and the integrated bsd gene.

P. falciparum cell culture

Parasites were cultured as described elsewhere (81). In brief, parasites were propagated in A^+ red blood cells in complete media (CM) composed of RPMI 1640 medium supplemented with 0.5% Albumax, 9 mM glucose, 0.2 mM hypoxanthine, 2.1 mM L-glutamine, 25 mM HEPES, and 22 µg/mL gentamicin at 3.3% hematocrit and 37°C under 3% O_2 and 3% CO_2. Cells were synchronized via 5% sorbitol at least three times before each measurement. Cells were treated with sorbitol in their developmental cycles preceding the cycle of the measurement.

In vitro P. falciparum drug susceptibility assay

Half maximal effective concentration (EC_{50}) of PYRO against *P. falciparum* NF54*attB* cell line was performed using SYBR Green I-based fluorescence assays according to Ekland et al. (82). Serial double dilutions of the compound in CM were performed in 96-well plates (black, half area, µClear, Greiner Bio-One GmbH, Frickenhausen, Germany). Synchronized ring-stage parasites were added to each well to 0.15% parasitemia and 1.25% hematocrit and incubated at 37°C for 48 h. Subsequently, SYBR Green in lysis buffer (20 mM Tris-HCl, 5 mM EDTA, 0.16%, wt/vol saponin, and 1.6% vol/vol Triton X-100) was added to each well for 24 h at RT in the dark. Fluorescence was measured in a Clariostar plate reader (BMG Labtech, Ortenberg, Germany) at 494 nm excitation and 530 nm emission sensing. Curve fitting of the growth inhibition against log compound concentration with a variable slope sigmoidal function led to the EC_{50} value.

Trophozoite enrichment via MACS

Briefly, sorbitol-synchronized iRBCs were transferred to MACS cell separation LD columns (Miltenyi Biotec, Bergisch Gladbach, Germany), washed, and eluted in CM. For

measurements using live-cell microscopy, cells were washed and resuspended in Ringer's solution (122.5 mM NaCl, 5.4 mM KCl, 1.2 mM $CaCl_2$, 0.8 mM $MgCl_2$, 11 mM D-glucose, 25 mM HEPES, and 1 mM NaH_2PO_4, pH 7.4) to a density leading to approximately 30 parasites per field of view. For plate reader measurements, cells were counted using the improved Neubauer hemocytometer (Brand GmbH, Wertheim, Germany) and diluted to the desired parasite count.

Western blot analysis

Western blot analysis was conducted with MACS-enriched trophozoite-iRBCs. For each sample, 5 million cells were either first incubated with 100× compound stock solution or vehicle control in CM or directly washed with PBS and cOmplete Protease Inhibitor Cocktail Tablets (Roche Diagnostics GmbH, Mannheim, Germany) and lysed using M-PER buffer (ThermoFisher Scientific, Waltham, MA, USA). Cell debris was pelleted, and the supernatant was incubated at 95°C with 4× sample buffer + DTT and separated using sodium dodecyl sulfate-polyacrylamide gel electrophoresis according to reference (83). Proteins were blotted on polyvinylidene difluoride membrane. The membrane was stained with Ponceau S protein stain, washed, blocked in 5% milk, and probed with α-GFP (1:1,000 in 5% milk; Roche Diagnostics GmbH, Mannheim, Germany) for GFP-based sensor probing, followed by secondary α-mouse IgG antibodies (1:10,000 in 5% milk; Dianova, Hamburg, Germany). Equal loading via housekeeping genes was verified via α-aldolase or α-HSP90 western blot, after GFP probing. All solutions for western blot staining were dissolved in Tris-buffered saline with 0.05% polysorbate 20.

Measurements of sensor cell lines via plate reader

For plate reader measurements, 2 million NF54*attB*$^{[ATeam1.03YEMK]}$/NF54*attB*$^{[ATeam1.03-nD/nA]}$ or 1 million NF54*attB*$^{[sfpHluorin]}$ MACS-enriched trophozoite-iRBCs were washed in Ringer's solution, mixed in 384-well small volume plates (Greiner Bio-One GmbH, Frickenhausen, Germany), and measured in Clariostar plate reader (BMG Labtech, Ortenberg, Germany) at 37°C. For NF54*attB*$^{[ATeam1.03YEMK]}$ and NF54*attB*$^{[ATeam1.03-nD/nA]}$, measurement settings were chosen as described for recombinant ATeam protein earlier. For NF54*attB*$^{[sfpHluorin]}$, spectral excitation scan was collected via emission sensing at 530/40 nm and excitation from 350 to 490 nm for every nanometer with 10 nm bandwidth. The ratio was calculated after background subtraction of emission at 530/20 nm and excitation at 390/15 or 482/16 nm, respectively. Dynamic measurements over time were monitored every 10 s.

Measurements of sensor cell lines via live-cell microscopy

For imaging, Axio Observer.Z1/7 microscope (Zeiss, Oberkochen, Germany) with plan-apochromat 63×/1.40 oil immersion DIC M27 objective and Axiocam 506 camera were used. For measurements, CM was washed off with Ringer's solution, and parasites were allowed to settle on pre-heated ibidiTreat µ-Dish 35 mm Quad microcopy dishes (ibidi GmbH, Gräfelfing, Germany) at 37°C. The emission ratio of NF54*attB*$^{[ATeam1.03YEMK]}$ was measured using Zeiss filter set 47 (EX BP 436/20, BS FT 455, EM BP 480/40) and 48 (EX BP 436/20, BS FT 455, EM BP 535/30) for CFP and CFP-YFP-FRET signal, respectively. Colibri 7 LED module 430 nm was used for excitation. FRET ratio equals background-corrected YFP signal at 535 nm divided by background-corrected CFP signal at 480 nm. The excitation ratio of NF54*attB*$^{[sfpHluorin]}$ was measured using Zeiss filter set 38 HE without excitation filter [BS FT 495 (HE), EM BP 525/50 (HE)]. The excitation ratio equals background-corrected GFP signal at 525 nm and excitation at 385 nm divided by background-corrected GFP signal at 525 nm and excitation at 475 nm. ROIs were defined using a semi-automatic ImageJ script. The background area was selected manually. Image analysis was conducted via ImageJ Fiji (84) 1.54f.

Statistical analysis

Statistical analyses were performed via GraphPad Prism 10.02. Analysis of drug effects on sensor-expressing cell lines was conducted via repeated measure two-way ANOVA using a general linear model for the analysis of the selected randomized block design. Correction for multiple comparisons was conducted using the false discovery rate with the two-staged step-up method described by Benjamini et al. (44). The desired FDR was set at 5%. Calibration curves for interpolation of pH values were generated using a sigmoidal, four-parameter logistic model.

ACKNOWLEDGMENTS

The authors gratefully thank Hiromi Imamura for providing the ATeam1.03YEMK sequence and Markus Schwarzländer for providing the ATeam1.03-nD/nA sequence.

This research was funded by the German Research Foundation (grant BE1540/23-2 within the DFG Priority Program 1710 on Thiol Switches, awarded to K.B.) and the LOEWE Center DRUID (Project E3 awarded to K.B., J.M.P., and S.R.) within the Hessian Excellence Program.

AUTHOR AFFILIATION

[1]Biochemistry and Molecular Biology, Interdisciplinary Research Center, Justus Liebig University, Giessen, Germany

PRESENT ADDRESS

Kim C. Heimsch, Institute of Virology, Charité, Berlin, Germany
Katja Becker, German Research Foundation (DFG), Bonn, Germany

AUTHOR ORCIDs

Eric Springer http://orcid.org/0000-0002-8092-1453
Jude M. Przyborski http://orcid.org/0000-0002-3494-7767

FUNDING

Funder	Grant(s)	Author(s)
Deutsche Forschungsgemeinschaft (DFG)	BE1540/23-2	Eric Springer Katja Becker
HMWK	DRUID_E3	Eric Springer Stefan Rahlfs Katja Becker Jude M. Przyborski

AUTHOR CONTRIBUTIONS

Eric Springer, Conceptualization, Formal analysis, Investigation, Writing – original draft, Writing – review and editing | Kim C. Heimsch, Investigation, Writing – review and editing | Stefan Rahlfs, Funding acquisition, Project administration, Supervision, Writing – review and editing | Katja Becker, Conceptualization, Funding acquisition, Project administration, Supervision, Writing – review and editing | Jude M. Przyborski, Project administration, Supervision, Writing – review and editing

ADDITIONAL FILES

The following material is available online.

Supplemental Material

Supplemental material (AAC01690-23-s0001.docx). Figures S1 to S11; Tables S1 to S10.

REFERENCES

1. WHO. 2023 Nov 30. World malaria report 2023. World Health Organization.
2. MacRae JI, Dixon MW, Dearnley MK, Chua HH, Chambers JM, Kenny S, Bottova I, Tilley L, McConville MJ. 2013. Mitochondrial metabolism of sexual and asexual blood stages of the malaria parasite *Plasmodium falciparum*. BMC Biol 11:67. https://doi.org/10.1186/1741-7007-11-67
3. Sakata-Kato T, Wirth DF. 2016. A novel methodology for bioenergetic analysis of *Plasmodium falciparum* reveals a glucose-regulated metabolic shift and enables mode of action analyses of mitochondrial inhibitors. ACS Infect Dis 2:903–916. https://doi.org/10.1021/acsinfecdis.6b00101
4. Jortzik E, Becker K. 2011. Energy metabolism as an antimalarial drug target, p 75–95. In Becker K (ed), Apicomplexan parasites: molecular approaches toward targeted drug development. Drug discovery in infectious diseases. Wiley.
5. Jiang X. 2022. An overview of the *Plasmodium falciparum* hexose transporter and its therapeutic interventions. Proteins 90:1766–1778. https://doi.org/10.1002/prot.26351
6. Ley-Ngardigal S, Bertolin G. 2022. Approaches to monitor ATP levels in living cells: where do we stand? FEBS J 289:7940–7969. https://doi.org/10.1111/febs.16169
7. Kanaani J, Ginsburg H. 1989. Metabolic interconnection between the human malarial parasite *Plasmodium falciparum* and its host erythrocyte. Regulation of ATP levels by means of an adenylate translocator and adenylate kinase. J Biol Chem 264:3194–3199.
8. Kanaani J, Ginsburg H. 1992. Effects of cinnamic acid derivatives on *in vitro* growth of *Plasmodium falciparum* and on the permeability of the membrane of malaria-infected erythrocytes. Antimicrob Agents Chemother 36:1102–1108. https://doi.org/10.1128/AAC.36.5.1102
9. Fry M, Webb E, Pudney M. 1990. Effect of mitochondrial inhibitors on adenosinetriphosphate levels in *Plasmodium falciparum*. Comp Biochem Physiol B 96:775–782. https://doi.org/10.1016/0305-0491(90)90230-q
10. Kirk K, Horner HA, Kirk J. 1996. Glucose uptake in *Plasmodium falciparum*-infected erythrocytes is an equilibrative not an active process. Mol Biochem Parasitol 82:195–205. https://doi.org/10.1016/0166-6851(96)02734-x
11. Saliba KJ, Kirk K. 1999. pH regulation in the intracellular malaria parasite, *Plasmodium falciparum*. H^+ extrusion via a V-type H^+-ATPase. J Biol Chem 274:33213–33219. https://doi.org/10.1074/jbc.274.47.33213
12. Ayi K, Liles WC, Gros P, Kain KC. 2009. Adenosine triphosphate depletion of erythrocytes simulates the phenotype associated with pyruvate kinase deficiency and confers protection against *Plasmodium falciparum in vitro*. J Infect Dis 200:1289–1299. https://doi.org/10.1086/605843
13. Khan T, van Brummelen AC, Parkinson CJ, Hoppe HC. 2012. ATP and luciferase assays to determine the rate of drug action in *in vitro* cultures of *Plasmodium falciparum*. Malar J 11:369. https://doi.org/10.1186/1475-2875-11-369
14. Lelièvre J, Almela MJ, Lozano S, Miguel C, Franco V, Leroy D, Herreros E. 2012. Activity of clinically relevant antimalarial drugs on *Plasmodium falciparum* mature gametocytes in an ATP bioluminescence "transmission blocking" assay. PLoS One 7:e35019. https://doi.org/10.1371/journal.pone.0035019
15. van Schalkwyk DA, Saliba KJ, Biagini GA, Bray PG, Kirk K. 2013. Loss of pH control in *Plasmodium falciparum* parasites subjected to oxidative stress. PLoS One 8:e58933. https://doi.org/10.1371/journal.pone.0058933
16. Miguel-Blanco C, Molina I, Bardera AI, Díaz B, de Las Heras L, Lozano S, González C, Rodrigues J, Delves MJ, Ruecker A, Colmenarejo G, Viera S, Martínez-Martínez MS, Fernández E, Baum J, Sinden RE, Herreros E. 2017. Hundreds of dual-stage antimalarial molecules discovered by a functional gametocyte screen. Nat Commun 8:15160. https://doi.org/10.1038/ncomms15160
17. Shi X, Wei M, Xu Z, Liu Y, Zhang M, Lv L, Wang Q. 2021. Vitamin C inhibits blood-stage *Plasmodium* parasites via oxidative stress. Front Cell Dev Biol 9:639944. https://doi.org/10.3389/fcell.2021.639944
18. Morais I, Medeiros MM, Carvalho M, Morello J, Teixeira SM, Maciel S, Nhantumbo J, Balau A, Rosa MTG, Nogueira F, Rodrigues JA, Carvalho FA, Antunes AMM, Arez AP. 2022. Synthetic red blood cell-specific glycolytic intermediate 2,3-diphosphoglycerate (2,3-DPG) inhibits *Plasmodium falciparum* development *in vitro*. Front Cell Infect Microbiol 12:840968. https://doi.org/10.3389/fcimb.2022.840968
19. Peatey CL, Leroy D, Gardiner DL, Trenholme KR. 2012. Anti-malarial drugs: how effective are they against *Plasmodium falciparum* gametocytes? Malar J 11:34. https://doi.org/10.1186/1475-2875-11-34
20. Cevenini L, Camarda G, Michelini E, Siciliano G, Calabretta MM, Bona R, Kumar TRS, Cara A, Branchini BR, Fidock DA, Roda A, Alano P. 2014. Multicolor bioluminescence boosts malaria research: quantitative dual-color assay and single-cell imaging in *Plasmodium falciparum* parasites. Anal Chem 86:8814–8821. https://doi.org/10.1021/ac502098w
21. Sheridan CM, Garcia VE, Ahyong V, DeRisi JL. 2018. The *Plasmodium falciparum* cytoplasmic translation apparatus: a promising therapeutic target not yet exploited by clinically approved anti-malarials. Malar J 17:465. https://doi.org/10.1186/s12936-018-2616-7
22. Imamura H, Nhat KPH, Togawa H, Saito K, Iino R, Kato-Yamada Y, Nagai T, Noji H. 2009. Visualization of ATP levels inside single living cells with fluorescence resonance energy transfer-based genetically encoded indicators. Proc Natl Acad Sci U S A 106:15651–15656. https://doi.org/10.1073/pnas.0904764106
23. Nakano M, Imamura H, Nagai T, Noji H. 2011. Ca^{2+} regulation of mitochondrial ATP synthesis visualized at the single cell level. ACS Chem Biol 6:709–715. https://doi.org/10.1021/cb100313n
24. Kotera I, Iwasaki T, Imamura H, Noji H, Nagai T. 2010. Reversible dimerization of *Aequorea victoria* fluorescent proteins increases the dynamic range of FRET-based indicators. ACS Chem Biol 5:215–222. https://doi.org/10.1021/cb900263z
25. Shaner NC, Steinbach PA, Tsien RY. 2005. A guide to choosing fluorescent proteins. Nat Methods 2:905–909. https://doi.org/10.1038/nmeth819
26. Wissing F, Sanchez CP, Rohrbach P, Ricken S, Lanzer M. 2002. Illumination of the malaria parasite *Plasmodium falciparum* alters intracellular pH. J Biol Chem 277:37747–37755. https://doi.org/10.1074/jbc.M204845200
27. Kuhn Y, Rohrbach P, Lanzer M. 2007. Quantitative pH measurements in *Plasmodium falciparum*-infected erythrocytes using pHluorin. Cell Microbiol 9:1004–1013. https://doi.org/10.1111/j.1462-5822.2006.00847.x
28. Rahbari M, Rahlfs S, Jortzik E, Bogeski I, Becker K. 2017. H_2O_2 dynamics in the malaria parasite *Plasmodium falciparum*. PLoS One 12:e0174837. https://doi.org/10.1371/journal.pone.0174837
29. Reifenrath M, Boles E. 2018. A superfolder variant of pH-sensitive pHluorin for *in vivo* pH measurements in the endoplasmic reticulum. Sci Rep 8:11985. https://doi.org/10.1038/s41598-018-30367-z
30. Schuh AK, Rahbari M, Heimsch KC, Mohring F, Gabryszewski SJ, Weder S, Buchholz K, Rahlfs S, Fidock DA, Becker K. 2018. Stable integration and comparison of hGrx1-roGFP2 and sfroGFP2 redox probes in the malaria parasite *Plasmodium falciparum*. ACS Infect Dis 4:1601–1612. https://doi.org/10.1021/acsinfecdis.8b00140
31. Schirmer RH, Adler H, Pickhardt M, Mandelkow E. 2011. "Lest we forget you — methylene blue …". Neurobiol Aging 32:2325. https://doi.org/10.1016/j.neurobiolaging.2010.12.012
32. Ehrhardt K, Deregnaucourt C, Goetz A-A, Tzanova T, Gallo V, Arese P, Pradines B, Adjalley SH, Bagrel D, Blandin S, Lanzer M, Davioud-Charvet E. 2016. The redox cycler plasmodione is a fast-acting antimalarial lead compound with pronounced activity against sexual and early asexual blood-stage parasites. Antimicrob Agents Chemother 60:5146–5158. https://doi.org/10.1128/AAC.02975-15
33. Dahl EL, Shock JL, Shenai BR, Gut J, DeRisi JL, Rosenthal PJ. 2006. Tetracyclines specifically target the apicoplast of the malaria parasite *Plasmodium falciparum*. Antimicrob Agents Chemother 50:3124–3131. https://doi.org/10.1128/AAC.00394-06

34. Fry M, Pudney M. 1992. Site of action of the antimalarial hydroxynaphthoquinone, 2-trans-4-(4'-chlorophenyl) cyclohexyl-3-hydroxy-1,4-naphthoquinone (566C80). Biochem Pharmacol 43:1545–1553. https://doi.org/10.1016/0006-2952(92)90213-3
35. Geary TG, Jensen JB. 1983. Effects of antibiotics on *Plasmodium falciparum in vitro*. Am J Trop Med Hyg 32:221–225. https://doi.org/10.4269/ajtmh.1983.32.221
36. Berneburg I, Peddibhotla S, Heimsch KC, Haeussler K, Maloney P, Gosalia P, Preuss J, Rahbari M, Skorokhod O, Valente E, Ulliers D, Simula LF, Buchholz K, Hedrick MP, Hershberger P, Chung TDY, Jackson MR, Schwarzer E, Rahlfs S, Bode L, Becker K, Pinkerton AB. 2022. An optimized dihydrodibenzothiazepine lead compound (SBI-0797750) as a potent and selective inhibitor of *Plasmodium falciparum* and *P. vivax* glucose 6-phosphate dehydrogenase 6-phosphogluconolactonase. Antimicrob Agents Chemother 66:e0210921. https://doi.org/10.1128/aac.02109-21
37. De Col V, Fuchs P, Nietzel T, Elsässer M, Voon CP, Candeo A, Seeliger I, Fricker MD, Grefen C, Møller IM, Bassi A, Lim BL, Zancani M, Meyer AJ, Costa A, Wagner S, Schwarzländer M. 2017. ATP sensing in living plant cells reveals tissue gradients and stress dynamics of energy physiology. Elife 6:e26770. https://doi.org/10.7554/eLife.26770
38. Storer AC, Cornish-Bowden A. 1976. Concentration of MgATP2- and other ions in solution. Calculation of the true concentrations of species present in mixtures of associating ions. Biochem J 159:1–5. https://doi.org/10.1042/bj1590001
39. Adjalley SH, Johnston GL, Li T, Eastman RT, Ekland EH, Eappen AG, Richman A, Sim BKL, Lee MCS, Hoffman SL, Fidock DA. 2011. Quantitative assessment of *Plasmodium falciparum* sexual development reveals potent transmission-blocking activity by methylene blue. Proc Natl Acad Sci U S A 108:E1214–E1223. https://doi.org/10.1073/pnas.1112037108
40. Nkrumah LJ, Muhle RA, Moura PA, Ghosh P, Hatfull GF, Jacobs WR, Fidock DA. 2006. Efficient site-specific integration in *Plasmodium falciparum* chromosomes mediated by mycobacteriophage Bxb1 integrase. Nat Methods 3:615–621. https://doi.org/10.1038/nmeth904
41. Wick AN, Drury DR, Nakada HI, Wolfe JB. 1957. Localization of the primary metabolic block produced by 2-deoxyglucose. J Biol Chem 224:963–969. https://doi.org/10.1016/S0021-9258(18)64988-9
42. Thomas JA, Buchsbaum RN, Zimniak A, Racker E. 1979. Intracellular pH measurements in Ehrlich ascites tumor cells utilizing spectroscopic probes generated *in situ*. Biochemistry 18:2210–2218. https://doi.org/10.1021/bi00578a012
43. Hayashi M, Yamada H, Mitamura T, Horii T, Yamamoto A, Moriyama Y. 2000. Vacuolar H^+-ATPase localized in plasma membranes of malaria parasite cells, *Plasmodium falciparum*, is involved in regional acidification of parasitized erythrocytes. J Biol Chem 275:34353–34358. https://doi.org/10.1074/jbc.M003323200
44. Benjamini Y, Krieger AM, Yekutieli D. 2006. Adaptive linear step-up procedures that control the false discovery rate. Biometrika 93:491–507. https://doi.org/10.1093/biomet/93.3.491
45. Sullivan DJ, Gluzman IY, Russell DG, Goldberg DE. 1996. On the molecular mechanism of chloroquine's antimalarial action. Proc Natl Acad Sci U S A 93:11865–11870. https://doi.org/10.1073/pnas.93.21.11865
46. Famin O, Ginsburg H. 2002. Differential effects of 4-aminoquinoline-containing antimalarial drugs on hemoglobin digestion in *Plasmodium falciparum*-infected erythrocytes. Biochem Pharmacol 63:393–398. https://doi.org/10.1016/s0006-2952(01)00878-4
47. Lerchundi R, Huang N, Rose CR. 2020. Quantitative imaging of changes in astrocytic and neuronal adenosine triphosphate using two different variants of ATeam. Front Cell Neurosci 14:80. https://doi.org/10.3389/fncel.2020.00080
48. Yaginuma H, Kawai S, Tabata KV, Tomiyama K, Kakizuka A, Komatsuzaki T, Noji H, Imamura H. 2014. Diversity in ATP concentrations in a single bacterial cell population revealed by quantitative single-cell imaging. Sci Rep 4:6522. https://doi.org/10.1038/srep06522
49. Choi I, Mikkelsen RB. 1990. *Plasmodium falciparum*: ATP/ADP transport across the parasitophorous vacuolar and plasma membranes. Exp Parasitol 71:452–462. https://doi.org/10.1016/0014-4894(90)90071-j
50. Akkaya C, Shumilina E, Bobballa D, Brand VB, Mahmud H, Lang F, Huber SM. 2009. The *Plasmodium falciparum*-induced anion channel of human erythrocytes is an ATP-release pathway. Pflugers Arch 457:1035–1047. https://doi.org/10.1007/s00424-008-0572-8
51. Yayon A, Cabantchik ZI, Ginsburg H. 1984. Identification of the acidic compartment of *Plasmodium falciparum*-infected human erythrocytes as the target of the antimalarial drug chloroquine. EMBO J. 3:2695–2700. https://doi.org/10.1002/j.1460-2075.1984.tb02195.x
52. Mohring F, Rahbari M, Zechmann B, Rahlfs S, Przyborski JM, Meyer AJ, Becker K. 2017. Determination of glutathione redox potential and pH value in subcellular compartments of malaria parasites. Free Radic Biol Med 104:104–117. https://doi.org/10.1016/j.freeradbiomed.2017.01.001
53. Adjepon-Yamoah KK, Ofori-Adjei D, Woolhouse NM, Lindström B. 1986. Whole-blood single-dose kinetics of chloroquine and desethylchloroquine in Africans. Ther Drug Monit 8:195–199. https://doi.org/10.1097/00007691-198606000-00012
54. Anyorigiya TA, Castel S, Mauff K, Atuguba F, Ogutu B, Oduro A, Dosoo D, Asante K-P, Owusu-Agyei S, Dodoo A, Hodgson A, Binka F, Workman LJ, Allen EN, Denti P, Wiesner L, Barnes KI. 2021. Pharmacokinetic profile of amodiaquine and its active metabolite desethylamodiaquine in Ghanaian patients with uncomplicated falciparum malaria. Malar J 20:18. https://doi.org/10.1186/s12936-020-03553-6
55. Chu W-Y, Dorlo TPC. 2023. Pyronaridine: a review of its clinical pharmacology in the treatment of malaria. J Antimicrob Chemother 78:2406–2418. https://doi.org/10.1093/jac/dkad260
56. Ezzet F, Mull R, Karbwang J. 1998. Population pharmacokinetics and therapeutic response of CGP 56697 (artemether + benflumetol) in malaria patients. Br J Clin Pharmacol 46:553–561. https://doi.org/10.1046/j.1365-2125.1998.00830.x
57. Gutman J, Green M, Durand S, Rojas OV, Ganguly B, Quezada WM, Utz GC, Slutsker L, Ruebush TK, Bacon DJ. 2009. Mefloquine pharmacokinetics and mefloquine-artesunate effectiveness in Peruvian patients with uncomplicated *Plasmodium falciparum* malaria. Malar J 8:58. https://doi.org/10.1186/1475-2875-8-58
58. Kayumba PC, Twagirumukiza M, Huyghebaert N, Ntawukuliryayo JD, van Bortel L, Vervaet C, Remon JP. 2008. Taste-masked quinine sulphate pellets: bio-availability in adults and steady-state plasma concentrations in children with uncomplicated *Plasmodium falciparum* malaria. Ann Trop Paediatr 28:103–109. https://doi.org/10.1179/146532808X302116
59. Rijken MJ, McGready R, Phyo AP, Lindegardh N, Tarning J, Laochan N, Than HH, Mu O, Win AK, Singhasivanon P, White N, Nosten F. 2011. Pharmacokinetics of dihydroartemisinin and piperaquine in pregnant and nonpregnant women with uncomplicated falciparum malaria. Antimicrob Agents Chemother 55:5500–5506. https://doi.org/10.1128/AAC.05067-11
60. Walter-Sack I, Rengelshausen J, Oberwittler H, Burhenne J, Mueller O, Meissner P, Mikus G. 2009. High absolute bioavailability of methylene blue given as an aqueous oral formulation. Eur J Clin Pharmacol 65:179–189. https://doi.org/10.1007/s00228-008-0563-x
61. Newton PN, Chaulet J-F, Brockman A, Chierakul W, Dondorp A, Ruangveerayuth R, Looareesuwan S, Mounier C, White NJ. 2005. Pharmacokinetics of oral doxycycline during combination treatment of severe falciparum malaria. Antimicrob Agents Chemother 49:1622–1625. https://doi.org/10.1128/AAC.49.4.1622-1625.2005
62. Russell JB, Cook GM. 1995. Energetics of bacterial growth: balance of anabolic and catabolic reactions. Microbiol Rev 59:48–62. https://doi.org/10.1128/mr.59.1.48-62.1995
63. Sánchez-Alcázar JA, Ruı´z-Cabello J, Hernández-Muñoz I, Pobre PS, de la Torre P, Siles-Rivas E, Garcı´a I, Kaplan O, Muñoz-Yagüe MT, Soli´s-Herruzo JA. 1997. Tumor necrosis factor-α increases ATP content in metabolically inhibited L929 cells preceding cell death. J Biol Chem 272:30167–30177. https://doi.org/10.1074/jbc.272.48.30167
64. Combrinck JM, Mabotha TE, Ncokazi KK, Ambele MA, Taylor D, Smith PJ, Hoppe HC, Egan TJ. 2013. Insights into the role of heme in the mechanism of action of antimalarials. ACS Chem Biol 8:133–137. https://doi.org/10.1021/cb300454t
65. Fitch CD. 2004. Ferriprotoporphyrin IX, phospholipids, and the antimalarial actions of quinoline drugs. Life Sci 74:1957–1972. https://doi.org/10.1016/j.lfs.2003.10.003
66. Ward KE, Fidock DA, Bridgford JL. 2022. *Plasmodium falciparum* resistance to artemisinin-based combination therapies. Curr Opin Microbiol 69:102193. https://doi.org/10.1016/j.mib.2022.102193

67. Fitch CD. 1998. Involvement of heme in the antimalarial action of chloroquine. Trans Am Clin Climatol Assoc 109:97–105;
68. Wong W, Bai X-C, Sleebs BE, Triglia T, Brown A, Thompson JK, Jackson KE, Hanssen E, Marapana DS, Fernandez IS, Ralph SA, Cowman AF, Scheres SHW, Baum J. 2017. Mefloquine targets the *Plasmodium falciparum* 80S ribosome to inhibit protein synthesis. Nat Microbiol 2:17031. https://doi.org/10.1038/nmicrobiol.2017.31
69. Dziekan JM, Yu H, Chen D, Dai L, Wirjanata G, Larsson A, Prabhu N, Sobota RM, Bozdech Z, Nordlund P. 2019. Identifying purine nucleoside phosphorylase as the target of quinine using cellular thermal shift assay. Sci Transl Med 11:eaau3174. https://doi.org/10.1126/scitranslmed.aau3174
70. Bielitza M, Belorgey D, Ehrhardt K, Johann L, Lanfranchi DA, Gallo V, Schwarzer E, Mohring F, Jortzik E, Williams DL, Becker K, Arese P, Elhabiri M, Davioud-Charvet E. 2015. Antimalarial NADPH-consuming redox-cyclers as superior glucose-6-phosphate dehydrogenase deficiency copycats. Antioxid Redox Signal 22:1337–1351. https://doi.org/10.1089/ars.2014.6047
71. Kehr S, Jortzik E, Delahunty C, Yates JR, Rahlfs S, Becker K. 2011. Protein S-glutathionylation in malaria parasites. Antioxid Redox Signal 15:2855–2865. https://doi.org/10.1089/ars.2011.4029
72. Yeh E, DeRisi JL. 2011. Chemical rescue of malaria parasites lacking an apicoplast defines organelle function in blood-stage *Plasmodium falciparum*. PLoS Biol 9:e1001138. https://doi.org/10.1371/journal.pbio.1001138
73. Okada M, Guo P, Nalder S-A, Sigala PA. 2020. Doxycycline has distinct apicoplast-specific mechanisms of antimalarial activity. Elife 9:e60246. https://doi.org/10.7554/eLife.60246
74. Painter HJ, Morrisey JM, Mather MW, Vaidya AB. 2007. Specific role of mitochondrial electron transport in blood-stage *Plasmodium falciparum*. Nature 446:88–91. https://doi.org/10.1038/nature05572
75. Wilson DW, Langer C, Goodman CD, McFadden GI, Beeson JG. 2013. Defining the timing of action of antimalarial drugs against *Plasmodium falciparum*. Antimicrob Agents Chemother 57:1455–1467. https://doi.org/10.1128/AAC.01881-12
76. Birrell GW, Challis MP, De Paoli A, Anderson D, Devine SM, Heffernan GD, Jacobus DP, Edstein MD, Siddiqui G, Creek DJ. 2020. Multi-omic characterization of the mode of action of a potent new antimalarial compound, JPC-3210, against *Plasmodium falciparum*. Mol Cell Proteomics 19:308–325. https://doi.org/10.1074/mcp.RA119.001797
77. Roberts L, Egan TJ, Joiner KA, Hoppe HC. 2008. Differential effects of quinoline antimalarials on endocytosis in *Plasmodium falciparum*. Antimicrob Agents Chemother 52:1840–1842. https://doi.org/10.1128/AAC.01478-07
78. Hoppe HC, van Schalkwyk DA, Wiehart UIM, Meredith SA, Egan J, Weber BW. 2004. Antimalarial quinolines and artemisinin inhibit endocytosis in *Plasmodium falciparum*. Antimicrob Agents Chemother 48:2370–2378. https://doi.org/10.1128/AAC.48.7.2370-2378.2004
79. Bertani G. 1951. Studies on lysogenesis. I. The mode of phage liberation by lysogenic *Escherichia coli*. J Bacteriol 62:293–300. https://doi.org/10.1128/jb.62.3.293-300.1951
80. Bradford MM. 1976. A rapid and sensitive method for the quantitation of microgram quantities of protein utilizing the principle of protein-dye binding. Anal Biochem 72:248–254. https://doi.org/10.1006/abio.1976.9999
81. Trager W, Jensen JB. 1976. Human malaria parasites in continuous culture. Science 193:673–675. https://doi.org/10.1126/science.781840
82. Ekland EH, Schneider J, Fidock DA. 2011. Identifying apicoplast-targeting antimalarials using high-throughput compatible approaches. FASEB J 25:3583–3593. https://doi.org/10.1096/fj.11-187401
83. Laemmli UK. 1970. Cleavage of structural proteins during the assembly of the head of bacteriophage T4. Nature 227:680–685. https://doi.org/10.1038/227680a0
84. Schindelin J, Arganda-Carreras I, Frise E, Kaynig V, Longair M, Pietzsch T, Preibisch S, Rueden C, Saalfeld S, Schmid B, Tinevez J-Y, White DJ, Hartenstein V, Eliceiri K, Tomancak P, Cardona A. 2012. Fiji: an open-source platform for biological-image analysis. Nat Methods 9:676–682. https://doi.org/10.1038/nmeth.2019

SUPPLEMENTAL MATERIALS

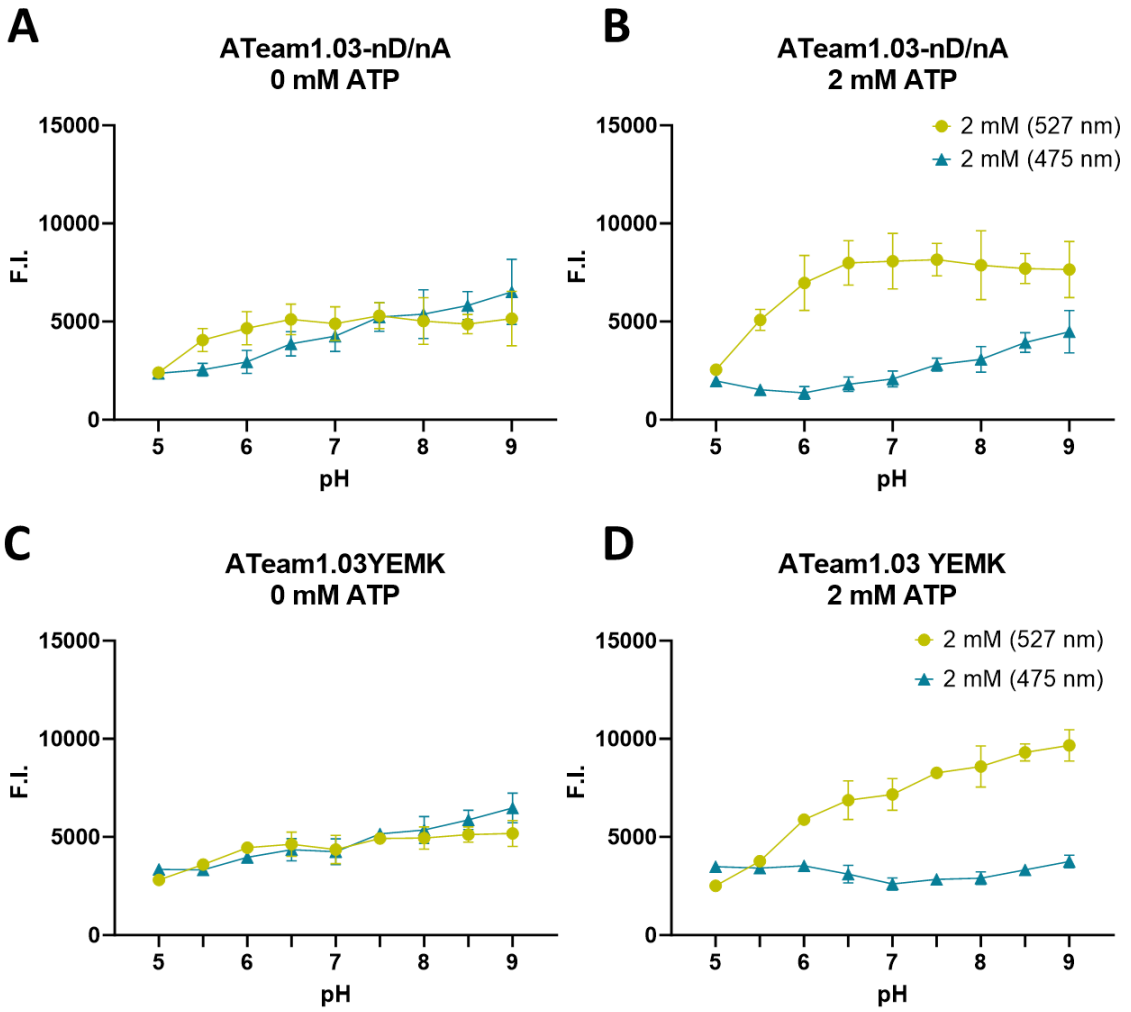

Fig S1: ATeam1.03-nD/nA shows less pH stability compared to ATeam1.03YEMK. A: CFP emission of ATeam1.03-nD/nA is effected by pH in the physiological range from pH 6 to 8; B: Increased dynamic range of ATeam1.03-nD/nA in response to 2 mM ATP is accompanied with decreased CFP emission; C: CFP and YFP fluorescence of ATeam1.03YEMK in the absence of ATP is stable in the physiological relevant range of pH 6 to 8; D: Ratio [527/475] decrease of ATeam1.03YEMK from pH 7 to 5 is accompanied with decreasing and increasing YFP and CFP fluorescence, respectively; Measurements were conducted via excitation at 435 nm and emission sensing at 527 nm for YFP and 475 nm for CFP. ATP was solved in equimolar solution of $MgCl_2$. 1 µM recombinant protein was used. Mean values of n = 3 independent experiments are shown. Error bars indicate SD.

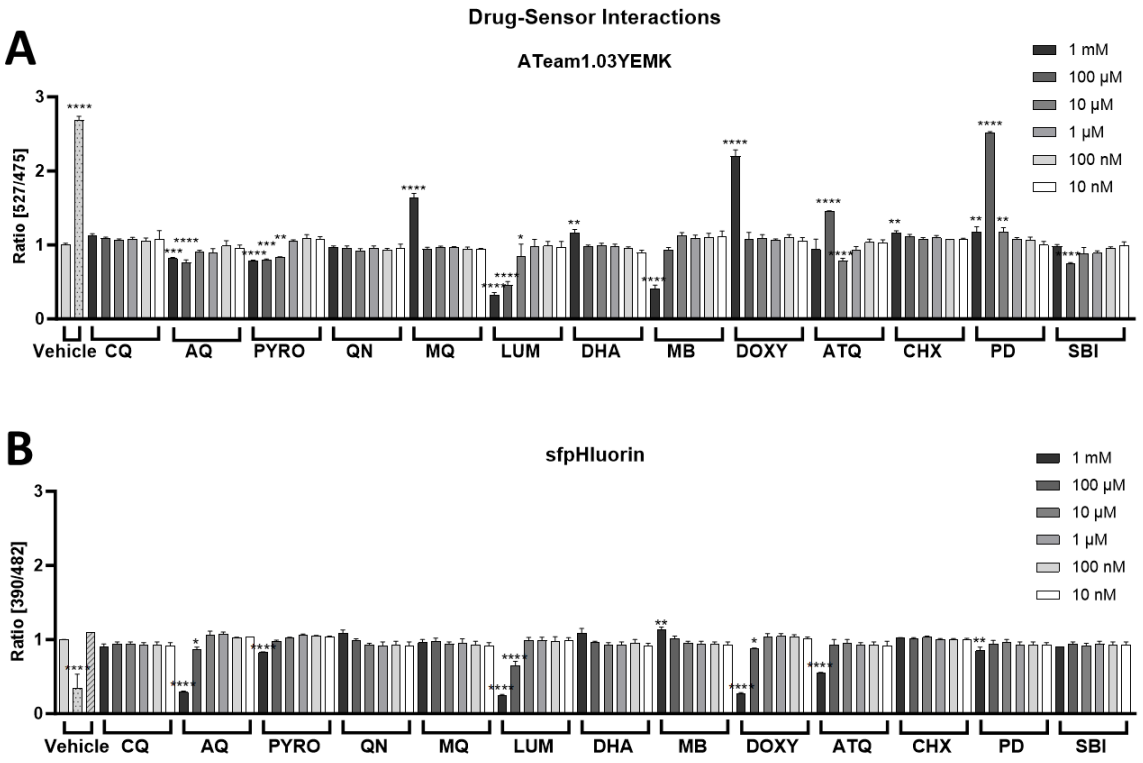

Fig. S2: ATeam1.03YEMK and sfpHluorin drug-sensor interactions. Recombinant sensor protein was incubated with the indicated drugs (1 mM, 100 µM, 10 µM, 1 µM, 100 nM, 10 nM); A: ATeam1.03YEMK measurements included vehicle treatment with 10 mM ATP dissolved in equimolar $MgCl_2$ solution (dotted); B: sfpHluorin measurements included vehicle treatment with buffers set to pH 5 (dotted) and pH 9 (diagonal); Chloroquine (CQ), amodiaquine (AQ), pyronaridine (PYRO), quinine (QN), mefloquine (MQ), lumefantrine (LUM), dihydroartemisinin (DHA), methylene blue (MB), doxycycline (DOXY), atovaquone (ATQ), cycloheximide (CHX), plasmodione (PD), SBI 0797750 (SBI). Background-corrected emission (A) or excitation (B) ratio relative to control is shown. Sensors were incubated for 5 min. Mean ratio of n = 3 independent experiments is shown. Error bars indicate SD. Ordinary one-way ANOVA with Dunnett's multiple comparisons testing was used. *: $p < 0.05$; **: $p < 0.01$; ***: $p < 0.001$; ****: $p < 0.0001$.

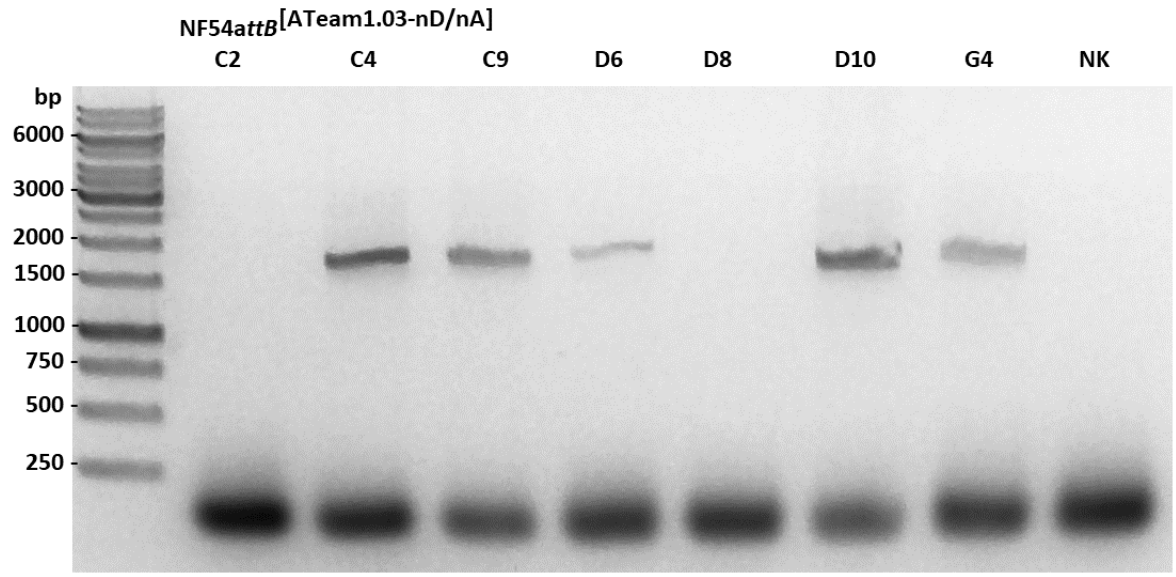

Fig. S3: Stable integration of ATeam1.03-nD/nA in NF54*attB*. Representative clonal cell-lines show PCR product based on genomic cg6 and integrated BSD genes, and thereby, demonstrating successful sensor integration.

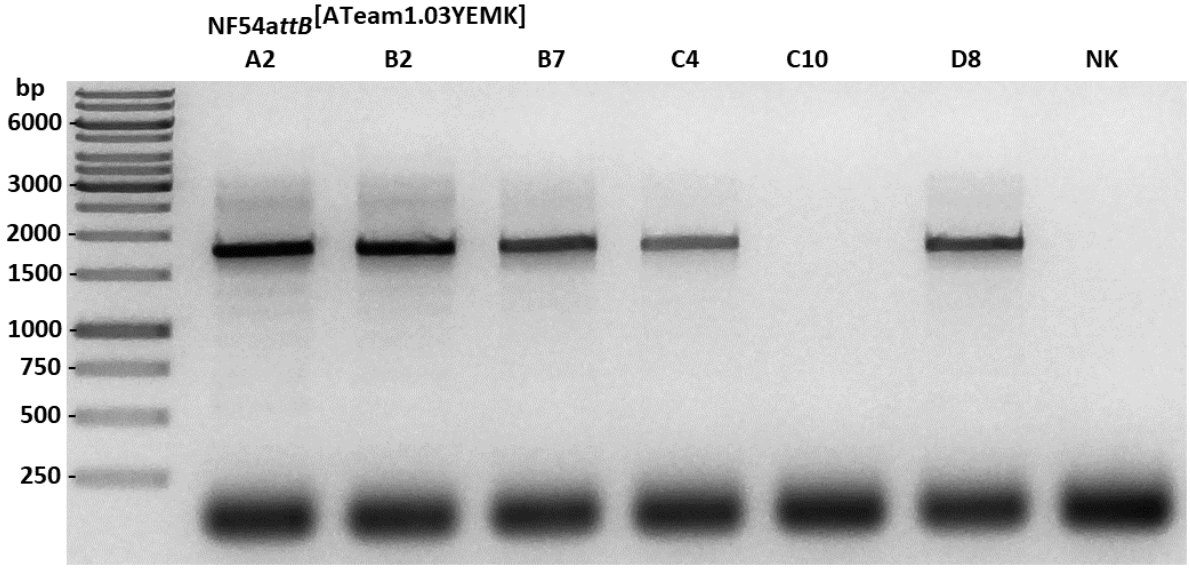

Fig. S4: Stable integration of ATeam1.03YEMK in NF54*attB*. Representative clonal cell-lines show PCR product based on genomic cg6 and integrated BSD genes, and thereby, demonstrating successful sensor integration.

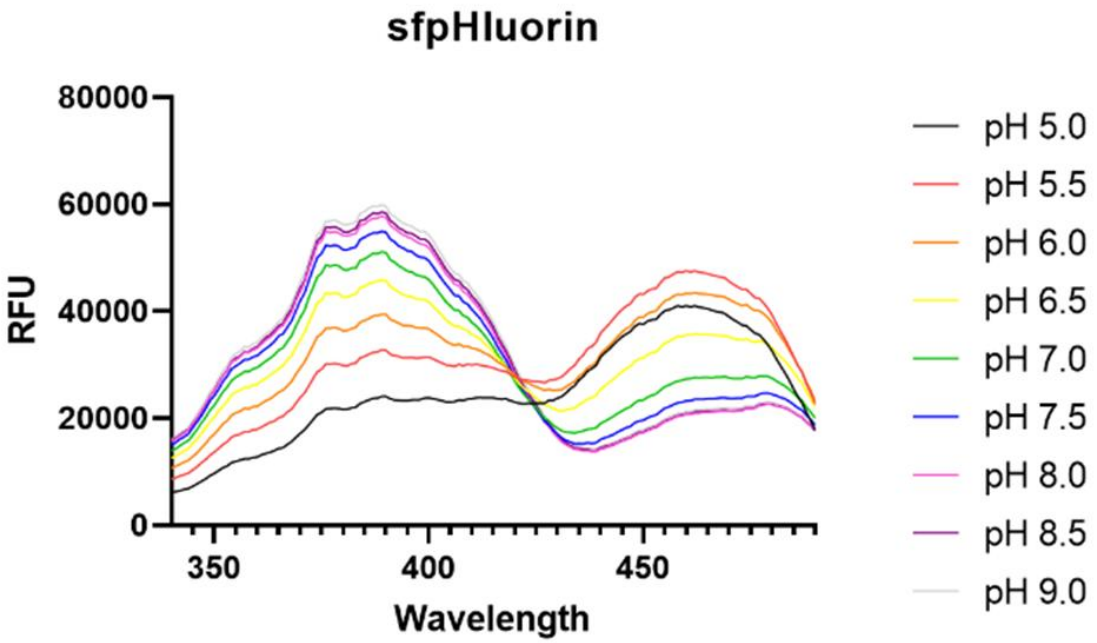

Fig. S5: NF54*attB*[sfpHluorin] *in vitro* calibration in a plate reader format. Excitation spectra from 350 to 490 nm with emission sensing at 530 nm show pH responsive peaks around 390 and 482 nm. Error bars were omitted for clarity. Means of n = 3 independent experiments are shown.

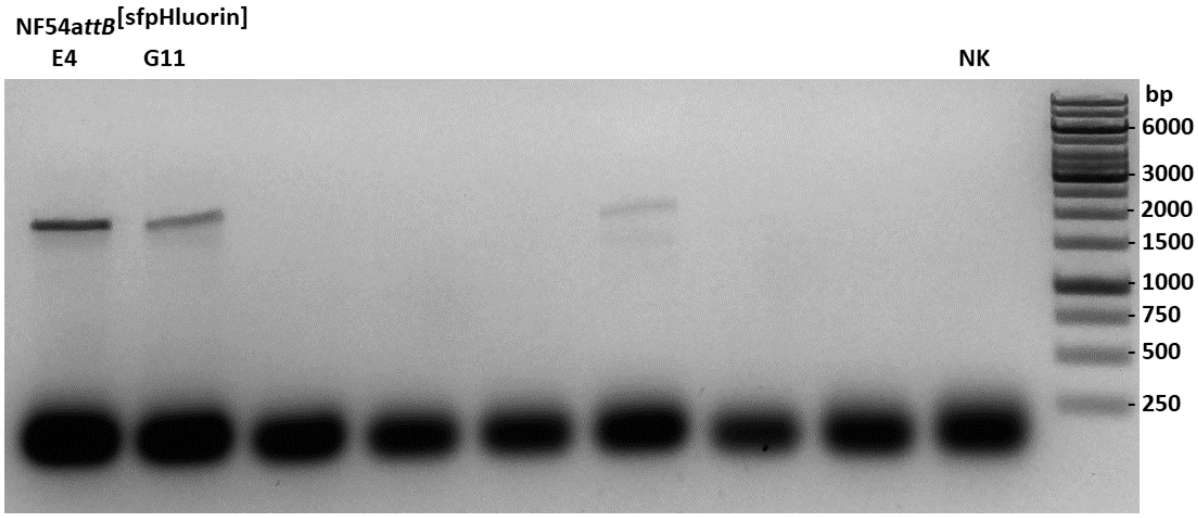

Fig. S6: Stable integration of sfpHluorin in NF54*attB*. Representative clonal cell-lines show PCR product based on genomic cg6 and integrated BSD genes, and thereby, demonstrating successful sensor integration.

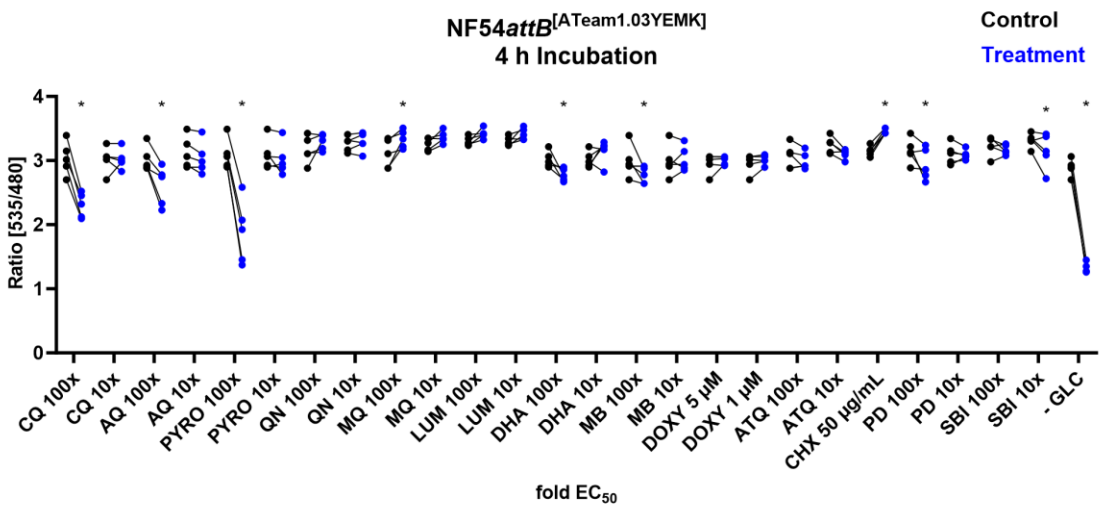

Fig. S7: NF54*attB*[ATeam1.03YEMK] shows distinct ratio changes in response towards different drug classes after 4 h incubation. Fluorescence microscopic measurement of MACS-enriched trophozite infected red blood cells. Each measurement corresponds to the 535 nm to 480 nm emission ratio after excitation at 430 nm. Mean of 100 single cell analyses of compound intervention (Treatment) and contemporaneous vehicle control (Control) with n = 5 independent experiments are shown. Treatment groups included chloroquine (CQ), amodiaquine (AQ), pyronaridine (PYRO), quinine (QN), mefloquine (MQ), lumefantrine (LUM), dihydroartemisinin (DHA), methylene blue (MB), doxycycline (DOXY), atovaquone (ATQ), cycloheximide (CHX), plasmodione (PD), SBI 0797750 (SBI), and glucose starvation (-GLC). Cells were starved from GLC through washing in PBS just before measurement. If not indicated otherwise, compounds were applied with 100x and 10x EC_{50} concentration. * indicates discovery with FDR = 5 %.

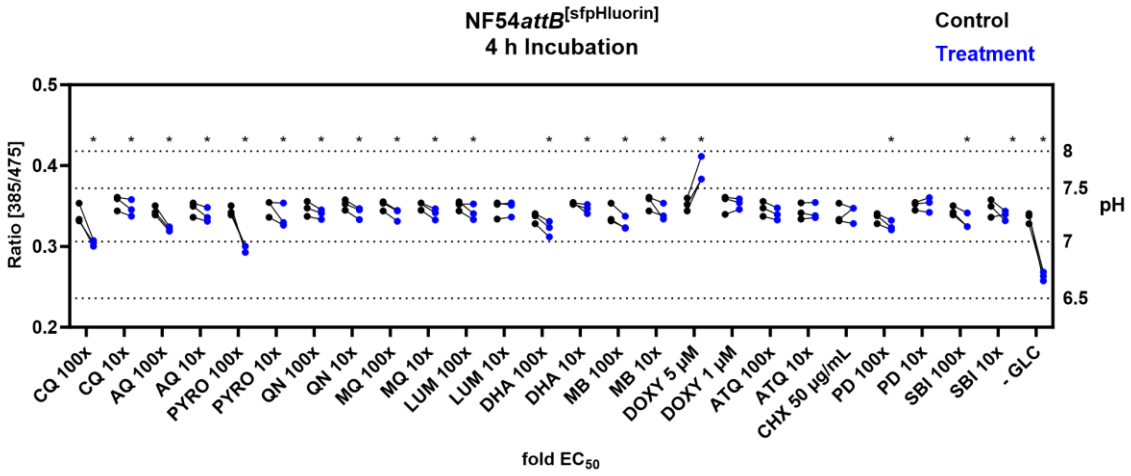

Fig. S8: NF54*attB*[sfpHluorin] shows predominantly marginal ratio changes in response towards different drug classes after 4 h incubation time. Fluorescence microscopic measurement of MACS-enriched trophozite infected red blood cells. Each measurement corresponds to the 385 to 475 nm excitation ratio at 525 nm emission. Mean of 100 single cell analyses of compound intervention (Treatment) and concurrent vehicle control (Control) with n = 3 independent experiments are shown. Treatment groups included chloroquine (CQ), amodiaquine (AQ), pyronaridine (PYRO), quinine (QN), mefloquine (MQ), lumefantrine (LUM), dihydroartemisinin (DHA), methylene blue (MB), doxycycline (DOXY), atovaquone (ATQ),

cycloheximide (CHX), plasmodione (PD), SBI 0797750 (SBI), and glucose starvation (-GLC). Cells were starved from GLC through washing in PBS just before measurement. If not indicated otherwise, compounds were applied with 100x and 10x EC_{50} concentration. * indicates discovery with FDR = 5 %.

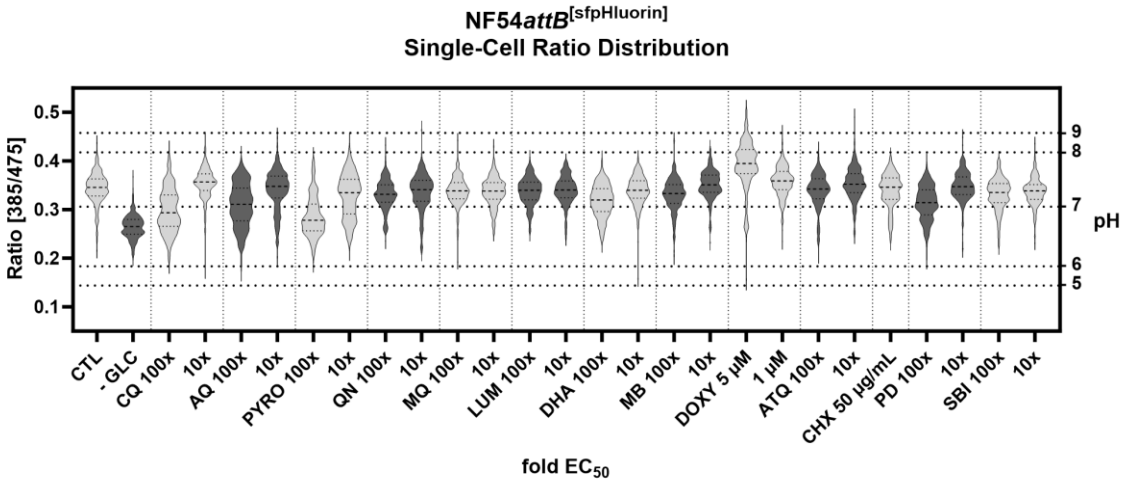

Fig. S9: NF54*attB*[sfpHluorin] shows distinct single-cell excitation ratio distribution in response towards different drug classes. Fluorescence microscopic measurement of MACS-enriched trophozite-iRBCs. Each measurement corresponds to the 385 to 475 nm excitation ratio at 525 nm emission. Pool of n = 3 independent experiments with each 100 single cell analyses is shown. Treatment groups included chloroquine (CQ), amodiaquine (AQ), pyronaridine (PYRO), quinine (QN), mefloquine (MQ), lumefantrine (LUM), dihydroartemisinin (DHA), methylene blue (MB), doxycycline (DOXY), atovaquone (ATQ), cycloheximide (CHX), plasmodione (PD), SBI 0797750 (SBI), and glucose starvation (-GLC). Cells were starved from GLC through washing in PBS just before measurement. If not indicated otherwise, compounds were applied with 100x and 10x EC_{50} concentration.

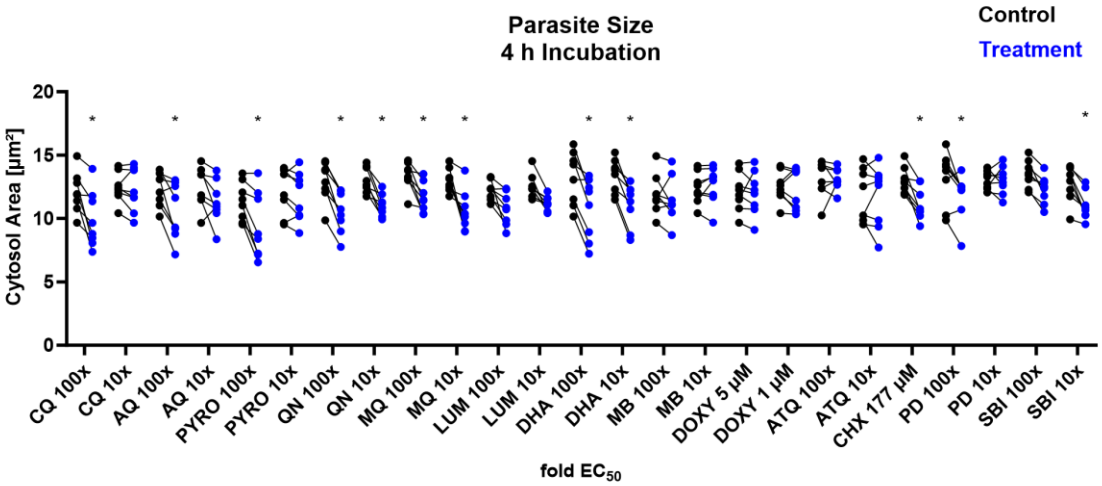

Fig. S10 NF54*attB*[ATeam1.03YEMK] and NF54*attB*[sfpHluorin] show decreased parasite size in response towards different drug classes after 4 h incubation. The mean cytosol size of 100 MACS-enriched trophozite infected red blood cells derived from automated ROI definition from fluorescence microscopic measurements of NF54*attB*[ATeam1.03YEMK] (n = 5) and NF54*attB*[sfpHluorin] (n = 3) is combined. Analyses of compound intervention

(Treatment) and concurrent vehicle control (Control) with in total n = 8 independent experiments are shown. Treatment groups included chloroquine (CQ), amodiaquine (AQ), pyronaridine (PYRO), quinine (QN), mefloquine (MQ), lumefantrine (LUM), dihydroartemisinin (DHA), methylene blue (MB), doxycycline (DOXY), atovaquone (ATQ), cycloheximide (CHX), plasmodione (PD), and SBI 0797750 (SBI). If not indicated otherwise, compounds were applied with 100x and 10x EC_{50} concentration. * indicates discovery with FDR = 5 %.

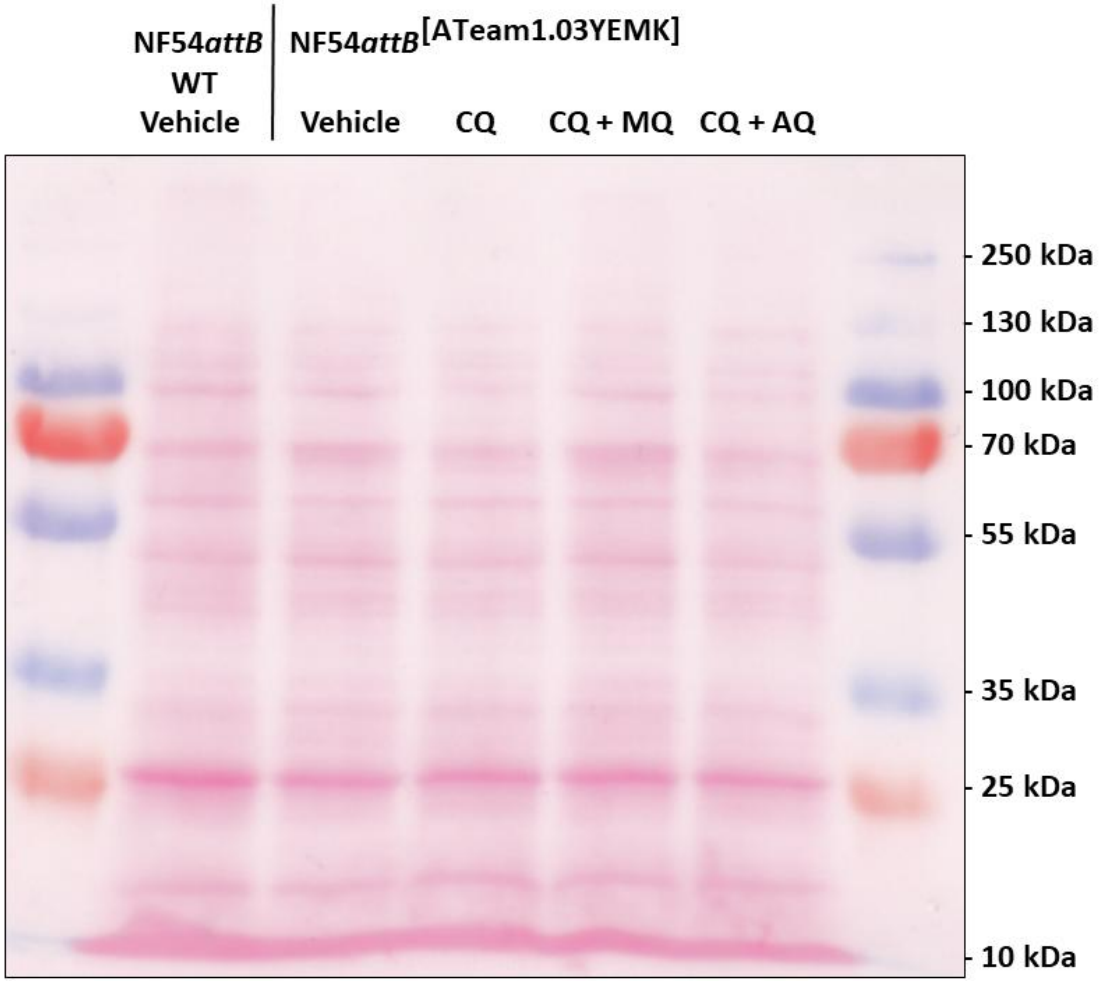

Fig. S11: Ponceau S protein staining demonstrates sample loading.

Table S1: EC_{50} concentrations used for drug incubation of sensor cell lines. EC_{50} values were either measured (PYRO) or orientated to results in the literature.

Compound	EC_{50}
CQ	6.9 nM (1)
AQ	3.4 nM (1)
PYRO	2.84 ± 0.77 (this study)
QN	66.2 nM (1)
MQ	23.4 nM (1)
LUM	10.7 nM (1)
DHA	5 nM (2)
MB	3.3 nM (3)

ATQ	0.5 nM (1)
PD	50 nM (4)
SBI	83.8 nM (5)

Table S2: Two-Way ANOVA analysis of for concurrent control and treatment of NF54*attB*$^{[ATeam1.03YEMK]}$ after 6 h incubation time with two-stage linear step-up.

Treatment	Mean Diff.	Discovery?	q value	Individual P Value
CQ 100x	1.000	Yes	<0.0001	<0.0001
CQ 10x	0.02959	No	0.3796	0.6928
AQ 100x	0.7095	Yes	<0.0001	<0.0001
AQ 10x	0.1803	Yes	0.0170	0.0175
PYRO 100x	1.608	Yes	<0.0001	<0.0001
PYRO 10x	0.2056	Yes	0.0080	0.0070
QN 100x	-0.1170	No	0.0843	0.1205
QN 10x	-0.07470	No	0.2120	0.3196
MQ 100x	-0.1774	Yes	0.0174	0.0194
MQ 10x	-0.1963	Yes	0.0104	0.0099
LUM 100x	-0.2276	Yes	0.0041	0.0029
LUM 10x	-0.2153	Yes	0.0061	0.0048
DHA 100x	0.5730	Yes	<0.0001	<0.0001
DHA 10x	-0.1431	Yes	0.0489	0.0582
MB 100x	0.3145	Yes	<0.0001	<0.0001
MB 10x	-0.01869	No	0.4148	0.8029
DOXY 5 µM	-0.01544	No	0.4148	0.8367
DOXY 1 µM	-0.01360	No	0.4148	0.8559
ATQ 100x	0.1178	No	0.0843	0.1179
ATQ 10x	0.05975	No	0.2438	0.4256
CHX 50 µg/mL	-0.3833	Yes	<0.0001	<0.0001
PD 100x	0.5180	Yes	<0.0001	<0.0001
PD 10x	0.07006	No	0.2208	0.3505
SBI 100x	-0.06399	No	0.2362	0.3936
SBI 10x	0.1360	No	0.0563	0.0714
- GLC	1.595	Yes	<0.0001	<0.0001

Table S3: Two-Way ANOVA analysis for concurrent control and treatment of NF54*attB*$^{[ATeam1.03YEMK]}$ after 4 h incubation time with two-stage linear step-up.

Treatment	Mean Diff.	Discovery?	q value	Individual P Value
CQ 100x	0.7303	Yes	<0.0001	<0.0001
CQ 10x	0.0006286	No	0.6415	0.9928
AQ 100x	0.4177	Yes	<0.0001	<0.0001
AQ 10x	0.08382	No	0.2274	0.2301
PYRO 100x	1.216	Yes	<0.0001	<0.0001
PYRO 10x	0.07649	No	0.2550	0.2732
QN 100x	-0.1189	No	0.1162	0.0899
QN 10x	-0.02805	No	0.4810	0.6871
MQ 100x	-0.2271	Yes	0.0035	0.0015

MQ 10x	-0.1097	No	0.1232	0.1173
LUM 100x	-0.1133	No	0.1232	0.1057
LUM 10x	-0.1103	No	0.1232	0.1151
DHA 100x	0.2387	Yes	0.0024	0.0008
DHA 10x	-0.1293	No	0.0916	0.0654
MB 100x	0.2240	Yes	0.0035	0.0017
MB 10x	-0.03194	No	0.4722	0.6465
DOXY 5 µM	-0.04523	No	0.3942	0.5163
DOXY 1 µM	-0.05024	No	0.3793	0.4710
ATQ 100x	0.06981	No	0.2803	0.3171
ATQ 10x	0.1436	No	0.0627	0.0411
CHX 50 µg/mL	-0.3122	Yes	<0.0001	<0.0001
PD 100x	0.2124	Yes	0.0053	0.0028
PD 10x	0.01526	No	0.5554	0.8264
SBI 100x	0.04988	No	0.3793	0.4742
SBI 10x	0.1692	Yes	0.0278	0.0165
- GLC	1.571	Yes	<0.0001	<0.0001

Table S4: Two-Way ANOVA analysis for concurrent control and treatment of NF54*attB*$^{[sfpHluorin]}$ after 6 h incubation time with two-stage linear step-up procedure.

Treatment	Mean Diff.	Discovery?	q value	Individual P Value
CQ 100x	0.04137	Yes	<0.0001	<0.0001
CQ 10x	7.927e-005	No	0.4383	0.9867
AQ 100x	0.03300	Yes	<0.0001	<0.0001
AQ 10x	0.01757	Yes	0.0007	0.0005
PYRO 100x	0.05615	Yes	<0.0001	<0.0001
PYRO 10x	0.02381	Yes	<0.0001	<0.0001
QN 100x	0.01447	Yes	0.0035	0.0036
QN 10x	0.01047	Yes	0.0231	0.0320
MQ 100x	0.008791	Yes	0.0426	0.0699
MQ 10x	0.01454	Yes	0.0035	0.0035
LUM 100x	0.008784	Yes	0.0426	0.0701
LUM 10x	0.01175	Yes	0.0137	0.0166
DHA 100x	0.02190	Yes	<0.0001	<0.0001
DHA 10x	0.01625	Yes	0.0014	0.0012
MB 100x	0.009468	Yes	0.0350	0.0515
MB 10x	0.003244	No	0.2613	0.4976
DOXY 5 µM	-0.04388	Yes	<0.0001	<0.0001
DOXY 1 µM	-0.001992	No	0.3398	0.6766
ATQ 100x	0.006393	No	0.1064	0.1842
ATQ 10x	0.001578	No	0.3567	0.7411
CHX 50 µg/mL	0.0006628	No	0.4110	0.8896
PD 100x	0.02671	Yes	<0.0001	<0.0001
PD 10x	0.003522	No	0.2540	0.4618
SBI 100x	0.01102	Yes	0.0187	0.0243
SBI 10x	0.01246	Yes	0.0102	0.0114
- GLC	0.07512	Yes	<0.0001	<0.0001

Table S5: Two-Way ANOVA analysis for concurrent control and treatment of NF54*attB*[sfpHluorin] after 4 h incubation time with two-stage linear step-up procedure.

Treatment	Mean Diff.	Discovery?	q value	Individual P Value
CQ 100x	0.7303	Yes	<0.0001	<0.0001
CQ 10x	0.0006286	No	0.6415	0.9928
AQ 100x	0.4177	Yes	<0.0001	<0.0001
AQ 10x	0.08382	No	0.2274	0.2301
PYRO 100x	1.216	Yes	<0.0001	<0.0001
PYRO 10x	0.07649	No	0.2550	0.2732
QN 100x	-0.1189	No	0.1162	0.0899
QN 10x	-0.02805	No	0.4810	0.6871
MQ 100x	-0.2271	Yes	0.0035	0.0015
MQ 10x	-0.1097	No	0.1232	0.1173
LUM 100x	-0.1133	No	0.1232	0.1057
LUM 10x	-0.1103	No	0.1232	0.1151
DHA 100x	0.2387	Yes	0.0024	0.0008
DHA 10x	-0.1293	No	0.0916	0.0654
MB 100x	0.2240	Yes	0.0035	0.0017
MB 10x	-0.03194	No	0.4722	0.6465
DOXY 5 µM	-0.04523	No	0.3942	0.5163
DOXY 1 µM	-0.05024	No	0.3793	0.4710
ATQ 100x	0.06981	No	0.2803	0.3171
ATQ 10x	0.1436	No	0.0627	0.0411
CHX 50 µg/mL	-0.3122	Yes	<0.0001	<0.0001
PD 100x	0.2124	Yes	0.0053	0.0028
PD 10x	0.01526	No	0.5554	0.8264
SBI 100x	0.04988	No	0.3793	0.4742
SBI 10x	0.1692	Yes	0.0278	0.0165
- GLC	1.571	Yes	<0.0001	<0.0001

Table S6: Two-Way ANOVA analysis of parasite size for concurrent control and treatment of NF54*attB*[ATeam1.03YEMK] and NF54*attB*[sfpHluorin] parasites after 6 h incubation time with two-stage linear step-up procedure.

Treatment	Mean Diff.	Discovery?	q value	Individual P Value
CQ 100x	2.145	Yes	<0.0001	<0.0001
CQ 10x	0.2619	No	0.2672	0.5371
AQ 100x	1.735	Yes	<0.0001	<0.0001
AQ 10x	1.163	Yes	0.0039	0.0067
PYRO 100x	1.924	Yes	<0.0001	<0.0001
PYRO 10x	0.4574	No	0.1566	0.2817
QN 100x	2.465	Yes	<0.0001	<0.0001
QN 10x	2.010	Yes	<0.0001	<0.0001
MQ 100x	1.775	Yes	<0.0001	<0.0001
MQ 10x	2.427	Yes	<0.0001	<0.0001
LUM 100x	1.475	Yes	0.0005	0.0006

LUM 10x	1.349	Yes	0.0012	0.0017
DHA 100x	2.428	Yes	<0.0001	<0.0001
DHA 10x	2.287	Yes	<0.0001	<0.0001
MB 100x	0.4181	No	0.1706	0.3249
MB 10x	-0.2114	No	0.2782	0.6183
DOXY 5 µM	0.1008	No	0.3415	0.8121
DOXY 1 µM	0.2199	No	0.2782	0.6043
ATQ 100x	0.009156	No	0.3715	0.9828
ATQ 10x	0.09041	No	0.3415	0.8312
CHX 177 µM	1.856	Yes	<0.0001	<0.0001
PD 100x	1.413	Yes	0.0008	0.0010
PD 10x	0.02024	No	0.3715	0.9619
SBI 100x	1.260	Yes	0.0021	0.0034
SBI 10x	1.761	Yes	<0.0001	<0.0001

Table S7: Two-Way ANOVA analysis of parasite size for concurrent control and treatment of NF54*attB*$^{[ATeam1.03YEMK]}$ and NF54*attB*$^{[sfpHluorin]}$ parasites after 4 h incubation time with two-stage linear step-up procedure.

Treatment	Mean Diff.	Discovery?	q value	Individual P Value
CQ 100x	1.470	Yes	0.0005	0.0003
CQ 10x	0.3620	No	0.2945	0.3667
AQ 100x	1.697	Yes	<0.0001	<0.0001
AQ 10x	0.3126	No	0.3302	0.4355
PYRO 100x	1.993	Yes	<0.0001	<0.0001
PYRO 10x	0.1888	No	0.4351	0.6375
QN 100x	2.475	Yes	<0.0001	<0.0001
QN 10x	1.266	Yes	0.0025	0.0018
MQ 100x	1.614	Yes	0.0002	<0.0001
MQ 10x	1.688	Yes	<0.0001	<0.0001
LUM 100x	0.6219	No	0.1133	0.1218
LUM 10x	-0.02293	No	0.5211	0.9544
DHA 100x	2.030	Yes	<0.0001	<0.0001
DHA 10x	1.449	Yes	0.0006	0.0004
MB 100x	-0.2095	No	0.4319	0.6012
MB 10x	0.1049	No	0.4513	0.7935
DOXY 5 µM	-0.1427	No	0.4513	0.7216
DOXY 1 µM	0.1050	No	0.4513	0.7932
ATQ 100x	-0.1195	No	0.4513	0.7656
ATQ 10x	-0.4707	No	0.2055	0.2409
CHX 177 µM	1.770	Yes	<0.0001	<0.0001
PD 100x	1.182	Yes	0.0044	0.0035
PD 10x	0.6174	No	0.1133	0.1245
SBI 100x	0.7174	No	0.0784	0.0746
SBI 10x	1.110	Yes	0.0070	0.0061

Table S8: pH values of compound interventions after 6 h incubation.

6 h Incubation	95 % Confidence Interval

Compound fold EC_{50}	Mean pH	Lower Limit	Upper Limit
CQ 100x	6.95	6.90	6.99
CQ 10x	7.35	7.30	7.40
AQ 100x	7.02	6.98	7.07
AQ 10x	7.18	7.13	7.22
PYRO 100x	6.86	6.82	6.90
PYRO 10x	7.15	7.11	7.20
QN 100x	7.17	7.13	7.22
QN 10x	7.26	7.21	7.31
MQ 100x	7.23	7.18	7.27
MQ 10x	7.21	7.17	7.26
LUM 100x	7.22	7.18	7.27
LUM 10x	7.24	7.19	7.29
DHA 100x	7.08	7.04	7.13
DHA 10x	7.23	7.19	7.28
MB 100x	7.17	7.12	7.22
MB 10x	7.33	7.28	7.38
DOXY 5 µM	7.68	7.62	7.75
DOXY 1 µM	7.38	7.32	7.43
ATQ 100x	7.23	7.18	7.28
ATQ 10x	7.29	7.24	7.34
CHX 50 µg/mL	7.23	7.19	7.28
PD 100x	7.05	7.01	7.09
PD 10x	7.30	7.25	7.35
SBI 100x	7.18	7.13	7.22
SBI 10x	7.22	7.18	7.27
- GLC	6.71	6.67	6.76

Table S9: pH values of compound interventions after 4 h incubation.

4 h Incubation		95 % Confidence Interval	
Compound fold EC_{50}	**Mean pH**	**Lower Limit**	**Upper Limit**
CQ 100x	6.98	6.94	7.03
CQ 10x	7.29	7.24	7.35
AQ 100x	7.11	7.06	7.15
AQ 10x	7.23	7.18	7.28
PYRO 100x	6.94	6.90	6.98
PYRO 10x	7.22	7.17	7.26
QN 100x	7.24	7.19	7.29
QN 10x	7.25	7.21	7.30
MQ 100x	7.24	7.19	7.29
MQ 10x	7.24	7.20	7.29
LUM 100x	7.26	7.21	7.31

LUM 10x	7.29	7.25	7.35
DHA 100x	7.11	7.07	7.16
DHA 10x	7.29	7.24	7.34
MB 100x	7.15	7.11	7.20
MB 10x	7.25	7.21	7.30
DOXY 5 µM	7.70	7.63	7.76
DOXY 1 µM	7.34	7.29	7.39
ATQ 100x	7.24	7.19	7.29
ATQ 10x	7.26	7.21	7.31
CHX 50 µg/mL	7.25	7.20	7.30
PD 100x	7.13	7.09	7.18
PD 10x	7.33	7.28	7.39
SBI 100x	7.17	7.12	7.22
SBI 10x	7.23	7.18	7.28
- GLC	6.70	6.65	6.75

Table S10: Primer Sequences.

Stable Integration	
cg6F	5'-GAAAATATTATTACAAAGGGTGAGG-3'
bsdR	5'-ACGAATTCTTAGCTAATTCGCTTGTAAGA-3'
Molecular Cloning	
ATeamF	5'-ATATGGATCCCCTAGGATGGTGAGCAAGGGCGAGGAGCTGT-3'
ATeamR	5'-ATATAAGCTTCTCGAGTTACTCGATGTTGTGGCGGATCTTGAAGTTGGCCTTG-3'
sfpHluprinF	5'-ATATGGATCCCCTAGGATGAGCAAAGGAGAAGAACTTTTCAC-3'
sfpHluprinR	5'-ATATAAGCTTCCCGGGTTATTTGTAGAGCTCATCCATGCC-3'

References

1. Schuh AK, Rahbari M, Heimsch KC, Mohring F, Gabryszewski SJ, Weder S, Buchholz K, Rahlfs S, Fidock DA, Becker K. 2018. Stable Integration and Comparison of hGrx1-roGFP2 and sfroGFP2 Redox Probes in the Malaria Parasite Plasmodium falciparum. ACS Infect Dis 4:1601–12. doi:10.1021/acsinfecdis.8b00140

2. Nardella F, Halby L, Hammam E, Erdmann D, Cadet-Daniel V, Peronet R, Ménard D, Witkowski B, Mecheri S, Scherf A, Arimondo PB. 2020. DNA Methylation Bisubstrate Inhibitors Are Fast-Acting Drugs Active against Artemisinin-Resistant Plasmodium falciparum Parasites. ACS Cent Sci 6:16–21. doi:10.1021/acscentsci.9b00874

3. Pascual A, Henry M, Briolant S, Charras S, Baret E, Amalvict R, Des Huyghues Etages E, Feraud M, Rogier C, Pradines B. 2011. In vitro activity of Proveblue (methylene blue) on Plasmodium falciparum strains resistant to standard

antimalarial drugs. Antimicrob Agents Chemother 55:2472–4. doi:10.1128/AAC.01466-10

4. Cichocki BA, Donzel M, Heimsch KC, Lesanavičius M, Feng L, Montagut EJ, Becker K, Aliverti A, Elhabiri M, Čėnas N, Davioud-Charvet E. 2021. Plasmodium falciparum Ferredoxin-NADP+ Reductase-Catalyzed Redox Cycling of Plasmodione Generates Both Predicted Key Drug Metabolites: Implication for Antimalarial Drug Development. ACS Infect Dis 7:1996–2012. doi:10.1021/acsinfecdis.1c00054

5. Berneburg I, Peddibhotla S, Heimsch KC, Haeussler K, Maloney P, Gosalia P, Preuss J, Rahbari M, Skorokhod O, Valente E, Ulliers D, Simula LF, Buchholz K, Hedrick MP, Hershberger P, Chung TDY, Jackson MR, Schwarzer E, Rahlfs S, Bode L, Becker K, Pinkerton AB. 2022. An Optimized Dihydrodibenzothiazepine Lead Compound (SBI-0797750) as a Potent and Selective Inhibitor of Plasmodium falciparum and P. vivax Glucose 6-Phosphate Dehydrogenase 6-Phosphogluconolactonase. Antimicrob Agents Chemother 66:e0210921. doi:10.1128/aac.02109-21

2.2 Publication II

Arylmethylamino steroid compound 1o interferes with *Plasmodium falciparum*'s hemoglobin metabolism

Springer, E., Heimsch, K. C., Sidiropoulos, N., Krijnse Locker, J., Przyborski J. M.

Antimicrobial Agents and Chemotherapy, *69*(8). e0033225.

2025

https://doi.org/10.1128/aac.00332-25

AMERICAN SOCIETY FOR MICROBIOLOGY | Antimicrobial Agents and Chemotherapy

Arylmethylamino steroid compound 1o interferes with *Plasmodium falciparum's* hemoglobin metabolism

Eric Springer,[1] Kim C. Heimsch,[1] Niklas Sidiropoulos,[1] Jacomina Krijnse Locker,[2] Jude M. Przyborski[1]

AUTHOR AFFILIATIONS See affiliation list on p. 18.

ABSTRACT The anti-parasitic compound arylmethylamino steroid 1o (1o) is a promising drug candidate with low nanomolar activity against the malaria parasite *Plasmodium falciparum*, but with a so far unknown mode of action. To address this, we applied previously developed live-cell ATP and pH assays to measure effects upon exposure of parasites to 1o. Furthermore, we analyzed the parasites' heme species distribution, the ultrastructural morphology, food vacuole (FV) appearance, and lifecycle development of different parasite stages. We found that 1o increases cytosolic [ATP] level and causes a slight drop in pH, similar to the effects of arylamino alcohols such as mefloquine. The compound also prevents chloroquine (CQ)-mediated proteolysis and limits cytosol acidification within the range of its EC_{50}. Additionally, 1o prevents CQ-mediated heme and hemoglobin accumulation, and preserves ultrastructural FV integrity. Furthermore, we can demonstrate that 1o blocks the development of ring and early trophozoite stages, while late trophozoite stages were unaffected. These findings suggest that the mechanism underlying the killing activity of 1o may be the interference of a pathway within or upstream of hemoglobin digestion, particularly during the highly metabolically active earlier parasite stages. Our data open a new perspective on the compound's mode of action, information critically needed for target identification and further drug development.

KEYWORDS ATeam1.03YEMK, ATP, sfpHluorin, arylmethylamino steroids, hemoglobin, heme, malaria, *Plasmodium*

Malaria remains one of the greatest public health burdens for humankind, with 263 million estimated cases worldwide in 2023. Of these, around 597,000 people died, the majority of victims being children under the age of five. Among *Plasmodium* species, *Plasmodium falciparum* causes most infections and leads to the deadliest form of the disease (1). Rising resistance against antimalarials is of increasing concern, and therefore, basic research on the development of new drugs is critical for global health. Known anti-malarial drugs appear to kill the parasite by inhibition of a number of different pathways, although for several well-known drugs, the exact mode of action (MoA) is unclear or still under discussion. An understanding of the MoA of these drugs can lead to an insight into how resistances generate and spreads across populations and allow optimization of existing and future compounds to avoid the development of resistance.

The arylmethylamino steroid compound 1o (1o) is a promising drug candidate and antiplasmodial compound. It shows low nanomolar activity against chloroquine (CQ) sensitive and resistant strains, drastic cure rates in a *Plasmodium berghei* animal model (2), and demonstrates a good toxicity profile in mammalian cells and mice (2, 3). Although it has been proposed that the compound exerts its effects by covalent protein crosslinking (2), experimental evidence for a specific mechanism of action is lacking.

Editor Audrey Odom John, The Children's Hospital of Philadelphia, Philadelphia, Pennsylvania, USA

Address correspondence to Jude M. Przyborski, Jude.Przyborski@ernaehrung.uni-giessen.de.

The authors declare no conflict of interest.

See the funding table on p. 19.

Received 27 February 2025
Accepted 12 May 2025
Published 23 June 2025

We used various MoA analysis techniques to advance a deeper understanding of the effects of compound 1o. We have previously used genetically-encoded biosensors to measure pH and [ATP] changes in response to various antimalarial drugs, including 4-aminoquinolines and arylamino alcohols. We observed distinct sensor-response patterns, depending on the class of compounds used (4). Here, we applied the same techniques to monitor responses to 1o. We detected increased [ATP], as well as a slight effect on pH in trophozoites upon exposure to 1o. These effects are similar to those we previously observed using established arylamino alcohol-based antimalarials, such as mefloquine (MQ). Though the exact parasite-killing mechanism of this class of compounds remains poorly understood, they are thought to exert specific effects on the parasite's heme species distribution, cause inhibition of endocytosis, and to interfere with certain modes of action of the long-established antimalarial CQ (5–10).

Based on our initial results with the biosensors, we sought to elucidate if 1o treatment demonstrates further similarities to the arylamino alcohol class of antimalarials, including interference in hemoglobin (Hb) metabolism and interaction with CQ-induced phenotypes. These experiments reveal that 1o prevents CQ-mediated proteolysis and limits cytosol acidification within the range of its EC_{50} at 72 h ($^{72h}EC_{50}$). Additionally, it prevents CQ-mediated heme and Hb accumulation, while it preserves ultrastructural food vacuole (FV) integrity. Furthermore, we can demonstrate that 1o prevents lifecycle progression of ring and early trophozoite stages, while it hardly affects the development of late trophozoite stages. These findings suggest that the parasite-killing effect of compound 1o could be interfering with a pathway within or upstream of Hb digestion and relevant for trophozoite development.

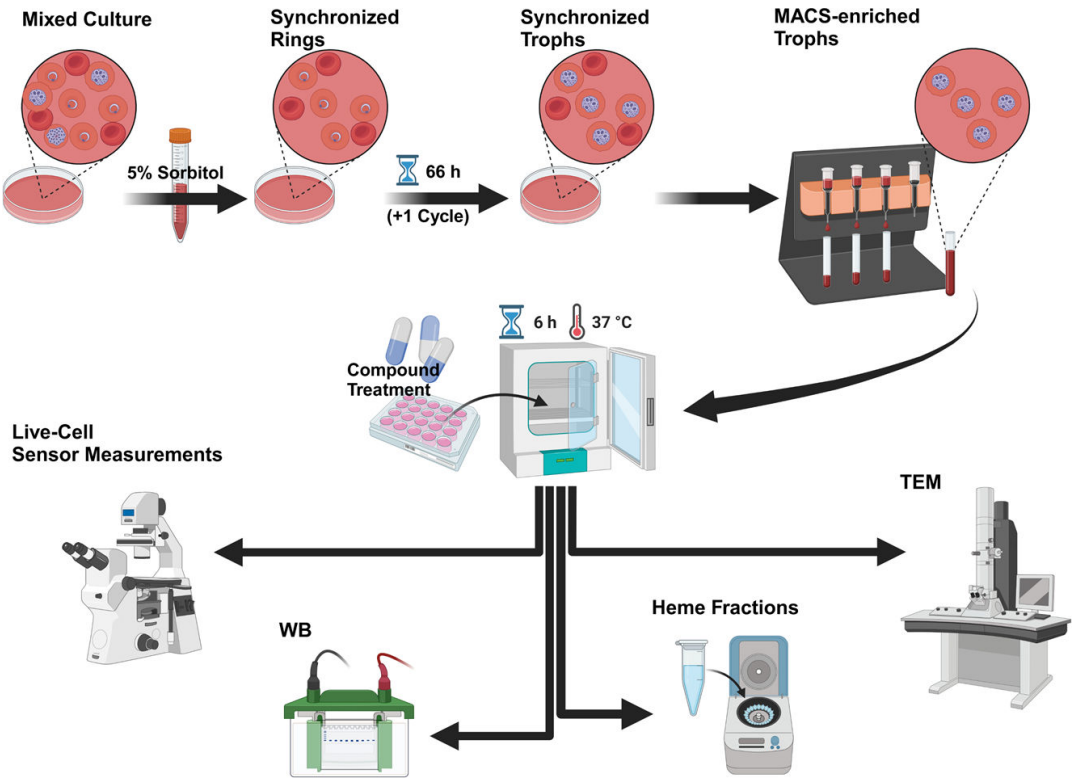

FIG 1 Workflow of trophozoite experiments. All parasites were synchronized for ring stages (Rings) via sorbitol for at least three consecutive cycles and were allowed to complete their last cycle prior to sample preparation. Trophozoites (Trophs) were enriched using magnetic activated cell sorting (MACS), treated with compounds or vehicle, and incubated under standard conditions prior to live-cell measurements, western blot (WB), heme fractionation, and transmission electron microscopy (TEM). Created in BioRender.

RESULTS

1o affects [ATP], pH, and parasite growth

To monitor changes in [ATP] upon 1o (Fig. S1) treatment, we applied our previously established techniques (4). To ensure comparability to our previously published results, we used an identical streamlined purification and incubation design for all experiments (Fig. 1). We started our time series with mid-trophozoite stage parasites, as these stages are highly metabolically active and are also easier to image than younger stages. We were interested in compound treatments with up to 100-fold of the $^{72h}EC_{50}$. To this end, we determined a $^{72h}EC_{50}$ of 4.6 ± 0.1 nM for compound 1o using the NF54*attB*$^{[ATeam1.03YEMK]}$ sensor cell line (Fig. S2A) and used this as the basis for all further experiments. Using recombinant ATeam1.03YEMK and sfpHluorin sensor protein, we could not detect significant interference within our desired concentration range, due to direct drug-sensor interactions (Fig. S2B and C).

The ATeam1.03YEMK ATP sensor (11) is based on intramolecular Förster resonance energy transfer (FRET [Fig. 2A]), and its emission ratio can be used as a measure of [ATP] (4). The sfpHluorin sensor (12) changes its excitation properties upon pH changes (Fig. 2B). Additionally, we used the fluorescence of the cytosolic sensor as a proxy for parasite size (Fig. 2C). We could detect significantly elevated cytosolic [ATP] in trophozoite stage parasites at the 6 h endpoint upon treatment with 2x and 10x $^{72h}EC_{50}$ 1o (Fig. 3A and B). We could detect a slight drop in mean cytosolic pH (95% confidence interval) from 7.27 to 7.18 (7.13–7.22) after 6 h 10x $^{72h}EC_{50}$ 1o incubation (Fig. 3C and D). Importantly, this is still within the pH range that allows reliable [ATP] measurements (4). Analysis of images allowed us to detect significantly lower mean parasite size after 10x $^{72h}EC_{50}$ 1o incubation compared to the control (Fig. 3E and F).

An increase in cytosolic [ATP], a drop in pH, and a reduced parasite size upon 1o treatment is a similar phenotypic pattern to that observed when treating parasites with the arylamino alcohols MQ and lumefantrine (LUM [4]). For this reason, we measured further effects known to be induced by MQ, including inhibition of CQ-mediated phenotypes, upon 1o treatment.

1o prevents CQ-induced sensor phenotypes around its parasite-killing $^{72h}EC_{50}$

We previously showed that CQ causes degradation of the FRET-based ATP sensor ATeam1.03YEMK, causing distinct fluorescence and western blot (WB) signal attenuations, as well as cytosol acidification, which can be prevented by the arylamino alcohol MQ but not by the 4-aminoquinoline amodiaquine (AQ [4]). We attribute these effects to CQ-induced heme accumulation that is potentially lysing the parasite's FV and thereby causing proteolytic degradation in the cytosol (13–17). We wished to study whether these effects, at or around the $^{72}EC_{50}$, could be responsible for the parasite-killing activity. Thus, we determined the dose-response of 1o for correlation to its parasite-killing activity. To analyze a possible interference with Hb metabolism in more detail, we investigated effects on heme species distribution, analysis of FV integrity by transmission electron microscopy (TEM), as well as treatment of different parasite developmental stages.

We recently showed that treatment of parasites with 690 nM CQ (100x EC_{50}) causes a distinct bimodal single-cell ATP and pH level distribution, and this effect can be prevented through co-incubation with MQ (4). Co-incubation of trophozoite stage parasites of the ATP sensor cell line with 100x $^{72h}EC_{50}$ CQ and increasing concentrations of 1o (0.01x – 100x $^{72h}EC_{50}$) reveals that 1o prevents this CQ phenotype, in an apparent dose-dependent manner (Fig. 4A). The bimodal data distribution of the CQ-treated parasites shows an apparent correlation with the 25th and 75th percentile markers (Fig. 4A). In particular, the 25th percentile marker was representative of the CQ effect (in comparison to vehicle control). To enable further data analysis, we thus used this 25th percentile marker as a numerical surrogate for the CQ effect. We then used this marker for quantification of the

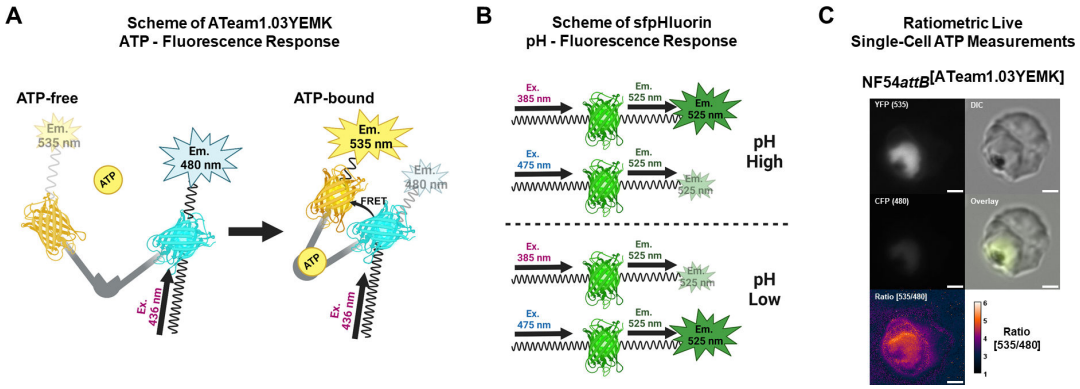

FIG 2 ATP, pH, and size determinations using genetically-encoded parasite lines. Sensor sequences were stably integrated into the *Plasmodium falciparum* NF54*attB* strain. (A) ATP measurements via ATeam1.03YEMK are based on changes in intramolecular FRET upon ATP binding, which allows ratiometric measurements of ATP levels. (B) The GFP-based sfpHlourin pH sensor changes its excitation properties upon pH changes, which is the basis for ratiometric measurements of the pH level. (C) The NF54*attB*$^{[ATeam1.03YEMK]}$ ATP sensor cell line exemplarily demonstrates ratiometric live-cell measurements via fluorescence microscopy based on the signal intensity ratio of different fluorescence channels. The mean signal intensity after background subtraction is used for ratio calculation, while the fluorescence area is used as a proxy for the parasite size. Created in BioRender.

CQ effect level. We normalized the 25th percentile ratio of the 1o co-incubations (CQ set to 100%; vehicle set to 0%) for dose-response analysis (Fig. 4B). We calculated the half-maximal effective concentration for this 1o-CQ interaction ($^{1o\text{-}CQ}EC_{50}$) and found that 1o prevents the CQ-mediated phenotype with 0.83x ± 0.36 (mean ± SD) of its parasite-killing $^{72h}EC_{50}$ (Fig. 4B). As recently shown, 100x $^{72h}EC_{50}$ CQ also causes a ratio distribution shift in trophozoites of the pH sensor cell line NF54*attB*$^{[sfpHluorin]}$ responsive to MQ (4). Using the identical experimental conditions of the previously described experiment for NF54*attB*$^{[sfpHluorin]}$, we found that 1o also prevents the CQ-characteristic sfpHluorin ratio distribution in a dose-dependent manner (Fig. 5A). Again, we used the 25th percentile as a marker for the CQ phenotype and determined the $^{1o\text{-}CQ}EC_{50}$ to equal 0.65x ± 0.10 (mean ± SD) of the parasite-killing $^{72h}EC_{50}$ (Fig. 5B).

1o prevents CQ-induced sensor degradation

In our previous study, we found that the CQ-mediated bimodal drop of the ATeam1.03YEMK ratio is accompanied by degradation of the ATeam sensor and the PfHSP90 housekeeping control protein on WB, which could be prevented by MQ (4). To investigate 1o's capabilities to prevent such degradation in red blood cells (RBCs) infected with trophozoite stage NF54*attB*$^{[ATeam1.03YEMK]}$ parasites, we used the identical experimental setup of the two previously described experiments and carried out WB analysis. Using an anti-GFP antibody that recognizes ATeam, we could detect a signal just below 70 kDa, representing intact ATeam1.03YEMK sensor (68 kDa), as well as a faint signal intensity around 25 kDa, correlating to protease-resistant GFP-based degradation products in the vehicle control parasites (Fig. 6A). CQ treatment causes the disappearance of the ATeam signal, while the signal from GFP degradation products drastically increases. Co-incubation with increasing 1o concentrations prevented ATeam degradation and fragment appearance. We could detect a similar phenomenon while analyzing PfHSP90. CQ treatment caused the disappearance of the PfHSP90 signal, while increasing 1o concentrations could prevent this effect. Normalization of the sensor fragment (Fig. 6B) and the ATeam sensor intensity (Fig. 6C) demonstrates a dose-dependent relationship of the described 1o-CQ interaction.

1o alters the parasites' heme species distribution

As arylamino alcohols such as MQ and quinine have been shown to interfere with CQ-mediated alteration of Hb and heme species (7, 10, 18, 19), we analyzed 1o's effects on absolute amounts and relative fractions of Hb, "free" heme, and hemozoin (Hz) in

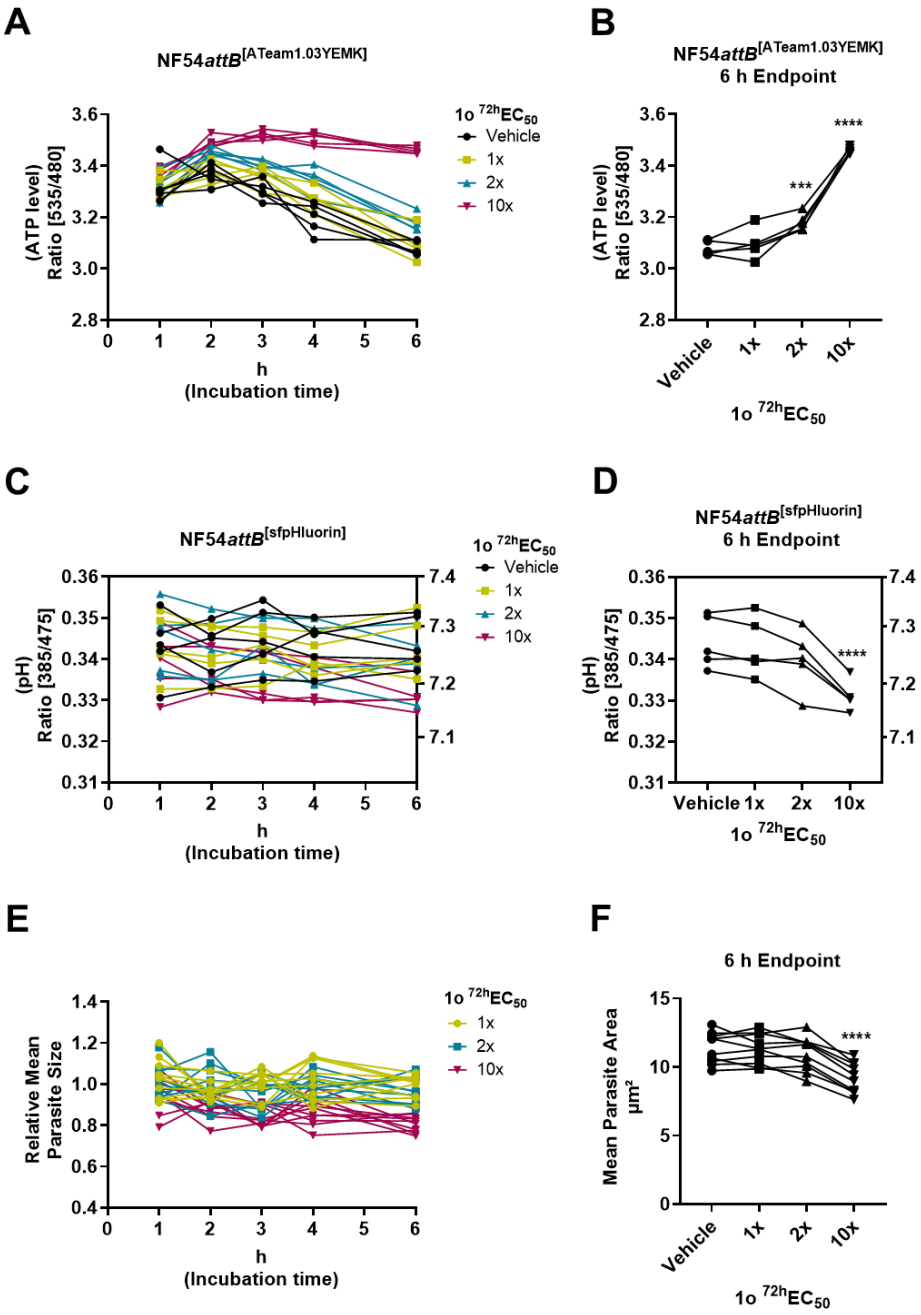

FIG 3 Compound 1o causes elevated ATP levels, a slight pH drop, and reduced parasite size in the cytosol of trophozoite stage parasites. *Plasmodium falciparum* sensor cell lines were used to measure ATP and pH levels of MACS-enriched trophozoite-infected red blood cells (iRBCs) via fluorescence microscopy 1, 2, 3, 4, and 6 h after incubation with multiples of the parasite-killing $^{72h}EC_{50}$ or vehicle control. (A and B) ATP levels were determined using the NF54*attB*$^{[ATeam1.03YEMK]}$ ATP sensor cell line via excitation at 430 nm and emission sensing at 535 and 480 nm for the YFP and CFP channels, respectively. The background-corrected YFP–CFP ratio is equivalent to the ATP level. After 6 h, the ATP level of 2x (P = 0.0004) and 10x (P < 0.0001) $^{72h}EC_{50}$-treated parasites were elevated compared to vehicle-treated controls. (C and D) pH levels were determined using the NF54*attB*$^{[sfpHluorin]}$ pH sensor cell line via excitation at 385 or 475 nm and emission sensing at 525 nm. Background-corrected emission ratio after 385 and 475 nm excitation is equivalent to the pH level. pH scale (right y-axis) was gained using nigericin *in cellulo* calibration. After 6 h, the mean pH (95% CI) of 10x (P < 0.0001) $^{72h}EC_{50}$-treated parasites was reduced to 7.18 (7.13–7.22) compared to vehicle-treated control parasites, pH 7.27 (7.22–7.32). (E and F) Cytosolic fluorescence of the sensor cell lines was used as a proxy for the parasite size. The relative mean parasite size was normalized using the concurrent vehicle-treated control in each microscopic dish. (A–D) n = 5 independent experiments. Each measurement is

(Continued on next page)

Fig 3 (Continued)

derived from the mean of 200 parasites. Statistical analysis after 6 h was conducted via two-way analysis of variance (ANOVA) and Dunnett's multiple comparisons test. Asterisks indicate significance level (***$P < 0.001$; ****$P < 0.0001$).

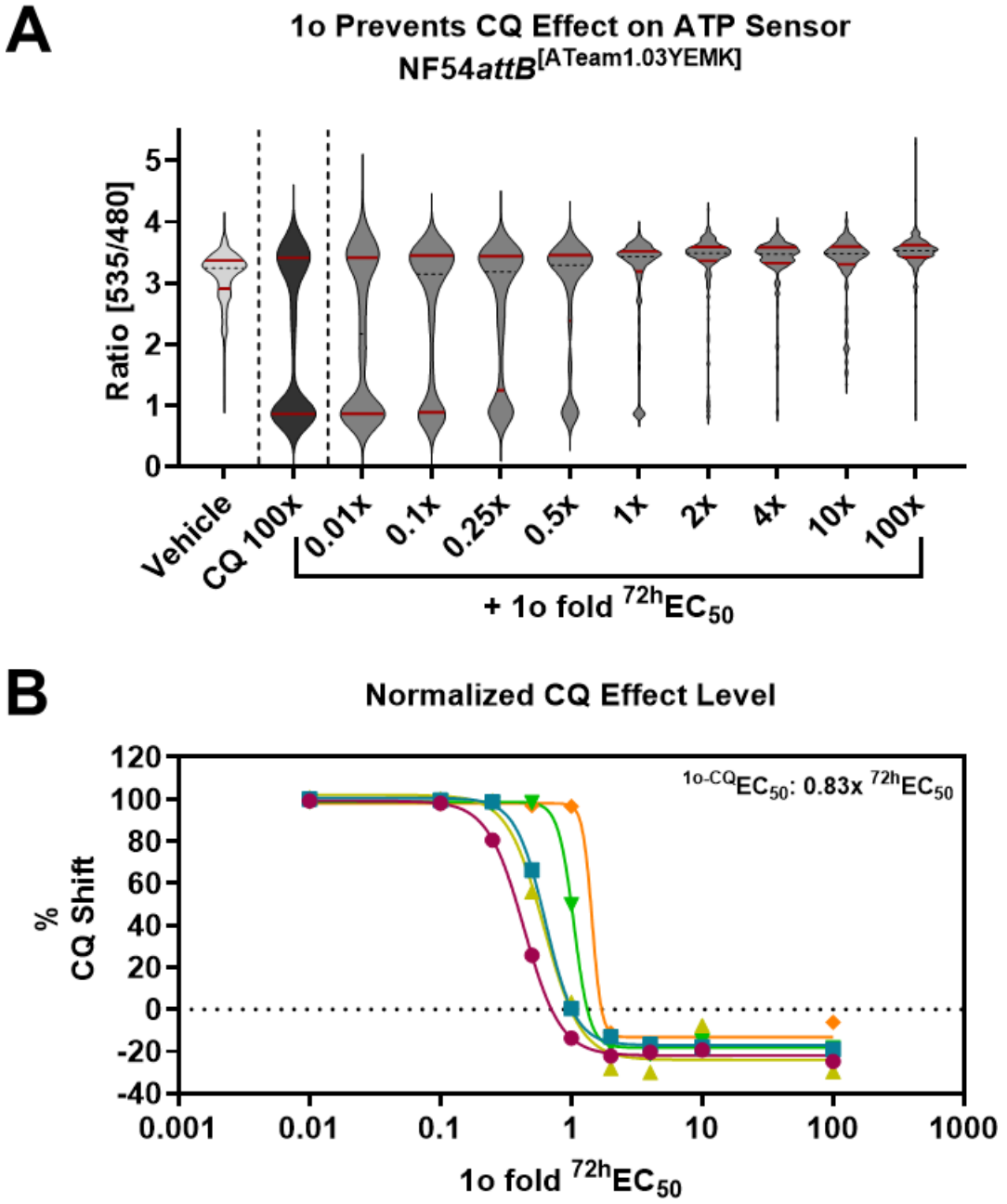

FIG 4 1o prevents CQ-mediated ATeam1.03YEMK ratio drop. (A) 100x $^{72h}EC_{50}$ CQ causes a distinct bimodal drop of the NF54*attB*$^{[ATeam1.03YEMK]}$ single-cell ratio distribution (black) compared to vehicle-treated control parasites (light gray) after excitation at 430 nm and emission sensing at 535 and 475 nm in MACS-enriched trophozoite iRBCs within the fluorescence microscopy setup. Co-incubation with increasing concentrations of 1o (0.01x – 100x $^{72h}EC_{50}$; light gray) prevents the appearance of a CQ-induced lower distribution mode in a dose-dependent manner. The solid red lines indicate the 25th and 75th percentiles. (B) Normalization of 1o's effects on the 25th percentile and plotting on a sigmoidal 4-factoral dose-response curve allows the calculation of a half-maximal effective dose of 1o on the CQ phenotype ($^{1o\text{-}CQ}EC_{50}$). $N = 5$ independent experiments are shown. The mean (±SD) $^{1o\text{-}CQ}EC_{50}$ is equivalent to 0.83x (±0.34) of the parasite-killing $^{72h}EC_{50}$. Different colored points and fit lines indicate independent replicates.

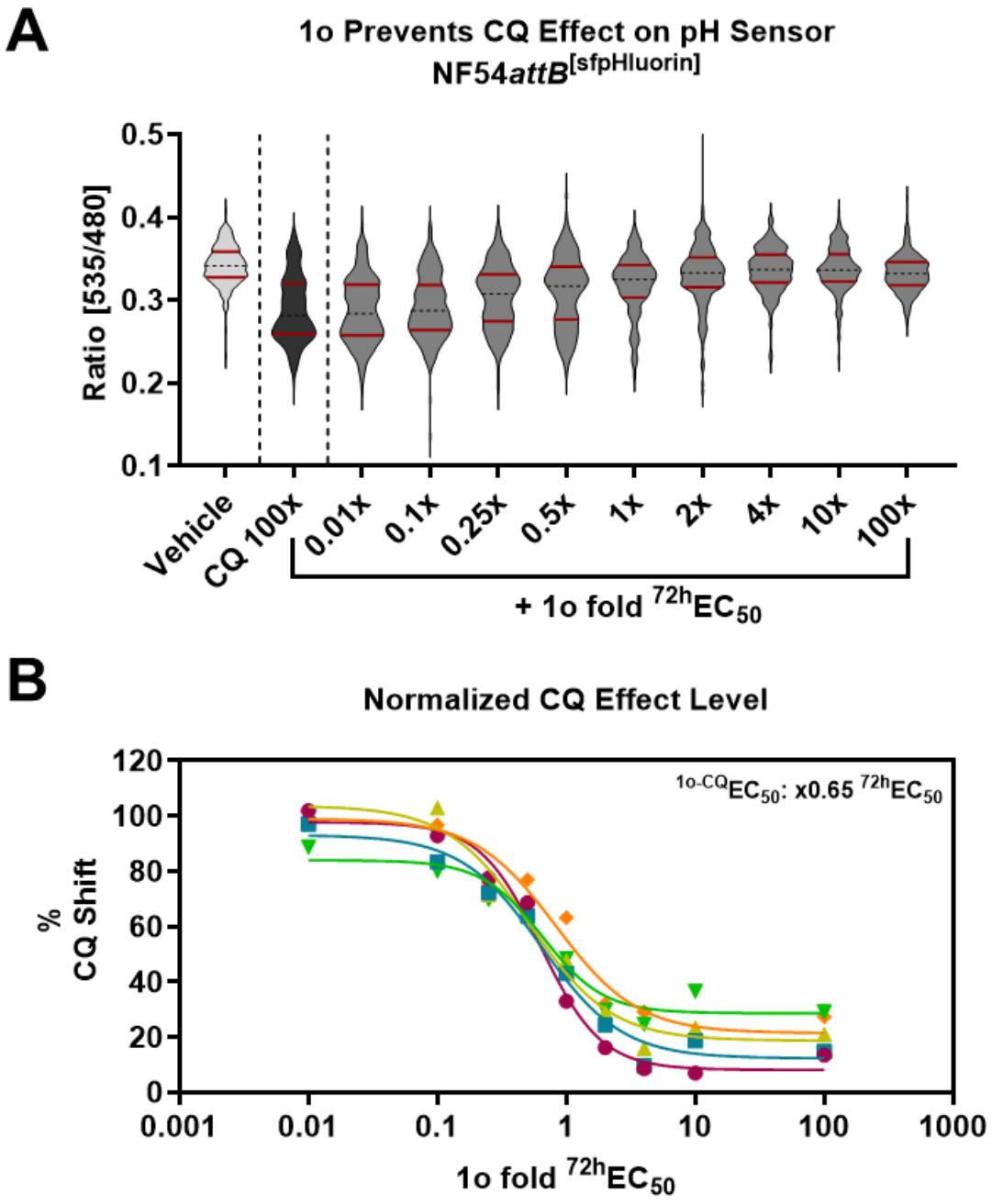

FIG 5 1o prevents CQ-mediated sfpHluorin ratio drop. (A) 100x $^{72h}EC_{50}$ CQ causes a distinct bimodal shift of the NF54*attB*$^{[sfpHluorin]}$ single-cell ratio distribution (black) compared to vehicle-treated control parasites (light gray) after excitation at 385 and 475 nm with emission sensing at 525 nm in MACS-enriched trophozoite iRBCs within the fluorescence microscopy setup. Co-incubation with increasing concentrations of 1o (0.01x – 100x $^{72h}EC_{50}$; light gray) prevents the appearance of a CQ-induced lower distribution mode in a dose-dependent manner. The solid red lines indicate the 25th and 75th percentiles. (B) Normalization of 1o's effects on the 25th percentile allows the calculation of a half-maximal effective dose of 1o on the CQ phenotype ($^{1o\text{-}CQ}EC_{50}$). *n* = 5 independent experiments are shown. The mean (±SD) $^{1o\text{-}CQ}EC_{50}$ is equivalent to 0.65x (±0.10) of the parasite-killing $^{72h}EC_{50}$. Different colored points and fit lines indicate independent replicates.

trophozoites treated with 1o. As we incubated a defined number of parasites per group, the pyridine-heme complex measured at A_{410} is equivalent to an absolute amount of the respective heme species per parasite, while the relative heme fractions reflect a heme species distribution that is independent of the parasite size. As in the previous experiments, we incubated parasites for 6 h in the presence of increasing doses of 1o (0x, 1x, 2x, 10x, 100x $^{72h}EC_{50}$) alone (Fig. 7A through F), or in co-incubation with 100x $^{72h}EC_{50}$ CQ

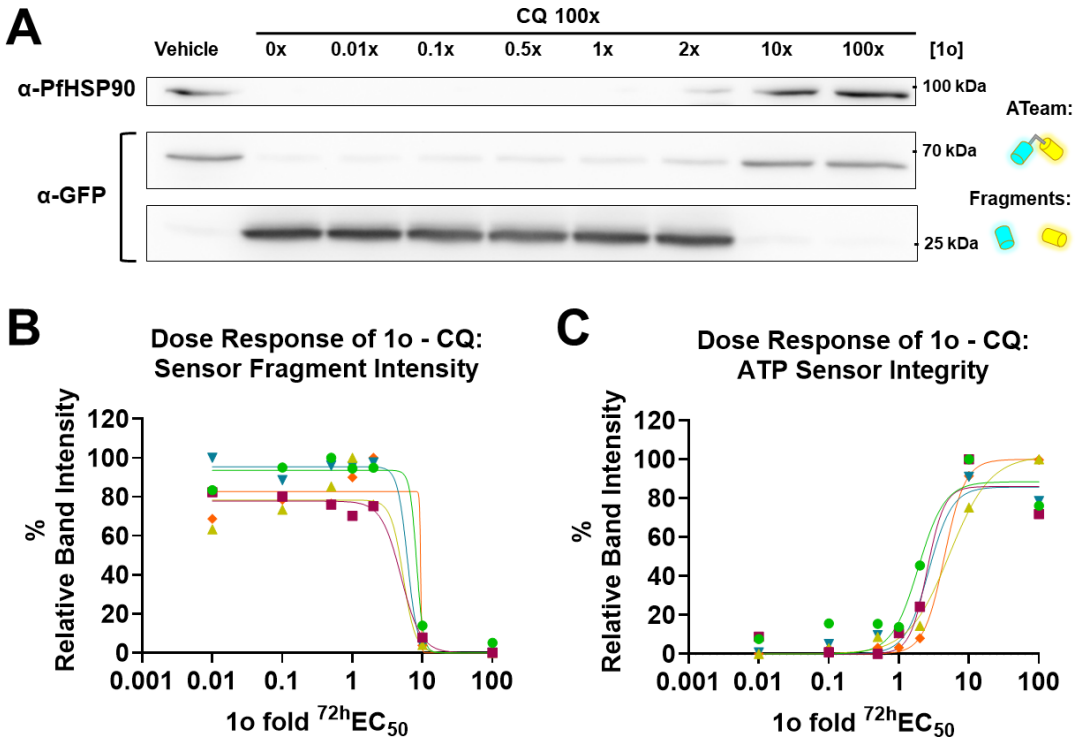

FIG 6 1o prevents CQ-mediated ATeam1.03YEMK sensor degradation. (A) WB of MACS-enriched NF54*attB*$^{[ATeam1.03YEMK]}$ trophozoite iRBCs treated with 100x $^{72h}EC_{50}$ CQ co-incubated with increasing concentrations of 1o (0.01x – 100x $^{72h}EC_{50}$) for 6 h. CQ causes the disappearance of the housekeeping control (PfHSP90; 90 kDa) and the GFP-based ATeam1.03YEMK (68 kDa) signal, concomitant with increased signal intensity around the size of GFP-based monomers (27 kDa; Fragments). (B and C) Normalization of WB to vehicle control and CQ alone signals shows a dose dependency. Band intensities were normalized to Ponceau S total protein stain. $n = 5$ independent experiments with 2.5×10^6 parasites per group are shown. Different colored points and fit lines indicate independent replicates.

(Fig. 7G through L). To exclude that the 1o effect is due to a non-specific negative effect on parasite metabolism or viability, we used the protein synthesis inhibitor cycloheximide (CHX) as a control in all experiments.

As previously reported, assays of this kind show high background noise, likely due to the low basal parasitic Hb content of less than 1%. Nevertheless, measurement of intraparasitic Hb without CQ co-incubation reveals a statistically significant lowered Hb amount (Fig. 7A) as well as relative Hb fraction (Fig. 7D) in the group incubated with 100x $^{72h}EC_{50}$ 1o compared to the control, while we could neither detect any effects of lower doses, nor of CHX (Fig. 7A and D). We detected a reduced occurrence of "free" heme after 10x and 100x $^{72h}EC_{50}$ 1o treatment (Fig. 7B), as well as less Hz after 2x, 10x, and 100x $^{72h}EC_{50}$ 1o and CHX treatment. However, the observed lowered "free" heme and Hz quantities caused by 1o do not cause a significant change in their relative fractions. For the relative "free" heme and Hz fractions, we could not detect any effects of 1o or CHX alone, even at high concentrations of 1o (Fig. 7E and F).

We detected increased Hb, increased "free" heme, and decreased Hz species caused by CQ, both on the absolute and relative level (Fig. 7G through L), which is in line with previous literature (8, 9). Compared to CQ alone, co-incubation with 1o showed a dose-dependent reduction of the absolute Hb amounts and relative fractions, already noticeable at its' 2x $^{72h}EC_{50}$ (Fig. 7G and J). For "free" heme, co-incubation with 1o caused a decrease in both parameters with a dose-dependent trend (Fig. 7H and K), which was statistically significant at 10x and 100x $^{72h}EC_{50}$ 1o. Co-incubation with 1o did not show an effect on absolute Hz (Fig. 7I). However, it showed a dose-dependent increase of the Hz fraction (Fig. 7L), significant at 2x, 10x, and 100x $^{72h}EC_{50}$ 1o, which should be reflected in a consequential alteration of the Hb and "free" heme species. Additionally, CHX showed a significant attenuation of the Hz fraction after CQ treatment, but levels did not reach those of the vehicle control (Fig. 7L).

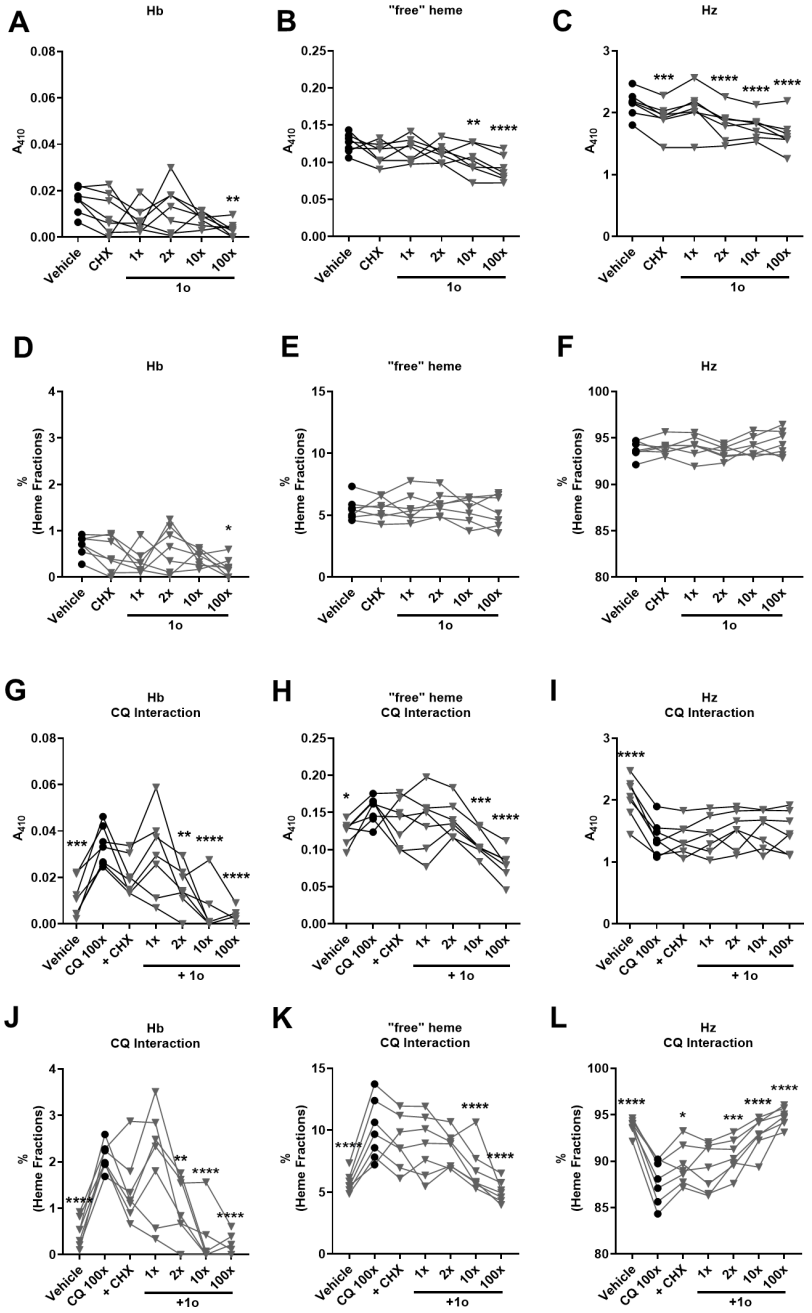

FIG 7 1o depresses Hb metabolism, lowers Hb fraction, and prevents CQ-mediated effects on Hb and "free" heme species. Fractionated analysis of heme species (Hb: hemoglobin; "free" heme; Hz: hemozoin) of MACS-enriched NF54*attB*$^{[ATeam1.03YEMK]}$ trophozoite iRBCs after compound incubation for 6 h (CQ and 1o: multiples of $^{72h}EC_{50}$; CHX: 50 µg/mL). Solitary 1o or CHX treatment (A–F) and CQ interaction (G–L) is presented as absolute amount of heme species, via absorbance of heme-pyridine complexes at A_{410} (A–C and G–I) and the relative fractions of the heme species distribution (D–F and J–L). (A) 100x $^{72h}EC_{50}$ 1o reduces the Hb amount in the parasites (P = 0.0027). (B) 10x and 100x $^{72h}EC_{50}$ 1o reduce the amount of "free" heme (10x: P = 0.0055; 100x: P < 0.0001). (C) CHX and 2x, 10x, 100x $^{72h}EC_{50}$ 1o reduce the amount of Hz (CHX: P = 0.0004; 1o 2x: P < 0.0001; 10x: P < 0.0001; 100x: P < 0.0001). (D) 100x $^{72h}EC_{50}$ 1o reduces the fraction of Hb (P = 0.016). (E and F) Solitary 1o or CHX incubations do not show effects on "free" heme or Hz fractions. (G) 100x $^{72h}EC_{50}$ CQ treatment elevates the amount of Hb (P = 0.0004). Co-incubation with 2x, 10x, and 100x $^{72h}EC_{50}$ 1o causes a reduced Hb amount compared to CQ treatment alone (2x: P = 0.0053; 10x: P < 0.0001; 100x: P < 0.0001). (H) 100x $^{72h}EC_{50}$ CQ treatment elevates the amount of "free"

(Continued on next page)

Fig 7 (Continued)

heme (P = 0.0325). Co-incubation with 10x and 100x $^{72h}EC_{50}$ 1o causes a reduced "free" heme amount (10x: P = 0.0005; 100x: P < 0.0001). (I) 100x $^{72h}EC_{50}$ CQ treatment reduces the amount of Hz (P < 0.0001). Co-incubations with CHX or 1o do not alter the Hz amount. (J) 100x $^{72h}EC_{50}$ CQ causes higher Hb fractions than vehicle control parasites (P < 0.0001). Co-incubation with 1o (2x: P = 0.005; 10x: P < 0.0001; 100x: P < 0.0001) causes reduced Hb fractions. (K) 100x $^{72h}EC_{50}$ CQ causes higher "free" heme fractions than vehicle control parasites (P < 0.0001). Co-incubation with 1o (10x: P < 0.0001; 100x: P < 0.0001) causes reduced "free" heme fractions. (L) 100x $^{72h}EC_{50}$ CQ causes lower Hz fractions than vehicle control parasites (P < 0.0001). Co-incubation with CHX (P = 0.0408) and 1o (2x: P = 0.0005; 10x: P < 0.0001; 100x: P < 0.0001) causes increased Hz fractions. n = 7 independent experiments derived from 1.5×10^7 parasites/treatment group. Statistical analysis was conducted via two-way ANOVA and Dunnett's multiple comparisons test. Reference group for multiple comparisons is indicated as black circles. Asterisks indicate significance level (*P < 0.05; **P < 0.01; ***P < 0.001; ****P < 0.0001).

1o preserves FV morphology under CQ treatment

Drug treatment, including using CQ, is known to alter the ultrastructure of trophozoites, including the FV (17, 20–22). We used transmission electron microscopy to investigate if 1o also caused such alterations, and additionally, if 1o was able to prevent the changes observed upon CQ treatment. For quantification, we trained a "blinded" non-parasitologist to count the percentage of parasites with Hz outside of a distinguishable subcellular parasite compartment, equivalent to the FV, of all parasites with visible Hz crystals. Without treatment (Vehicle), we observed a spectrum of different phenotypes, ranging from Hz being contained within a clearly defined-membrane delineated compartment, representing the FV (Fig. 8A, Vehicle, upper panel) to strongly condensed Hz which was less clearly separated from the cytosol by a bounding membrane (Fig. 8A, Vehicle, lower panel). This variation is likely due to differences in parasite stage or as a result of sample preparation. Treatment with 1o alone did not appear to lead to any pronounced phenotypic changes, and a similar population of phenotypes was observed (Fig. 8A, 1o 2x – 100x). CHX appeared to cause a change in the phenotype population, with Hz now seen less condensed and free in the parasite cytosol (Fig. 8A, CHX 50 µg/mL). As previously reported, CQ caused Hz to be less condensed and not found in a clearly distinguishable subcellular parasite compartment (Fig. 8B, CQ 100x), and co-treatment with CHX led to similar results (Fig. 8B, CQ + CHX). Co-incubation with CQ and increasing concentrations of 1o shifted the population phenotype away from the CQ appearance, more toward the appearance of untreated parasites (Fig. 8B, CQ + 1o 2x – 100x). These observations are consistent with the statistical analysis of n = 3 independent TEM replicates, apart from that of CHX alone (Fig. 9).

Late trophozoites are less affected by 1o than ring or early trophozoite stage parasites

To narrow down the targeted metabolic pathway of 1o's relevant parasite-killing activity, we treated different parasite stages (ring stage, early trophozoite, late trophozoite) of infected red blood cell (iRBC) culture with a fixed dose of 1o (5x $^{72h}EC_{50}$) or a vehicle control and monitored morphology and parasitemia over time (Fig. 10A through C). Untreated ring stages are expected to develop into trophozoites and then schizonts prior to egress as merozoites, second cycle invasion, ring stage, and trophozoite development (Fig. 10D). Ring stages were sampled just before and 24, 48, and 66 h post-treatment and used as a reference time scale for all other stages. When initiating treatment in ring stages, parasites did not, in contrast to the control group, propagate over the course of the experiment (Fig. 10A). Light microscopy revealed that, while control parasites progressed in their developmental stage to trophozoites, treated parasites took on a condensed morphology, likely representing degenerate ring stages (Fig. 10A). Treatment of early-trophozoite stage parasites in the same manner showed similar results, but with parasite growth in the treatment samples now blocked at the early trophozoite stage

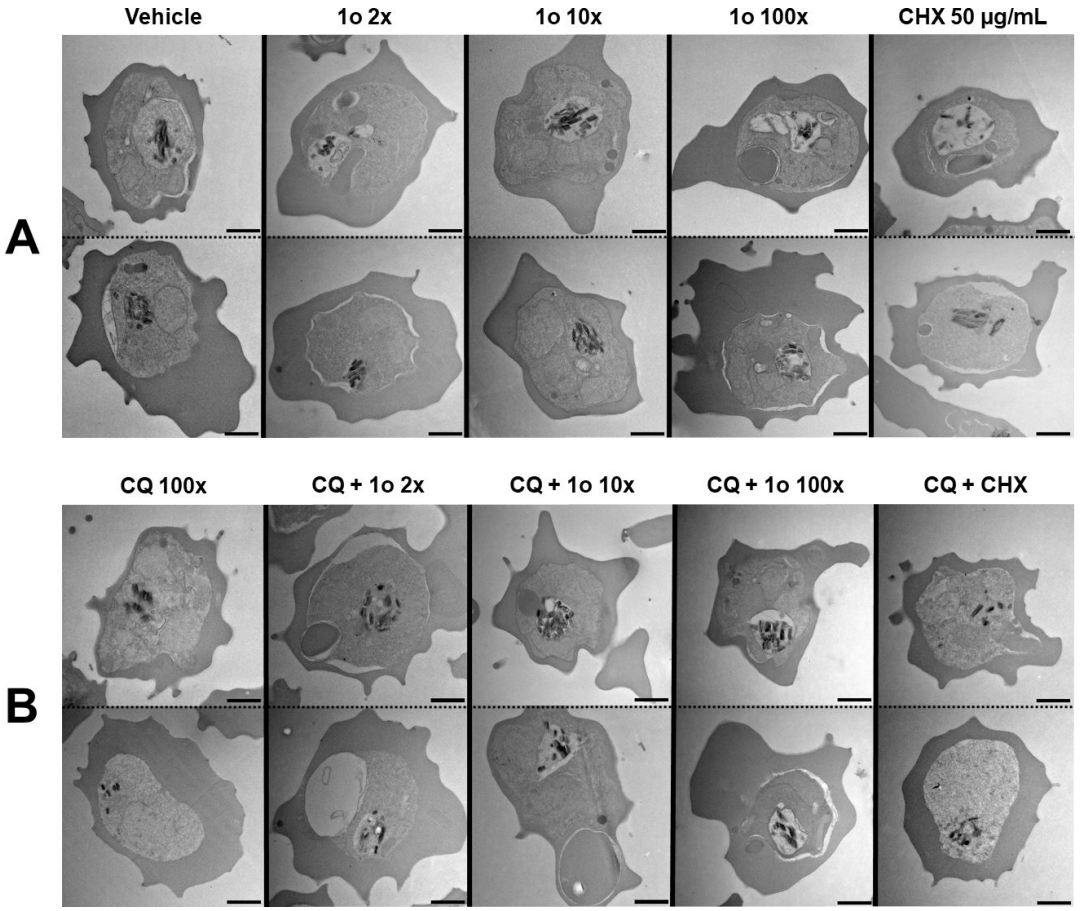

FIG 8 1o prevents CQ-mediated ultrastructural food vacuole alterations. TEM of MACS-enriched NF54*attB*$^{[ATeam1.03YEMK]}$ trophozoite iRBCs after compound incubation for 6 h (CQ and 1o: multiples of $^{72h}EC_{50}$; CHX: 50 µg/mL). (A) Vehicle-treated cells w/o co-incubation with 1o or CHX. (B) CQ-treated cells w/o co-incubation with 1o or CHX. Electron-dense hemozoin (Hz) is usually found within a distinguishable subcellular food vacuole compartment in vehicle-treated controls. Treatment with 100x CQ causes elevated parasite counts with disseminated Hz or Hz outside of a subcellular compartment. Co-incubation with 1o prevents such CQ-characteristic phenotypes. CHX does not appear to prevent the CQ action. Two representative images are shown. Scale bar equals 1 µm.

(Fig. 10B). Initiating the experiment with late-trophozoite stages, we observed that both treated and non-treated parasites increased in number over time (Fig. 10C). However, while untreated parasites, upon new invasion, developed into second generation trophozoite stages, parasites in the treated samples were blocked in their second cycle of development at the rings stage and again appeared degenerated (Fig. 10C). A comparison of all endpoint parasitemias from the above experiment revealed that the development of late trophozoites is significantly less compromised compared to treatment of ring and early trophozoite stages (Fig. 10E).

DISCUSSION

We aimed to investigate the MoA of 1o and present here the first detailed study of its effects on parasites at the cellular level. We applied our established ATeam1.03YEMK ATP assay for our measurements in trophozoite stages (4, 11) to detect changes in cytosolic [ATP]. We ruled out confounding factors such as temperature, differences in parasite development, and pH through simultaneous measurement of 1o- and vehicle-treated cells within the same microscopic dish and control measurements with the pH sensor sfpHluorin. Strikingly, together with the parasite size, 1o's response pattern at 10x $^{72h}EC_{50}$ reveals parallels to MQ's and LUM's responses. Both cause an increased [ATP], a similar pH decrease, and reduced parasite size (4). An increase in cellular [ATP] can be caused by increased ATP production or decreased consumption. ATP is likely to be in high demand

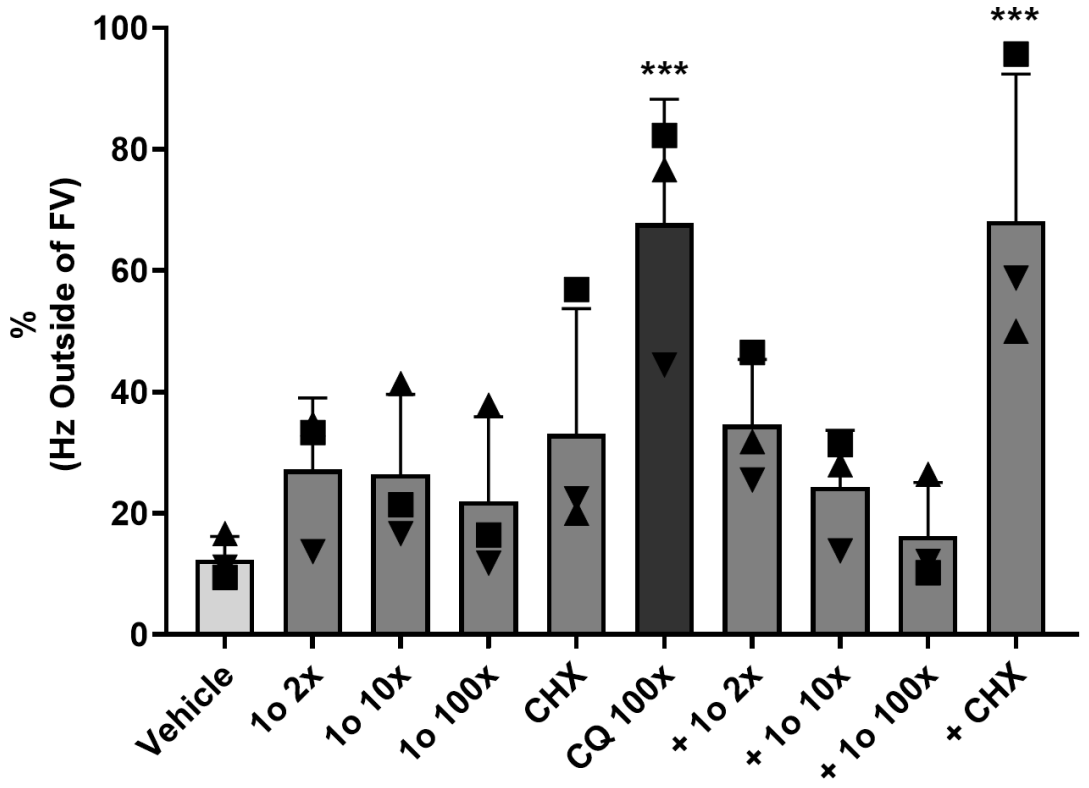

FIG 9 1o prevents CQ-mediated Hz dissemination. Quantification of TEM images of MACS-enriched NF54*attB*$^{[ATeam1.03YEMK]}$ trophozoite iRBCs after compound incubation for 6 h (CQ and 1o: multiples of $^{72h}EC_{50}$; CHX: 50 µg/mL). CQ (P = 0.003) and CQ + CHX (P = 0.003) treatment cause a significant increase in parasites with Hz outside of an FV structure compared to vehicle control. CHX alone and 1o alone or in co-incubation with CQ do not cause significantly increased levels. Readout is the percentage of parasites with Hz outside of a subcellular parasitic FV compartment of all parasite images with noticeable Hz crystals. n = 3 independent experiments with 12–97 Hz-containing parasite sections per data point. Statistical analysis was conducted via two-way ANOVA and Dunnett's multiple comparisons test. Each group was compared to the mean of the vehicle control. Asterisks indicate significance level (***P < 0.001).

for protein synthesis in the metabolically highly active trophozoite stages, and this is backed up by our previous observations that inhibition of protein synthesis via CHX causes an increase in [ATP] (4). Therefore, one possible explanation for the observed effects could be inhibition (either direct or indirect) of protein synthesis, which could also result in reduced parasite size.

Following up on the parallels to MQ, we analyzed 1o's interaction with CQ. CQ inhibits heme detoxification to Hz crystals (19), while it also inhibits Hb degradation (18), as well as heme detoxification via glutathione (14, 23). Ultimately, this leads to elevated levels of toxic free heme (9) and heme-inhibitor complexes (15), which are thought to kill the parasites (24), including lysis of the FV (17) and proteolysis in the cytosol (16, 17, 21). Drug effects can unfold on many levels and are dependent on incubation conditions, compound concentration, parasite strain and density, and incubation time. Within our assay conditions, with trophozoite iRBCs treated with 100x $^{72h}EC_{50}$ CQ for 6 h, we could replicate phenotypes that are already described in the literature. These include a characteristic shift of ATeam1.03YEMK and sfpHluorin single-cell distribution, ATeam1.03YEMK and PfHSP90 degradation (4), Hb and "free" heme fraction increase, Hz fraction decrease (8, 9), and FV alterations with Hz dissemination (17). Taken together, our observations can be explained through CQ-mediated Hz formation inhibition, with concomitant free heme increase that could lyse the FV and cause proteolytic degradation in the cytosol. We use this concept for the interpretation of our interaction analyses.

We found that 1o prevents CQ-mediated ATeam1.03YEMK and sfpHluorin ratio drop and ATeam sensor degradation, similar to the effect noted for MQ (4). We found the interaction $^{1o\text{-}CQ}EC_{50}$ to be in a similar range as the parasite-killing $^{72h}EC_{50}$ of 1o. This

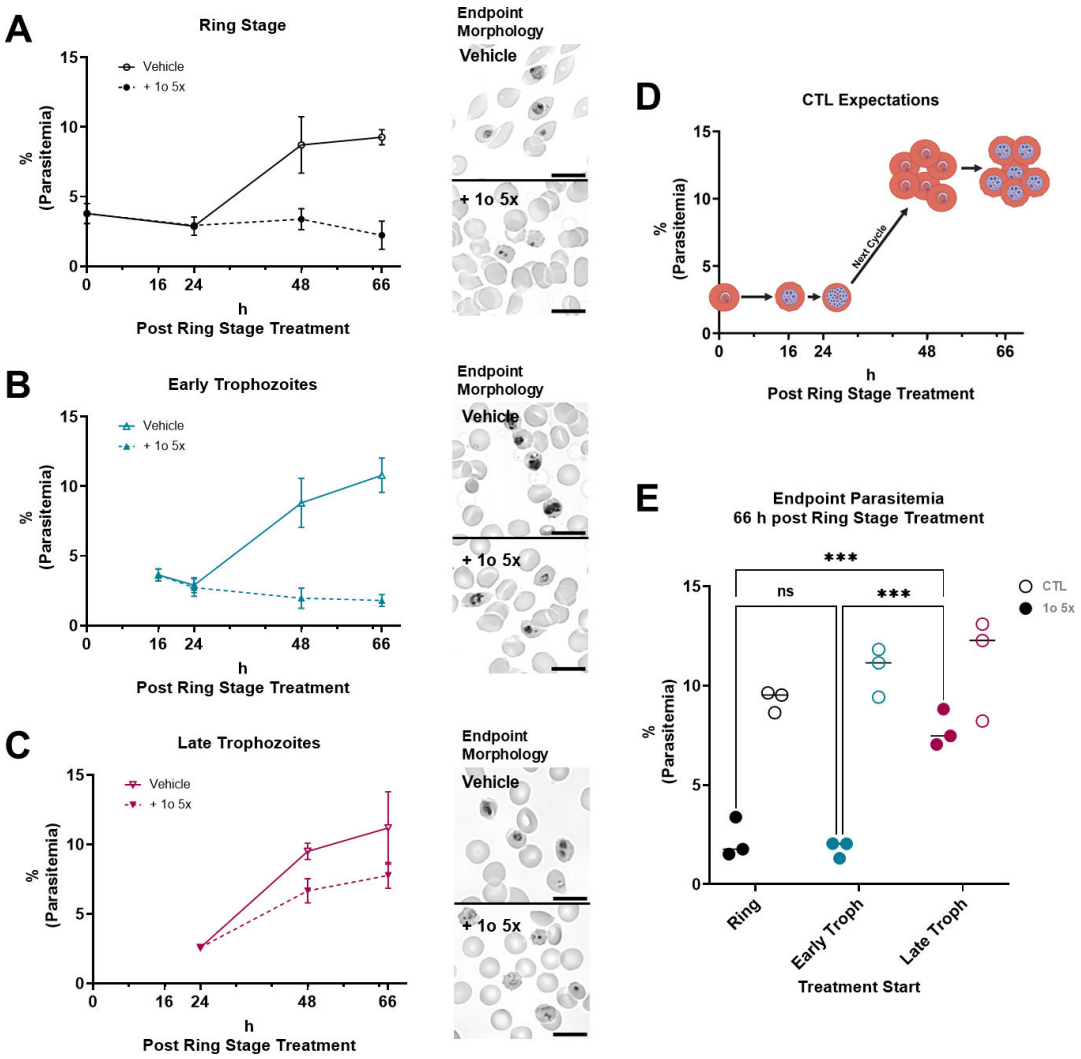

FIG 10 1o-treated late trophozoites can complete their life cycle until the following ring stage, in contrast to early trophozoites or ring stages. NF54*attB*$^{[ATeam1.03YEMK]}$ ring stage (A), early trophozoite (B), and late trophozoite (C) iRBC cultures were treated with 5x $^{72h}EC_{50}$ 1o (closed symbols, dotted line) or vehicle control (open symbols, solid line) and monitored for morphology and parasite count at the indicated time points. (D) Ring stages are expected to develop into trophozoites and then schizonts prior to merozoite egress, second cycle invasion, ring stage, and trophozoite development. (A) After 66 h, control parasites (Vehicle) proliferated and developed into trophozoites, while 1o-treated parasites did not increase parasitemia, nor develop into trophozoites. (B) 1o-treated early trophozoites on the same time scale did not proliferate and continuously appeared to be early trophozoites. (C) 1o-treatment of late trophozoites allowed proliferation into new ring stages, but not into trophozoites. (E) The endpoint parasitemia of each incubated parasite stage in the 1o-treatment and control groups was compared to each other's parasite stage in each group. The parasitemia in late trophozoite 1o-treated cultures is significantly different from ring (P = 0.0007) and early trophozoite (P = 0.0004) 1o-treated cultures. Parasitemia of all vehicle-treated stages is not significantly different. Statistical analysis was conducted via two-way ANOVA and the Tukey multiple comparisons test. Asterisks indicate significance level (***P < 0.001). n = 3 independent experiments; error bars indicate standard deviation. Scale bar equals 10 µm. Created in BioRender.

suggests that the mechanism involved in the 1o block of CQ effects is indeed highly likely to represent the parasite-killing mechanism of 1o itself. In line with this, 1o prevents the ATeam1.03YEMK sensor degradation in a dose-dependent manner, which could reflect the bi-modal ATeam ratio drop. It should be emphasized that, under these conditions, the sensor readout does not represent changes in [ATP] but rather is being applied as a measure of sensor degradation.

Our 1o-CQ sensor interaction studies uncovered parallels to MQ and therefore implicate a similar interference with the parasites' heme metabolism. To study this, we analyzed the relevant heme fractions in the parasites (9). Within our assay conditions, we can reproduce previous values for CQ-treated trophozoites (9), such as increased Hb,

increased “free” heme, and decreased Hz fractions. For 1o treatment alone, we detected reduced absolute amounts of Hb, “free” heme, and Hz. While the relative “free” heme and Hz fractions did not significantly change under 1o treatment, these observations could be explained by general impaired parasite growth. Additionally, the level of "free" heme in the cytosol of blood stage parasites appears to be tightly regulated throughout its lifecycle and might possibly be balanced by import of heme via new permeability pathways (25, 26). Nevertheless, we could detect a decreased relative Hb fraction, which implicates altered Hb metabolism. While we could not detect a significant effect on the Hb fraction with concentrations lower than 100x $^{72h}EC_{50}$ 1o, this may be explained by the low signal-to-noise ratio of the data produced under these conditions. Remarkably, within conditions of elevated Hb levels caused by CQ, 1o causes decreased Hb levels already at its 2x $^{72h}EC_{50}$. Additionally, 1o also causes decreased “free” heme levels starting with its 10x $^{72h}EC_{50}$ within the same scenario. At the same time, the absolute Hz amount is not affected by 1o. CHX, in contrast, does not affect the analyzed heme species in a similar manner, excluding a general effect caused by reduced parasite viability. Therefore, this data led us to conclude that the observed 1o effects and CQ interaction do not reflect unspecific effects caused by downstream inhibition of protein synthesis or simple parasite death, but rather support a mechanism for 1o interference in either uptake of Hb or Hb digestion to “free” heme. 1o has been reported to inhibit Hz formation *in vitro* (2). *In cellulo*, we could not detect an increase in the “free” heme fraction, suggesting that such effects are unlikely to represent the main parasite-killing activity of 1o.

We analyzed the ultrastructure of CQ- and 1o-treated iRBCs to investigate whether our biochemical findings match with the morphological changes of the parasites. CQ is known to cause the appearance of membranous structures within the FV, Hz in unusual vacuoles (20), as well as less discrete Hz crystals, vacuole rupture, and Hz outside of the FV (17). Additionally, using electron spectroscopic imaging, Combrinck et al. detected increased cytoplasmic iron in trophozoites after CQ treatment, indicative of heme diffusion outside of the FV and association with organelle membranes, which possibly kills the parasites (9). In line with this, we detected Hz dissemination into the cytosol, while 1o treatment already at 2x EC_{50} prevented the CQ effect. We detected increased “free” heme fractions caused by CQ under identical conditions, with 1o limiting this increase. A possible explanation for our observations could be that the CQ-mediated heme accumulation causes FV lysis with consequential Hz dissemination, which can be prevented by either directly or indirectly limiting heme accumulation.

Based on our hypothesis that 1o could interfere in a process within or upstream of Hb digestion, we analyzed its effect on the parasite development of different metabolic stages. We found that 1o-treatment blocked further development of ring or early trophozoite stage parasites, while parasites treated at the late trophozoite stage continued their lifecycle at a level approaching controls. This slight difference may be due to a small number of slightly asynchronous parasites in the population. This data suggests that a relevant metabolic pathway affected by 1o’s parasite-killing mechanism must be especially active during ring and early trophozoite development. The development from ring stage to early trophozoites is characterized by rapid growth and uptake of host Hb, while the subsequent late trophozoite and schizont stages are characterized by nuclear and eventual cellular division to merozoites (27). Together with our findings on the interaction of 1o with CQ, our data are consistent with a model in which 1o kills parasites by affecting their ability to uptake enough Hb to fulfil their metabolic requirements.

Our data give us a first idea of 1o’s MoA. We propose that 1o’s parasite-killing activity disrupts a metabolic pathway that is crucial for trophozoite development, possibly interfering with Hb uptake or digestion, and, thereby, superimposing CQ action. Our study is far from target identification, and 1o’s MoA may be pleiotropic in nature. However, we could narrow down a relevant metabolic pathway, which will benefit from the integration of further studies regarding resistance and omics analyses that are beyond the scope of our manuscript.

MATERIALS AND METHODS

Expression and purification of recombinant ATeam and sfpHluorin protein

ATeam10.3YEMK (11) and sfpHluorin (12) sequences in pQE-30 in *E. coli* strain M15 were used for overexpression and protein purification as previously published (4).

Drug-sensor interaction studies

Drug-sensor interaction studies with ATeam1.03YEMK and sfpHluorin were conducted as reported (4). In brief, pre-heated ATeam1.03YEMK protein in ATeam buffer (100 mM HEPES, 50 mM KCl, 0.5 mM $MgCl_2$, pH 7.34) with a final concentration of 1 µM was measured in black half-area 96-well plates in a Clariostar plate reader (BMG Labtech, Ortenberg, Germany) together with 1o (10 nM–1 µM), 10 mM $MgATP^{2-}$ solution, or dimethyl sulfoxide (DMSO) vehicle control at 37°C after incubation for 5 min. Background-corrected emission ratios were calculated by division of 527/10 nm and 475/10 nm emission after excitation at 435/10 nm, respectively. Mean values were calculated from $n = 3$ independently produced proteins. For sfpHluorin, preparation was conducted accordingly. Measurements were conducted in sfpHluorin buffer (100 mM potassium phosphate, 100 mM NaCl, and 0.5 mM Na_2-EDTA, pH 7.0), control buffer pH 5 (MES-KOH, 100 mM NaCl, and 5 mM EDTA), and control buffer pH 9 (100 mM Tris-HCl, 100 mM NaCl, and 5 mM EDTA). Excitation ratio was calculated from 390/15 nm and 482/16 nm excitation at 530/20 nm emission, respectively. Compound and vehicle treatments were normalized to the H_2O control.

P. falciparum cell culture

Transgenic sensor-expressing NF54*attB*$^{[ATeam1.03YEMK]}$ and NF54*attB*$^{[sfpHluorin]}$ parasite lines have been previously described (4). Blood stage parasites were cultured as previously described (28). Briefly, the parasites were cultured in complete media (CM) composed of RPMI 1640 medium with 2.1 mM L-glutamine, 25 mM HEPES supplemented with 0.5% Albumax, 9 mM glucose, 0.2 mM hypoxanthine, and 22 µg/mL gentamicin at 3.3% hematocrit and 37°C under 3% O_2 and 3% CO_2, respectively.

Sorbitol synchronization

Parasites were synchronized using a 5% D-sorbitol solution (29) for 8 min at 37°C for at least three consecutive cycles prior to measurements. To exclude confounding effects from the sorbitol treatment, parasites were allowed to complete their lifecycle after sorbitol treatment, before measurements. At the latest, 72 h post-last sorbitol treatment, the population of iRBCs was defined as the trophozoite stage and used for measurements. Early trophozoites refer to parasites that are 6 h younger.

In vitro P. falciparum drug susceptibility assay

The half maximal effective concentration of 1o against *P. falciparum* NF54*attB*$^{[ATeam1.03YEMK]}$ after 72 h ($^{72h}EC_{50}$) was performed using a SYBR Green I-based fluorescence assay (30). A 10 mM 1o stock solution dissolved in DMSO was diluted in CM for serial double dilutions in black half-area 96-well plates (final assay concentrations: 160, 80, 40, 20, 10, 5, 2.5, 1.25, 0.625, and 0.3125 nM) with two technical replicates for each measurement. Wells were equipped with synchronized ring stage parasites to 1.5% hematocrit with 0.5% parasitemia. After incubation for 72 h under standard conditions, plates were wrapped in aluminum foil and stored frozen at −80°C overnight. The plates were thawed for 2 h at RT. Afterward, plates were equipped with 1× SYBR Green I in lysis buffer (20 mM Tris-HCl, 5 mM EDTA, 0.16% wt/vol saponin, and 1.6% vol/vol Triton X-100) and incubated in the dark for 1 h. Subsequently, the fluorescence at 494 nm excitation and 530 nm emission was measured in a Clariostar Plate Reader (BMG Labtech, Ortenberg, Germany). $^{72h}EC_{50}$ determination was conducted via fitting a four-parametric variable slope using GraphPad Prism (version 10.4.1 for Windows, GraphPad Software, Boston, Massachusetts, USA, https://www.graphpad.com/).

Trophozoite enrichment via MACS

Trophozoite iRBCs were enriched by magnetic separation as previously published (4).

Drug and vehicle treatment

Magnetic activated cell sorting (MACS)-enriched trophozoite iRBC cultures were treated with 100× stock solutions in DMSO (1o) or H_2O (CQ). Each treatment and vehicle control group was treated with all respective solvents of the individual experimental setup and a maximal DMSO concentration of 1% (vol/vol). Vehicle controls indicate groups that were treated with all solvents of the respective experiment. Treated cells were incubated under standard culture conditions.

Measurements of sensor cell lines via live-cell microscopy

ATP and pH measurements in NF54*attB*$^{[ATeam1.03YEMK]}$ and NF54*attB*$^{[sfpHluorin]}$ were conducted as previously published (4). In brief, drug- and vehicle-incubated iRBCs were washed with Ringer's solution (122.5 mM NaCl, 5.4 mM KCl, 1.2 mM $CaCl_2$, 0.8 mM $MgCl_2$, 11 mM D-glucose, 25 mM HEPES, and 1 mM NaH_2PO_4, pH 7.4) and allowed to settle on pre-heated ibidiTreat µ-Dish 35 mm Quad microscopy dishes (ibidi GmbH, Gräfelfing, Germany) at 37°C for 10 min. Images were taken with an Axio Observer.Z1/7 microscope (Zeiss, Oberkochen, Germany) with plan-apochromat 63×/1.40 oil immersion DIC M27 objective and Axiocam 506 camera. ATeam1.03YEMK measurements were conducted using Zeiss filter set 47 (EX BP 436/20, BS FT 455, EM BP 480/40) and 48 (EX BP 436/20, BS FT 455, EM BP 535/30) for CFP and CFP-YFP-FRET emission signal, respectively. Excitation was facilitated using the Colibri 7 LED module 430 nm (300 ms, 90% intensity). Background-corrected YFP signal at 535 nm divided by background-corrected CFP signal at 480 nm equals FRET ratio. For sfpHluorin, the Zeiss filter set 38 HE without excitation filter (BS FT 495 [HE], EM BP 525/50 [HE]) and Colibri 7 LED module 525 nm and 475 nm was used (each at 300 ms, 30%). Background-corrected GFP signal at 525 nm and excitation at 385 nm divided by background-corrected GFP signal at 525 nm and excitation at 475 nm equals the excitation ratio. Image analysis was conducted via ImageJ Fiji (31) 1.54f. Each measurement was gained using the mean sensor ratio of 200 iRBCs. $n = 5$ independent experiments were conducted. Each microscopic dish contained a control group as a simultaneously treated reference.

Nigericin pH calibration

pH calibration via nigericin (32) of NF54*attB*$^{[sfpHluorin]}$ was conducted as previously described (4).

Western blot analysis

For western blot analysis, 2.5×10^6 MACS-enriched and 6 h compound-treated trophozoite iRBCs were washed in phosphate-buffered saline (PBS [pH 7.3–7.5, 154.004 mM, 5.599 Na_2HPO_4, 1.058 KH_2PO_4]) containing 1× cOmplete Protease Inhibitor Cocktail Tablets (Roche Diagnostics GmbH, Mannheim, Germany) and lysed using M-PER buffer (ThermoFisher Scientific, Waltham, MA, USA) containing 1× cOmplete Protease Inhibitor Cocktail Tablets for 10 min. After centrifugation of cell debris, the supernatant was incubated at 95°C together with 4× sample buffer + dithiothreitol and separated using sodium dodecyl sulfate (SDS)-polyacrylamide gel electrophoresis according to Laemmli (33). Separated proteins were blotted on polyvinylidene difluoride membranes and stained with Ponceau S protein stain. Intensity of the Ponceau S staining was used for normalization of gel loading (34). After washing in TBST (Tris-buffered saline with 0.05% polysorbate 20), membranes were blocked in 5% TBST milk and probed using α-GFP (1:1,000; Roche Diagnostics GmbH, Mannheim, Germany) antibody in 5% milk in TBST, followed by secondary goat α-mouse IgG HRP antibodies (1:10,000 Dako, Agilent Technologies Deutschland GmbH, Waldbronn, Germany) in 5% milk in

TBST. Probing of the PfHSP90 housekeeping control was conducted via α-PfHSP90 (1:500, a gift of Addmore Shonhai) antibody in 5% milk in TBST, followed by secondary goat α-rabbit IgG HRP antibody (1:2,000; Dako, Agilent Technologies Deutschland GmbH, Waldbronn, Germany). Band intensities were quantified using GelAnalyzer 19.1. (available at www.gelanalyzer.com by Istvan Lazar Jr., Ph.D., and Istvan Lazar Sr., Ph.D., CSc).

1o-chloroquine interaction

Dose-response analysis of 1o-chloroquine interaction (1o-CQ) of sensor readouts and WB signals was conducted via fitting of a four-parametric variable slope using GraphPad Prism (version 10.4.1 for Windows, GraphPad Software, Boston, Massachusetts, USA, https://www.graphpad.com/) for each of the $n = 5$ independent replicate series of each experimental setup. Measurements were set up as outlined above. For measurements of NF54*attB*$^{[ATeam1.03YEMK]}$ and NF54*attB*$^{[sfpHluorin]}$ sensor readouts, a CQ-treated contemporaneous control was used for normalization of the 25th percentile sensor ratio in each 4-well ibidiTreat µ-Dish 35 mm Quad (ibidi GmbH, Gräfelfing, Germany) microscopy dish. The 25th percentile of CQ alone- and vehicle-treated cells was set to 100% and 0%, respectively.

Heme species distribution

The pyridine assay for determination of heme fractions was adapted from Combrinck et al. (9) to our trophozoite assay setup. In brief, 1.5×10^7 MACS-enriched trophozoite RBCs were incubated with drugs or vehicle control under standard incubation conditions for 6 h. Afterward, cells were centrifuged at 2,100 × *g* and freed from host Hb using saponin lysis buffer (0.02% saponin in PBS) 2× for 10 min at 37°C. Cells were washed with saponin lysis buffer, subsequently with PBS, and stored in 100 µL PBS stocks at −80°C. For analysis, stocks were thawed, and 50 µL H_2O was added prior to sonication for 5 min. A total of 50 µL HEPES buffer (0.2 M pH 7.5) and 50 µL H_2O were added, followed by centrifugation at 16,000 × *g* for 20 min. The supernatant was used for Hb determination. The remaining pellet was resuspended in 50 µL H_2O and 50 µL 4% SDS, followed by sonication for 10 min, vortex mixing, and incubation at 37°C for 30 min. Afterward, 50 µL HEPES buffer, 50 µL 0.3 M NaCl, and 50 µL 25% pyridine were added, followed by centrifugation for 20 min at 16,000 × *g*. The supernatant was used for the determination of the "free" heme fraction. The remaining pellet was mixed with 50 µL H_2O and 50 µL 0.3 M NaOH and sonicated for 15 min. After incubation at 37°C for 30 min, 50 µL HEPES buffer, 50 µL 0.3 M HCl, 50 µL 25% pyridine, and 150 µL H_2O were added. The solution corresponds to the Hz fraction. The supernatant designated for Hb analysis was mixed with 50 µL 4% SDS and sonicated for 5 min prior to incubation at 37°C for 30 min. Subsequently, 50 µL 0.3 M NaCl and 50 µL pyridine 25% (vol/vol) in HEPES buffer were added. The solution corresponds to the Hb fraction. The supernatant designated for "free" heme analysis was filled up to 400 µL with H_2O and corresponds to the "free" heme fraction. The corresponding fractions were analyzed for absorbance of the heme-pyridine complex at 410 nm in a Mettler Toledo UV5 Bio spectrophotometer (Mettler Toledo GmbH, Giessen, Germany). Mean of $n = 7$ independent experiments, each calculated as the mean of 5 technical replicates, were used for fraction determination. The relative fraction (%) was calculated via division of the absorbance of each fraction by the sum of the absorbance of all fractions.

Transmission electron microscopy

For TEM samples, MACS-enriched trophozoite iRBCs were incubated with 100× compound stock solutions and/or vehicle control (1% final DMSO concentration) for 6 h in complete media under standard incubation conditions. After harvest, cells were fixed with 500 µL TEM-fixing buffer (2% glutaraldehyde, 2% paraformaldehyde, 100 mM CaCo pH 7.4, [Electron Microscopy Sciences, Hatfield, PA 19440, USA]) at RT. For fixation, cells

were shaken overnight at 4°C with consecutive storage at 4°C. Prior to sample preparation, fixed cells were washed three times with 500 µM PBS. Cell pellets were mixed with equal volumes of 3% agarose solution and hardened on ice. Cells in agarose were cut into cubes of about 1 mm length and soaked in PBS. After incubation with 1% osmium tetroxide for 1 h, cells were washed three times with H_2O for 5 min. Afterward, cells were incubated with uranyl acetate at 4°C overnight. Uranyl acetate was washed off twice with H_2O for 10 min. Dehydration was conducted with increasing acetone aqueous solutions (30%, 50%, 70%, 90%) and twice with 100% acetone for 10 min each. Afterward, cells were soaked with increasing SPURR (Electron Microscopy Sciences) in acetone solutions (25%, 50%, 75%) for 45 min each and 100% SPURR overnight at 4°C. The next day, cells were immersed in fresh SPURR for 4 h at RT, embedded in gelatin capsules (Electron Microscopy Sciences), and polymerized for 12 h at 70°C. After polymerization, the resin was washed and cut to 70 nm slices. Images were taken using the Joel JEM-1400 Flash.

Stage-specific lifecycle effects

We synchronized for ring stages via sorbitol synchronization. Parasites were allowed to complete their lifecycle before treatment and were defined as ring stage culture 48 h after the last sorbitol treatment. After a further 16 and 24 h, the parasites were defined as early and late trophozoites, respectively. For quantification and analysis of parasite morphology, Giemsa-stained blood smears were sampled at the indicated time points. For each group and $n = 3$ independent replicates, at least 1,000 parasites were counted.

Statistical analysis

Parasite experiments were set up in the fashion of a randomized block design, with each parasite culture of an independent experiment resembling an individual block. Statistical analysis was conducted using GraphPad Prism (version 10.4.1 for Windows, GraphPad Software, Boston, Massachusetts USA, www.graphpad.com).

Generation of figures

Figures 1 (https://BioRender.com/t80p940), 2 (https://BioRender.com/z33s681 and https://BioRender.com/i96g461) and 10 (https://BioRender.com/f26j068) were assembled using BioRender.com.

ACKNOWLEDGMENTS

This work was supported by the Loewe Initiative DRUID (awarded to J.M.P. and J.K.L.).

We thank the University of Giessen blood bank for erythrocyte concentrate, Regina Eberle for assistance with electron microcopy, and Reimar Krieg for synthesis of arylmethylamino steroid compound 1o.

AUTHOR AFFILIATIONS

[1]Biochemistry and Molecular Biology, Interdisciplinary Research Center, Justus Liebig University, Giessen, Germany
[2]Justus Liebig University, Giessen, Germany

PRESENT ADDRESS

Kim C. Heimsch, Institute of Virology, Charité – Universitätsmedizin Berlin, Berlin, Germany
Jacomina Krijnse Locker, Electron microscopy of pathogens, Paul Ehrlich Institute, Langen, Germany

AUTHOR ORCIDs

Eric Springer http://orcid.org/0000-0002-8092-1453

Jude M. Przyborski http://orcid.org/0000-0002-3494-7767

FUNDING

Funder	Grant(s)	Author(s)
Hessisches Ministerium für Wissenschaft und Kunst (Hessian Ministry for Science and Art)	LOEWE-DRUID	Jacomina Krijnse Locker Jude M. Przyborski

AUTHOR CONTRIBUTIONS

Eric Springer, Conceptualization, Data curation, Formal analysis, Investigation, Methodology, Visualization, Writing – original draft, Writing – review and editing | Kim C. Heimsch, Investigation, Writing – review and editing | Niklas Sidiropoulos, Investigation, Writing – review and editing | Jacomina Krijnse Locker, Investigation, Resources, Supervision | Jude M. Przyborski, Conceptualization, Funding acquisition, Methodology, Project administration, Resources, Supervision, Writing – original draft, Writing – review and editing

ADDITIONAL FILES

The following material is available online.

Supplemental Material

Supplemental material (AAC00332-25-s0001.pdf). Fig. S1 and S2.

REFERENCES

1. World Health Organisation. 2024. World malaria report 2024: addressing inequity in the global malaria response.
.
2. Krieg R, Jortzik E, Goetz A-A, Blandin S, Wittlin S, Elhabiri M, Rahbari M, Nuryyeva S, Voigt K, Dahse H-M, Brakhage A, Beckmann S, Quack T, Grevelding CG, Pinkerton AB, Schönecker B, Burrows J, Davioud-Charvet E, Rahlfs S, Becker K. 2017. Arylmethylamino steroids as antiparasitic agents. Nat Commun 8:14478. https://doi.org/10.1038/ncomms14478
3. Blum L, Gul S, Ulshöfer T, Henke M, Krieg R, Berneburg I, Thomas D, Trautmann S, Kurz J, Geyer J, Geisslinger G, Becker K, Parnham MJ, Schiffmann S. 2020. *In-vitro* safety and off-target profile of the antiparasitic arylmethylaminosteroid 1o. Sci Rep 10:7534. https://doi.org/10.1038/s41598-020-64382-w
4. Springer E, Heimsch KC, Rahlfs S, Becker K, Przyborski JM. 2024. Real-time measurements of ATP dynamics via ATeams in *Plasmodium falciparum* reveal drug-class-specific response patterns. Antimicrob Agents Chemother 68:e0169023. https://doi.org/10.1128/aac.01690-23
5. Hoppe HC, van Schalkwyk DA, Wiehart UIM, Meredith SA, Egan J, Weber BW. 2004. Antimalarial quinolines and artemisinin inhibit endocytosis in *Plasmodium falciparum*. Antimicrob Agents Chemother 48:2370–2378. https://doi.org/10.1128/AAC.48.7.2370-2378.2004
6. Roberts L, Egan TJ, Joiner KA, Hoppe HC. 2008. Differential effects of quinoline antimalarials on endocytosis in *Plasmodium falciparum*. Antimicrob Agents Chemother 52:1840–1842. https://doi.org/10.1128/AAC.01478-07
7. Chou AC, Fitch CD. 1993. Control of heme polymerase by chloroquine and other quinoline derivatives. Biochem Biophys Res Commun 195:422–427. https://doi.org/10.1006/bbrc.1993.2060
8. Combrinck JM, Fong KY, Gibhard L, Smith PJ, Wright DW, Egan TJ. 2015. Optimization of a multi-well colorimetric assay to determine haem species in *Plasmodium falciparum* in the presence of anti-malarials. Malar J 14:253. https://doi.org/10.1186/s12936-015-0729-9
9. Combrinck JM, Mabotha TE, Ncokazi KK, Ambele MA, Taylor D, Smith PJ, Hoppe HC, Egan TJ. 2013. Insights into the role of heme in the mechanism of action of antimalarials. ACS Chem Biol 8:133–137. https://doi.org/10.1021/cb300454t
10. Fitch CD, Cai G, Chen Y, Ryerse JS. 2003. Relationship of chloroquine-induced redistribution of a neutral aminopeptidase to hemoglobin accumulation in malaria parasites. Arch Biochem Biophys 410:296–306. https://doi.org/10.1016/s0003-9861(02)00688-4
11. Imamura H, Nhat KPH, Togawa H, Saito K, Iino R, Kato-Yamada Y, Nagai T, Noji H. 2009. Visualization of ATP levels inside single living cells with fluorescence resonance energy transfer-based genetically encoded indicators. Proc Natl Acad Sci USA 106:15651–15656. https://doi.org/10.1073/pnas.0904764106
12. Reifenrath M, Boles E. 2018. A superfolder variant of pH-sensitive pHluorin for *in vivo* pH measurements in the endoplasmic reticulum. Sci Rep 8:11985. https://doi.org/10.1038/s41598-018-30367-z
13. Ch'ng J-H, Lee Y-Q, Gun SY, Chia W-N, Chang Z-W, Wong L-K, Batty KT, Russell B, Nosten F, Renia L, Tan K-W. 2014. Validation of a chloroquine-induced cell death mechanism for clinical use against malaria. Cell Death Dis 5:e1305. https://doi.org/10.1038/cddis.2014.265
14. Ginsburg H, Famin O, Zhang J, Krugliak M. 1998. Inhibition of glutathione-dependent degradation of heme by chloroquine and amodiaquine as a possible basis for their antimalarial mode of action. Biochem Pharmacol 56:1305–1313. https://doi.org/10.1016/s0006-2952(98)00184-1
15. Sullivan DJ, Gluzman IY, Russell DG, Goldberg DE. 1996. On the molecular mechanism of chloroquine's antimalarial action. Proc Natl Acad Sci USA 93:11865–11870. https://doi.org/10.1073/pnas.93.21.11865
16. Ch'ng J-H, Kotturi SR, Chong AG-L, Lear MJ, Tan KS-W. 2010. A programmed cell death pathway in the malaria parasite *Plasmodium falciparum* has general features of mammalian apoptosis but is mediated by clan CA cysteine proteases. Cell Death Dis 1:e26–e26. https://doi.org/10.1038/cddis.2010.2
17. Ch'ng J-H, Liew K, Goh A-P, Sidhartha E, Tan K-W. 2011. Drug-induced permeabilization of parasite's digestive vacuole is a key trigger of programmed cell death in *Plasmodium falciparum*. Cell Death Dis 2:e216. https://doi.org/10.1038/cddis.2011.97
18. Famin O, Ginsburg H. 2002. Differential effects of 4-aminoquinoline-containing antimalarial drugs on hemoglobin digestion in Plasmodium falciparum-infected erythrocytes. Biochem Pharmacol 63:393–398. https://doi.org/10.1016/s0006-2952(01)00878-4
19. Fitch CD. 1998. Involvement of heme in the antimalarial action of chloroquine. Trans Am Clin Climatol Assoc 109:97–105.
20. Reiling SJ, Krohne G, Friedrich O, Geary TG, Rohrbach P. 2018. Chloroquine exposure triggers distinct cellular responses in sensitive versus resistant *Plasmodium falciparum* parasites. Sci Rep 8:11137. https://doi.org/10.1038/s41598-018-29422-6

21. Totino PRR, Daniel-Ribeiro CT, Corte-Real S, de Fátima Ferreira-da-Cruz M. 2008. *Plasmodium falciparum*: erythrocytic stages die by autophagic-like cell death under drug pressure. Exp Parasitol 118:478–486. https://doi.org/10.1016/j.exppara.2007.10.017
22. Sachanonta N, Chotivanich K, Chaisri U, Turner GDH, Ferguson DJP, Day NPJ, Pongponratn E. 2011. Ultrastructural and real-time microscopic changes in *P. falciparum*-infected red blood cells following treatment with antimalarial drugs. Ultrastruct Pathol 35:214–225. https://doi.org/10.3109/01913123.2011.601405
23. Famin O, Krugliak M, Ginsburg H. 1999. Kinetics of inhibition of glutathione-mediated degradation of ferriprotoporphyrin IX by antimalarial drugs. Biochem Pharmacol 58:59–68. https://doi.org/10.1016/s0006-2952(99)00059-3
24. de Villiers KA, Egan TJ. 2021. Heme detoxification in the malaria parasite: a target for antimalarial drug development. Acc Chem Res 54:2649–2659. https://doi.org/10.1021/acs.accounts.1c00154
25. Abshire JR, Rowlands CJ, Ganesan SM, So PTC, Niles JC. 2017. Quantification of labile heme in live malaria parasites using a genetically encoded biosensor. Proc Natl Acad Sci USA 114. https://doi.org/10.1073/pnas.1615195114
26. Martin RE, Ginsburg H, Kirk K. 2009. Membrane transport proteins of the malaria parasite. Mol Microbiol 74:519–528. https://doi.org/10.1111/j.1365-2958.2009.06863.x
27. Francis SE, Sullivan DJ, Goldberg DE. 1997. Hemoglobin metabolism in the malaria parasite *Plasmodium falciparum*. Annu Rev Microbiol 51:97–123. https://doi.org/10.1146/annurev.micro.51.1.97
28. Trager W, Jensen JB. 1976. Human malaria parasites in continuous culture. Science 193:673–675. https://doi.org/10.1126/science.781840
29. Lambros C, Vanderberg JP. 1979. Synchronization of *Plasmodium falciparum* erythrocytic stages in culture. J Parasitol 65:418–420. https://doi.org/10.2307/3280287
30. Smilkstein M, Sriwilaijaroen N, Kelly JX, Wilairat P, Riscoe M. 2004. Simple and inexpensive fluorescence-based technique for high-throughput antimalarial drug screening. Antimicrob Agents Chemother 48:1803–1806. https://doi.org/10.1128/AAC.48.5.1803-1806.2004
31. Schindelin J, Arganda-Carreras I, Frise E, Kaynig V, Longair M, Pietzsch T, Preibisch S, Rueden C, Saalfeld S, Schmid B, Tinevez J-Y, White DJ, Hartenstein V, Eliceiri K, Tomancak P, Cardona A. 2012. Fiji: an open-source platform for biological-image analysis. Nat Methods 9:676–682. https://doi.org/10.1038/nmeth.2019
32. Thomas JA, Buchsbaum RN, Zimniak A, Racker E. 1979. Intracellular pH measurements in ehrlich ascites tumor cells utilizing spectroscopic probes generated *in situ*. Biochemistry 18:2210–2218. https://doi.org/10.1021/bi00578a012
33. Laemmli UK. 1970. Cleavage of structural proteins during the assembly of the head of bacteriophage T4. Nature 227:680–685. https://doi.org/10.1038/227680a0
34. Romero-Calvo I, Ocón B, Martínez-Moya P, Suárez MD, Zarzuelo A, Martínez-Augustin O, de Medina FS. 2010. Reversible ponceau staining as a loading control alternative to actin in western blots. Anal Biochem 401:318–320. https://doi.org/10.1016/j.ab.2010.02.036

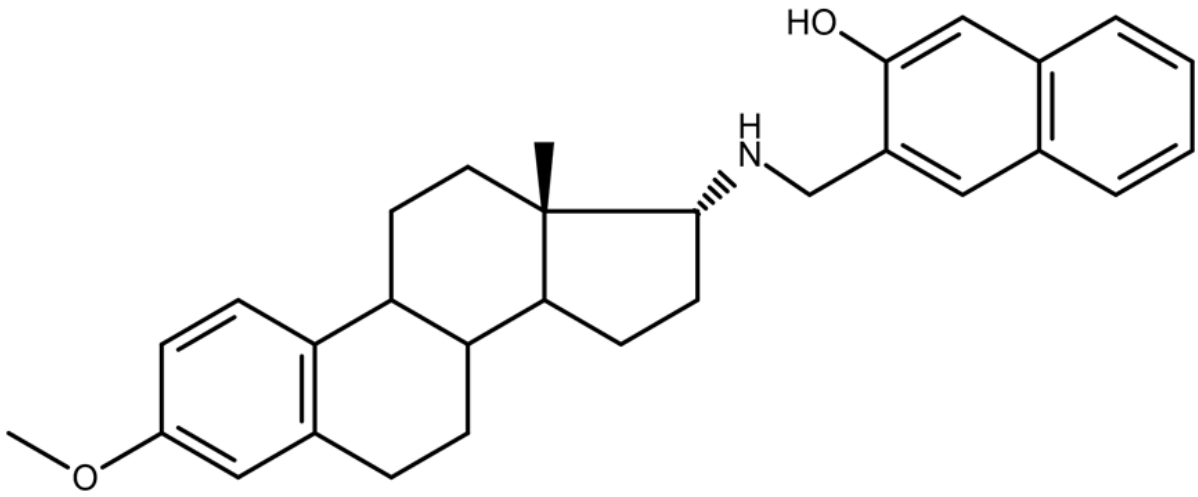

Fig. S1: Molecular structure of arylmethylamino steroid compound 1o

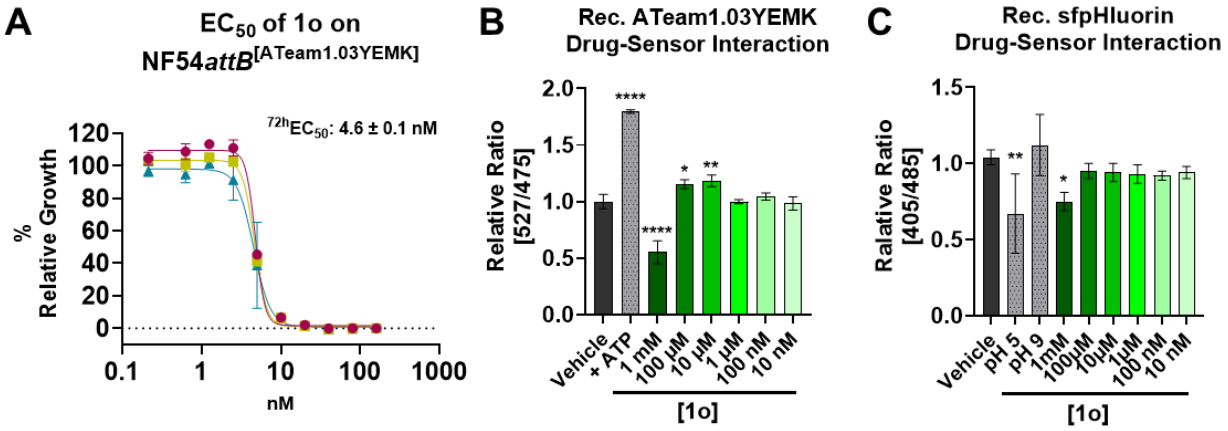

Fig. S2: 1o does not interfere with the ATP or pH sensor within biologically relevant doses. (A) Half maximal effective concentration on growth inhibition after 72 h ($^{72h}EC_{50}$) using SYBR green assay of 1o on the NF54*attB*[ATeam1.03YEMK] sensor cell line. Mean ± SD of n = 3 independent sigmoidal 4-parametric dose-response curves are shown. Each color (magenta (circles), yellow (squares), cyan (triangles)) represents an independent biological replicate. (B) Recombinant his-tagged ATeam1.03YEMK protein incubated with vehicle control, 10 mM ATP, or 1o (10 nM – 1 mM). Relative emission ratio of 527 nm and 475 nm after excitation at 435 nm in a plate reader. (C) Recombinant his-tagged sfpHluorin protein incubated with vehicle control, pH 5 and 9 buffer, or 1o (10 nM – 1 mM). Relative excitation ratio of 390 nm and 482 nm with emission sensing at 530 nm in a plate reader. n = 3 independent experiments are shown. Statistical analysis was conducted using ordinary one-way ANOVA and Dunnetts's multiple comparisons test. Error bars indicate standard deviation. Asterisks indicate significance level (*: $p < 0.05$; **: $p < 0.01$; ***: $p < 0.001$; ****: $p < 0.0001$) compared to the vehicle-treated control group.

3. DISCUSSION

The work presented here aimed to establish an ATP measurement platform that can be applied for drugs' MoA and other metabolic analyses, while overcoming limitations of previously available ATP analysis methods in *P. falciparum*. Furthermore, it was aimed to make this measurement system available for the broader malaria research community.

The work demonstrates for the first time that ATP sensors of the ATeam series (Imamura et al., 2009; Kotera et al., 2010) can successfully be applied for ATP measurements in *P. falciparum* and points out critical pitfalls to consider when using them (Springer et al., 2024). These include the selection of the different ATeam variants. Comparing ATeam1.03YEMK and ATeam1.03nD/nA side by side for the first time, the work uncovered a substantially lower signal intensity of ATeam1.03nD/nA in *P. falciparum*. When applying fluorescence techniques, the signal intensity is a feature that can determine the success or failure of an experiment in a confined analytical setting. Thus, these findings will likely contribute to considerations of future experiment designs. Additionally, the work describes the establishment and successful application of the advanced pH sensor sfpHluorin (Reifenrath & Boles, 2018) in *P. falciparum* (Springer et al., 2024). The pH measurements were intended to control for confounding factors affecting pH and possibly ATeam measurements. However, they also contributed to the further interpretations of ATeam measurements and are now established in *P. falciparum* for use in combination with other pH-affected sensors or even within entirely different research questions, as well.

Based on the establishment of the sensors in the cytosol of *P. falciparum*, we proved their feasibility for MoA analyses in trophozoite stage parasites treated with a selection of established and promising antiplasmodial compounds (Springer et al., 2024). Compared to other ATP analysis techniques, the sensors overcame previous limitations and allowed live-cell time-course measurements of ATP levels that are free from confounding by parasite size. Thus, they allow the comparison of physiologic [ATP] rather than ATP abundance. The measurements uncovered distinct response patterns that deepen our understanding of existing drugs and further elucidate the MoA of promising drug candidates. While the panel of selected compounds did not include representatives of all established compound classes, the selection includes the ones most relevant against *P. falciparum* malaria (WHO, 2024b).

While insightful on its own, the power of the presented ATP measurement system unfolds in particular through the complementation of other methodologies. The assessment of 1o's induced ATP and pH sensor responses revealed parallels to arylamino alcohols (Springer et al., 2025). As a consequence, this parallel led to further MoA analyses, resulting in the first proposal of a model of 1o's parasite-killing activity (Springer et al., 2025). This highlights the significance of the herein established system.

Additionally, within the time period of this work, the system already proved to benefit the broader malaria research community. The sfpHluorin sensor cell line was successfully applied for controlling measurements of the glutathione redox potential, the NADPH level, and the NADH:NAD^+ ratio in *P. falciparum* (Heimsch, 2022). Furthermore, the ATeam1.03YEMK cell line helped to uncover the importance of mitochondrial ATP synthesis for gametogenesis in *P. falciparum* (Sparkes et al., 2024), again, underlining its capability to address a broad variety of research questions.

The extent of the impact of this work is yet to be discovered. Future fields of its application are multifarious and range from comprehensive MoA studies, or the addressing of specific metabolic issues – potentially on the level of subcellular compartments. These applications include the investigation of the metabolic interconnection of the parasite with its human host or the deeper understanding of mitochandrial ATP generation in gametocytes. The presented system potentially further broadens our horizon on the level of basic parasite biology and in-depth understanding of drug effects, which both is critically needed to gain control of the perennial threat to global health that is posed by malaria throughout the centuries until today.

4. REFERENCES

Abshire, J. R., Rowlands, C. J., Ganesan, S. M., So, P. T. C., & Niles, J. C. (2017). Quantification of labile heme in live malaria parasites using a genetically encoded biosensor. *Proceedings of the National Academy of Sciences of the United States of America*, *114*(11), E2068-E2076. https://doi.org/10.1073/pnas.1615195114

Achan, J., Talisuna, A. O., Erhart, A., Yeka, A., Tibenderana, J. K., Baliraine, F. N., Rosenthal, P. J., & D'Alessandro, U. (2011). Quinine, an old anti-malarial drug in a modern world: Role in the treatment of malaria. *Malaria Journal*, *10*, 144. https://doi.org/10.1186/1475-2875-10-144

Alghamdi, J. M., Al-Qahtani, A. A., Alhamlan, F. S., & Al-Qahtani, A. A. (2024). Recent Advances in the Treatment of Malaria. *Pharmaceutics*, *16*(11), 1416. https://doi.org/10.3390/pharmaceutics16111416

Ando, T., Imamura, H., Suzuki, R., Aizaki, H., Watanabe, T., Wakita, T., & Suzuki, T. (2012). Visualization and measurement of ATP levels in living cells replicating hepatitis C virus genome RNA. *PLoS Pathogens*, *8*(3), e1002561. https://doi.org/10.1371/journal.ppat.1002561

Aronson, J. K., La Caze, A., Kelly, M. P., Parkkinen, V.-P., & Williamson, J. (2018). The use of mechanistic evidence in drug approval. *Journal of Evaluation in Clinical Practice*, *24*(5), 1166–1176. https://doi.org/10.1111/jep.12960

Atamna, H., Pascarmona, G., & Ginsburg, H. (1994). Hexose-monophosphate shunt activity in intact Plasmodium falciparum-infected erythrocytes and in free parasites. *Molecular and Biochemical Parasitology*, *67*(1), 79–89. https://doi.org/10.1016/0166-6851(94)90098-1

Ayi, K., Liles, W. C., Gros, P., & Kain, K. C. (2009). Adenosine triphosphate depletion of erythrocytes simulates the phenotype associated with pyruvate kinase deficiency and confers protection against Plasmodium falciparum in vitro. *The Journal of Infectious Diseases*, *200*(8), 1289–1299. https://doi.org/10.1086/605843

Baeza-Lehnert, F., Saab, A. S., Gutiérrez, R., Larenas, V., Díaz, E., Horn, M., Vargas, M., Hösli, L., Stobart, J., Hirrlinger, J., Weber, B., & Barros, L. F. (2019). Non-Canonical Control of Neuronal Energy Status by the Na+ Pump. *Cell Metabolism*, *29*(3), 668-680.e4. https://doi.org/10.1016/j.cmet.2018.11.005

Bhatt, S., Weiss, D. J., Cameron, E., Bisanzio, D., Mappin, B., Dalrymple, U., Battle, K., Moyes, C. L., Henry, A., Eckhoff, P. A., Wenger, E. A., Briët, O., Penny, M. A., Smith, T. A., Bennett, A., Yukich, J., Eisele, T. P., Griffin, J. T., Fergus, C. A., . . . Gething, P. W. (2015). The effect of malaria control on Plasmodium falciparum in Africa between 2000 and 2015. *Nature*, *526*(7572), 207–211. https://doi.org/10.1038/nature15535

Biddau, M., & Sheiner, L. (2019). Targeting the apicoplast in malaria. *Biochemical Society Transactions*, *47*(4), 973–983. https://doi.org/10.1042/BST20170563

Borges-Pereira, L., Thomas, S. J., dos Anjos e Silva, Amanda Laizy, Bartlett, P. J., Thomas, A. P., & Garcia, C. R. S. (2020). The genetic Ca2+ sensor GCaMP3 reveals multiple Ca2+ stores differentially coupled to Ca2+ entry in the human malaria parasite Plasmodium falciparum. *The Journal of Biological Chemistry*, *295*(44), 14998–15012. https://doi.org/10.1074/jbc.RA120.014906

Camarda, G., Jirawatcharadech, P., Priestley, R. S., Saif, A., March, S., Wong, M. H. L., Leung, S., Miller, A. B., Baker, D. A., Alano, P., Paine, M. J. I., Bhatia, S. N., O'Neill, P. M., Ward, S. A., & Biagini, G. A. (2019). Antimalarial activity of primaquine operates via a two-step biochemical relay. *Nature Communications*, *10*(1), 3226. https://doi.org/10.1038/s41467-019-11239-0

Cevenini, L., Camarda, G., Michelini, E., Siciliano, G., Calabretta, M. M., Bona, R., Kumar, T. R. S., Cara, A., Branchini, B. R., Fidock, D. A., Roda, A., & Alano, P. (2014). Multicolor bioluminescence boosts malaria research: Quantitative dual-color assay and single-cell imaging in Plasmodium falciparum parasites. *Analytical Chemistry*, *86*(17), 8814–8821. https://doi.org/10.1021/ac502098w

Chakraborty, A. (2016). Understanding the biology of the Plasmodium falciparum apicoplast; an excellent target for antimalarial drug development. *Life Sciences*, *158*, 104–110. https://doi.org/10.1016/j.lfs.2016.06.030

Combrinck, J. M., Mabotha, T. E., Ncokazi, K. K., Ambele, M. A., Taylor, D., Smith, P. J., Hoppe, H. C., & Egan, T. J. (2013). Insights into the role of heme in the mechanism of action of antimalarials. *ACS Chemical Biology*, *8*(1), 133–137. https://doi.org/10.1021/cb300454t

Conley, J. M., Radhakrishnan, S., Valentino, S. A., & Tantama, M. (2017). Imaging extracellular ATP with a genetically-encoded, ratiometric fluorescent sensor. *PloS One*, *12*(11), e0187481. https://doi.org/10.1371/journal.pone.0187481

Counihan, N. A., Modak, J. K., & Koning-Ward, T. F. de (2021). How Malaria Parasites Acquire Nutrients From Their Host. *Frontiers in Cell and Developmental Biology*, *9*, 649184. https://doi.org/10.3389/fcell.2021.649184

Cowman, A. F., Healer, J., Marapana, D., & Marsh, K. (2016). Malaria: Biology and Disease. *Cell*, *167*(3), 610–624. https://doi.org/10.1016/j.cell.2016.07.055

Croft, A. M. (2007). A lesson learnt: the rise and fall of Lariam and Halfan. *Journal of the Royal Society of Medicine*, *100*(4), 170–174. https://doi.org/10.1258/jrsm.100.4.170

Cui, L., & Su, X. (2009). Discovery, mechanisms of action and combination therapy of artemisinin. *Expert Review of Anti-Infective Therapy*, *7*(8), 999–1013. https://doi.org/10.1586/eri.09.68

Davis, R. L. (2020). Mechanism of Action and Target Identification: A Matter of Timing in Drug Discovery. *IScience*, *23*(9), 101487. https://doi.org/10.1016/j.isci.2020.101487

Delves, M., Plouffe, D., Scheurer, C., Meister, S., Wittlin, S., Winzeler, E. A., Sinden, R. E., & Leroy, D. (2012). The activities of current antimalarial drugs on the life cycle stages of Plasmodium: A comparative study with human and rodent parasites. *PLOS Medicine*, *9*(2), e1001169. https://doi.org/10.1371/journal.pmed.1001169

Desai, S. A., Bezrukov, S. M., & Zimmerberg, J. (2000). A voltage-dependent channel involved in nutrient uptake by red blood cells infected with the malaria parasite. *Nature*, *406*(6799), 1001–1005. https://doi.org/10.1038/35023000

Desai, S. A., Krogstad, D. J., & McCleskey, E. W. (1993). A nutrient-permeable channel on the intraerythrocytic malaria parasite. *Nature*, *362*(6421), 643–646. https://doi.org/10.1038/362643a0

Desai, S. A., & Rosenberg, R. L. (1997). Pore size of the malaria parasite's nutrient channel. *Proceedings of the National Academy of Sciences of the United States of America*, *94*(5), 2045–2049. https://doi.org/10.1073/pnas.94.5.2045

Djimdé, A., Doumbo, O. K., Cortese, J. F., Kayentao, K., Doumbo, S., Diourté, Y., Coulibaly, D., Dicko, A., Su, X. Z., Nomura, T., Fidock, D. A., Wellems, T. E., & Plowe, C. V. (2001). A molecular marker for chloroquine-resistant falciparum malaria. *The New England Journal of Medicine*, *344*(4), 257–263. https://doi.org/10.1056/NEJM200101253440403

Downie, M. J., Kirk, K., & Mamoun, C. B. (2008). Purine salvage pathways in the intraerythrocytic malaria parasite Plasmodium falciparum. *Eukaryotic Cell*, *7*(8), 1231–1237. https://doi.org/10.1128/EC.00159-08

Doysabas, K. C. C., Oba, M., Ishibashi, T., Shibata, H., Takemae, H., Shimoda, H., Tarigan, R., Mizutani, T., Iida, A., & Hondo, E. (2020). Ateam technology for detecting early signs of viral cytopathic effect. *The Journal of Veterinary Medical Science*, *82*(3), 387–393. https://doi.org/10.1292/jvms.20-0021

Duffy, P. E., Gorres, J. P., Healy, S. A., & Fried, M. (2024). Malaria vaccines: A new era of prevention and control. *Nature Reviews Microbiology*, *22*(12), 756–772. https://doi.org/10.1038/s41579-024-01065-7

Dziekan, J. M., Yu, H., Chen, D., Dai, L., Wirjanata, G., Larsson, A., Prabhu, N., Sobota, R. M., Bozdech, Z., & Nordlund, P. (2019). Identifying purine nucleoside phosphorylase as the target of quinine using cellular thermal shift assay. *Science Translational Medicine*, *11*(473). https://doi.org/10.1126/scitranslmed.aau3174

Edgar, R. C. S., Malcolm, T. R., Siddiqui, G., Giannangelo, C., Counihan, N. A., Challis, M., Duffy, S., Chowdhury, M., Marfurt, J., Dans, M., Wirjanata, G., Noviyanti, R., Daware, K., Suraweera, C. D., Price, R. N., Wittlin, S., Avery, V. M., Drinkwater, N., Charman, S. A., McGowan, S. (2024). On-target, dual aminopeptidase inhibition provides cross-species antimalarial activity. *MBio*, *15*(6), e0096624. https://doi.org/10.1128/mbio.00966-24

Egan, T. J., Ross, D. C., & Adams, P. A. (1994). Quinoline anti-malarial drugs inhibit spontaneous formation of beta-haematin (malaria pigment). *FEBS Letters*, *352*(1), 54–57. https://doi.org/10.1016/0014-5793(94)00921-X

Elliott, D. A., McIntosh, M. T., Hosgood, H. D., Chen, S., Zhang, G., Baevova, P., & Joiner, K. A. (2008). Four distinct pathways of hemoglobin uptake in the malaria parasite Plasmodium falciparum. *Proceedings of the National Academy of Sciences of the United States of America*, *105*(7), 2463–2468. https://doi.org/10.1073/pnas.0711067105

Famin, O., & Ginsburg, H. (2002). Differential effects of 4-aminoquinoline-containing antimalarial drugs on hemoglobin digestion in Plasmodium falciparum-infected erythrocytes. *Biochemical Pharmacology*, *63*(3), 393–398. https://doi.org/10.1016/S0006-2952(01)00878-4

Fidock, D. A., Nomura, T., Talley, A. K., Cooper, R. A., Dzekunov, S. M., Ferdig, M. T., Ursos, L. M., Sidhu, A. B., Naudé, B., Deitsch, K. W., Su, X. Z., Wootton, J. C., Roepe, P. D., & Wellems, T. E. (2000). Mutations in the P. Falciparum digestive vacuole transmembrane protein PfCRT and evidence for their role in chloroquine resistance. *Molecular Cell*, *6*(4), 861–871. https://doi.org/10.1016/s1097-2765(05)00077-8

Fitch, C. D. (1998). Involvement of heme in the antimalarial action of chloroquine. *Transactions of the American Clinical and Climatological Association*, *109*, 97-105; discussion 105-6. https://pubmed.ncbi.nlm.nih.gov/9601131/

Fitch, C. D. (2004). Ferriprotoporphyrin IX, phospholipids, and the antimalarial actions of quinoline drugs. *Life Sciences*, *74*(16), 1957–1972. https://doi.org/10.1016/j.lfs.2003.10.003

Forkink, M., Manjeri, G. R., Liemburg-Apers, D. C., Nibbeling, E., Blanchard, M., Wojtala, A., Smeitink, J. A. M., Wieckowski, M. R., Willems, P. H. G. M., & Koopman, W. J. H. (2014). Mitochondrial hyperpolarization during chronic complex I inhibition is sustained by low activity of complex II, III, IV and V. *Biochimica Et Biophysica Acta*, *1837*(8), 1247–1256. https://doi.org/10.1016/j.bbabio.2014.04.008

Frei, M. S., Mehta, S., & Zhang, J. (2024). Next-Generation Genetically Encoded Fluorescent Biosensors Illuminate Cell Signaling and Metabolism. *Annual Review of Biophysics*, *53*(1), 275–297. https://doi.org/10.1146/annurev-biophys-030722-021359

Fry, M., Webb, E., & Pudney, M. (1990). Effect of mitochondrial inhibitors on adenosinetriphosphate levels in Plasmodium falciparum. *Comparative Biochemistry and Physiology. B, Comparative Biochemistry*, *96*(4), 775–782. https://doi.org/10.1016/0305-0491(90)90230-q

Fujisawa, K., Wakazaki, M., Matsuzaki, A., Matsumoto, T., Yamamoto, N., Noma, T., & Takami, T. (2022). Adenylate Kinase Isozyme 3 Regulates Mitochondrial Energy

Metabolism and Knockout Alters HeLa Cell Metabolism. *International Journal of Molecular Sciences*, *23*(8), 4316. https://doi.org/10.3390/ijms23084316

Garten, M., Nasamu, A. S., Niles, J. C., Zimmerberg, J., Goldberg, D. E., & Beck, J. R. (2018). Exp2 is a nutrient-permeable channel in the vacuolar membrane of Plasmodium and is essential for protein export via PTEX. *Nature Microbiology*, *3*(10), 1090–1098. https://doi.org/10.1038/s41564-018-0222-7

Gemayel, R. (2017). Malaria, metabolism and mathematical models. *The FEBS Journal*, *284*(16), 2553–2555. https://doi.org/10.1111/febs.14161

Gerkau, N. J., Lerchundi, R., Nelson, J. S. E., Lantermann, M., Meyer, J., Hirrlinger, J., & Rose, C. R. (2019). Relation between activity-induced intracellular sodium transients and ATP dynamics in mouse hippocampal neurons. *The Journal of Physiology*, *597*(23), 5687–5705. https://doi.org/10.1113/JP278658

Ginsburg, H., Krugliak, M., Eidelman, O., & Cabantchik, Z. I. (1983). New permeability pathways induced in membranes of Plasmodium falciparum infected erythrocytes. *Molecular and Biochemical Parasitology*, *8*(2), 177–190. https://doi.org/10.1016/0166-6851(83)90008-7

Ginsburg, H., Kutner, S., Krugliak, M., & Cabantchik, Z. I. (1985). Characterization of permeation pathways appearing in the host membrane of Plasmodium falciparum infected red blood cells. *Molecular and Biochemical Parasitology*, *14*(3), 313–322. https://doi.org/10.1016/0166-6851(85)90059-3

Guttery, D. S., Zeeshan, M., Holder, A. A., Tromer, E. C., & Tewari, R. (2023). Meiosis in Plasmodium: How does it work? *Trends in Parasitology*, *39*(10), 812–821. https://doi.org/10.1016/j.pt.2023.07.002

Haynes, E. P., Rajendran, M., Henning, C. K., Mishra, A., Lyon, A. M., & Tantama, M. (2019). Quantifying Acute Fuel and Respiration Dependent pH Homeostasis in Live Cells Using the mCherryTYG Mutant as a Fluorescence Lifetime Sensor. *Analytical Chemistry*, *91*(13), 8466–8475. https://doi.org/10.1021/acs.analchem.9b01562

Heimsch, K. C (2022). Establishment of improved genetically encoded fluorescence-based biosensors to monitor redox and energy dynamics in the malaria parasite Plasmodium falciparum *Justus Liebig University Giessen*.

Henshall, I. G., & Spielmann, T. (2023). Critical interdependencies between Plasmodium nutrient flux and drugs. *Trends in Parasitology*, *39*(11), 936–944. https://doi.org/10.1016/j.pt.2023.08.008

Herraiz, T., Guillén, H., González-Peña, D., & Arán, V. J. (2019). Antimalarial Quinoline Drugs Inhibit β-Hematin and Increase Free Hemin Catalyzing Peroxidative Reactions and Inhibition of Cysteine Proteases. *Scientific Reports*, *9*(1), 15398. https://doi.org/10.1038/s41598-019-51604-z

Higgins, M., Manko, E., Ward, D., Phelan, J. E., Nolder, D., Sutherland, C. J., Clark, T. G., & Campino, S. (2024). New reference genomes to distinguish the sympatric malaria parasites, Plasmodium ovale curtisi and Plasmodium ovale wallikeri. *Scientific Reports*, *14*(1), 3843. https://doi.org/10.1038/s41598-024-54382-5

Hoppe, H. C., van Schalkwyk, D. A., Wiehart, U. I. M., Meredith, S. A., Egan, J., & Weber, B. W. (2004). Antimalarial quinolines and artemisinin inhibit endocytosis in Plasmodium falciparum. *Antimicrobial Agents and Chemotherapy*, *48*(7), 2370–2378. https://doi.org/10.1128/AAC.48.7.2370-2378.2004

Imamura, H., Nhat, K. P. H., Togawa, H., Saito, K., Iino, R., Kato-Yamada, Y., Nagai, T., & Noji, H. (2009). Visualization of ATP levels inside single living cells with fluorescence resonance energy transfer-based genetically encoded indicators. *Proceedings of the National Academy of Sciences of the United States of America*, *106*(37), 15651–15656. https://doi.org/10.1073/pnas.0904764106

ICH guideline S7A Safety pharmacology studies for human pharmaceuticals. (2000). https://database.ich.org/sites/default/files/S7A_Guideline.pdf

ICH guideline M3(R2) on non-clinical safety studies for the conduct of human clinical trials and marketing authorisation for pharmaceuticals. (2009). https://database.ich.org/sites/default/files/M3_R2__Guideline.pdf

Iworima, D. G., Pasqualotto, B. A., & Rintoul, G. L. (2016). Kif5 regulates mitochondrial movement, morphology, function and neuronal survival. *Molecular and Cellular Neurosciences*, *72*, 22–33. https://doi.org/10.1016/j.mcn.2015.12.014

Jonscher, E., Flemming, S., Schmitt, M., Sabitzki, R., Reichard, N., Birnbaum, J., Bergmann, B., Höhn, K., & Spielmann, T. (2019). Pfvps45 Is Required for Host Cell Cytosol Uptake by Malaria Blood Stage Parasites. *Cell Host & Microbe*, *25*(1), 166-173.e5. https://doi.org/10.1016/j.chom.2018.11.010

Jortzik, E., Wang, L., & Becker, K. (2012). Thiol-based posttranslational modifications in parasites. *Antioxidants & Redox Signaling*, *17*(4), 657–673. https://doi.org/10.1089/ars.2011.4266

Kahancová, A., Sklenář, F., Ježek, P., & Dlasková, A. (2020). Overexpression of native IF1 downregulates glucose-stimulated insulin secretion by pancreatic INS-1E cells. *Scientific Reports*, *10*(1), 1551. https://doi.org/10.1038/s41598-020-58411-x

Kanaani, J., & Ginsburg, H. (1989). Metabolic interconnection between the human malarial parasite Plasmodium falciparum and its host erythrocyte. Regulation of ATP levels by means of an adenylate translocator and adenylate kinase. *Journal of Biological Chemistry*, *264*(6), 3194–3199. https://pubmed.ncbi.nlm.nih.gov/2536737/

Kanaani, J., & Ginsburg, H. (1991). Transport of lactate in Plasmodium falciparum-infected human erythrocytes. *Journal of Cellular Physiology*, *149*(3), 469–476. https://doi.org/10.1002/jcp.1041490316

Kanaani, J., & Ginsburg, H. (1992). Effects of cinnamic acid derivatives on in vitro growth of Plasmodium falciparum and on the permeability of the membrane of malaria-infected erythrocytes. *Antimicrobial Agents and Chemotherapy*, *36*(5), 1102–1108. https://doi.org/10.1128/AAC.36.5.1102

Kasozi, D., Mohring, F., Rahlfs, S., Meyer, A. J., & Becker, K. (2013). Real-time imaging of the intracellular glutathione redox potential in the malaria parasite Plasmodium falciparum. *PLoS Pathogens*, *9*(12), e1003782. https://doi.org/10.1371/journal.ppat.1003782

Ke, H., Lewis, I. A., Morrisey, J. M., McLean, K. J., Ganesan, S. M., Painter, H. J., Mather, M. W., Jacobs-Lorena, M., Llinás, M., & Vaidya, A. B. (2015). Genetic investigation of tricarboxylic acid metabolism during the Plasmodium falciparum life cycle. *Cell Reports*, *11*(1), 164–174. https://doi.org/10.1016/j.celrep.2015.03.011

Khan, T., van Brummelen, A. C., Parkinson, C. J., & Hoppe, H. C. (2012). Atp and luciferase assays to determine the rate of drug action in in vitro cultures of Plasmodium falciparum. *Malaria Journal*, *11*(1), 369. https://doi.org/10.1186/1475-2875-11-369

Kim, H., Ju, J., Lee, H. N., Chun, H., & Seong, J. (2021). Genetically Encoded Biosensors Based on Fluorescent Proteins. *Sensors*, *21*(3), 795. https://doi.org/10.3390/s21030795

Kirk, K., Horner, H. A., & Kirk, J. (1996). Glucose uptake in Plasmodium falciparum-infected erythrocytes is an equilibrative not an active process. *Molecular and Biochemical Parasitology*, *82*(2), 195–205. https://doi.org/10.1016/0166-6851(96)02734-x

Kishikawa, J., Fujikawa, M., Imamura, H., Yasuda, K., Noji, H., Ishii, N., Mitani, S., & Yokoyama, K. (2012). Mrt letter: Expression of ATP sensor protein in Caenorhabditis elegans. *Microscopy Research and Technique*, *75*(1), 15–19. https://doi.org/10.1002/jemt.21103

Köhler, S., Schmidt, H., Fülle, P., Hirrlinger, J., & Winkler, U. (2020). A Dual Nanosensor Approach to Determine the Cytosolic Concentration of ATP in Astrocytes. *Frontiers in Cellular Neuroscience*, *14*, 565921. https://doi.org/10.3389/fncel.2020.565921

Korsinczky, M., Chen, N., Kotecka, B., Saul, A., Rieckmann, K., & Cheng, Q. (2000). Mutations in Plasmodium falciparum cytochrome b that are associated with atovaquone

resistance are located at a putative drug-binding site. *Antimicrobial Agents and Chemotherapy*, *44*(8), 2100–2108. https://doi.org/10.1128/AAC.44.8.2100-2108.2000

Kostyuk, A. I., Panova, A. S., Kokova, A. D., Kotova, D. A., Maltsev, D. I., Podgorny, O. V., Belousov, V. V., & Bilan, D. S. (2020). In Vivo Imaging with Genetically Encoded Redox Biosensors. *International Journal of Molecular Sciences*, *21*(21). https://doi.org/10.3390/ijms21218164

Kotera, I., Iwasaki, T., Imamura, H., Noji, H., & Nagai, T. (2010). Reversible dimerization of Aequorea victoria fluorescent proteins increases the dynamic range of FRET-based indicators. *ACS Chemical Biology*, *5*(2), 215–222. https://doi.org/10.1021/cb900263z

Krugliak, M., Zhang, J., & Ginsburg, H. (2002). Intraerythrocytic Plasmodium falciparum utilizes only a fraction of the amino acids derived from the digestion of host cell cytosol for the biosynthesis of its proteins. *Molecular and Biochemical Parasitology*, *119*(2), 249–256. https://doi.org/10.1016/s0166-6851(01)00427-3

Kuhn, Y., Rohrbach, P., & Lanzer, M. (2007). Quantitative pH measurements in Plasmodium falciparum-infected erythrocytes using pHluorin. *Cellular Microbiology*, *9*(4), 1004–1013. https://doi.org/10.1111/j.1462-5822.2006.00847.x

Lelièvre, J., Almela, M. J., Lozano, S., Miguel, C., Franco, V., Leroy, D., & Herreros, E. (2012). Activity of clinically relevant antimalarial drugs on Plasmodium falciparum mature gametocytes in an ATP bioluminescence "transmission blocking" assay. *PloS One*, *7*(4), e35019. https://doi.org/10.1371/journal.pone.0035019

Lerchundi, R., Huang, N., & Rose, C. R. (2020). Quantitative Imaging of Changes in Astrocytic and Neuronal Adenosine Triphosphate Using Two Different Variants of ATeam. *Frontiers in Cellular Neuroscience*, *14*, 80. https://doi.org/10.3389/fncel.2020.00080

Lerchundi, R., Kafitz, K. W., Winkler, U., Färfers, M., Hirrlinger, J., & Rose, C. R. (2019). Fret-based imaging of intracellular ATP in organotypic brain slices. *Journal of Neuroscience Research*, *97*(8), 933–945. https://doi.org/10.1002/jnr.24361

Lisk, G., & Desai, S. A. (2005). The plasmodial surface anion channel is functionally conserved in divergent malaria parasites. *Eukaryotic Cell*, *4*(12), 2153–2159. https://doi.org/10.1128/EC.4.12.2153-2159.2005

Liu, J., Istvan, E. S., Gluzman, I. Y., Gross, J., & Goldberg, D. E. (2006). Plasmodium falciparum ensures its amino acid supply with multiple acquisition pathways and redundant proteolytic enzyme systems. *Proceedings of the National Academy of Sciences of the United States of America*, *103*(23), 8840–8845. https://doi.org/10.1073/pnas.0601876103

MacRae, J. I., Dixon, M. W., Dearnley, M. K., Chua, H. H., Chambers, J. M., Kenny, S., Bottova, I., Tilley, L., & McConville, M. J. (2013). Mitochondrial metabolism of sexual and asexual blood stages of the malaria parasite Plasmodium falciparum. *BMC Biology*, *11*, 67. https://doi.org/10.1186/1741-7007-11-67

The Malaria Atlas Project. (2024). Plasmodium falciparum incidence rate in all age groups for 2022. Map version: 202406. https://data.malariaatlas.org/printables?metricId=pf_incidence_rate&version=202406&year=2022&colorRamp=RASTER_2019_Global_Pf_Incidence&geoLevel=global&adminCode=global

Mamudu, C. O., Tebamifor, M. E., Sule, M. O., Dokunmu, T. M., Ogunlana, O. O., & Iheagwam, F. N. (2024). Apicoplast-Resident Processes: Exploiting the Chink in the Armour of Plasmodium falciparum Parasites. *Advances in Pharmacological and Pharmaceutical Sciences*, *2024*, 9940468. https://doi.org/10.1155/2024/9940468

Mandal, S., Moudgil, M., & Mandal, S. K. (2009). Rational drug design. *European Journal of Pharmacology*, *625*(1-3), 90–100. https://doi.org/10.1016/j.ejphar.2009.06.065

Marchetti, R. V., Lehane, A. M., Shafik, S. H., Winterberg, M., Martin, R. E., & Kirk, K. (2015). A lactate and formate transporter in the intraerythrocytic malaria parasite, Plasmodium falciparum. *Nature Communications*, *6*(1), 6721. https://doi.org/10.1038/ncomms7721

Mayer, D. C. G. (2021). Protein Sorting in Plasmodium Falciparum. *Life*, *11*(9), 937. https://doi.org/10.3390/life11090937

McCarthy, J. S., & Price, R. N. (2015). 40 - Antimalarial Drugs. In J. E. Bennett, G. L. Mandell, & R. G. Douglas (Eds.), *Mandell, Douglas, and Bennett's principles and practice of infectious diseases* (495-509.e5). Elsevier Saunders. https://doi.org/10.1016/B978-1-4557-4801-3.00040-0

Mesén-Ramírez, P., Bergmann, B., Elhabiri, M., Zhu, L., Thien, H. von, Castro-Peña, C., Gilberger, T.-W., Davioud-Charvet, E., Bozdech, Z., Bachmann, A., & Spielmann, T. (2021a). The parasitophorous vacuole nutrient channel is critical for drug access in malaria parasites and modulates the artemisinin resistance fitness cost. *Cell Host & Microbe*, *29*(12), 1774-1787.e9. https://doi.org/10.1016/j.chom.2021.11.002

Mesén-Ramírez, P., Bergmann, B., Elhabiri, M., Zhu, L., Thien, H. von, Castro-Peña, C., Gilberger, T.-W., Davioud-Charvet, E., Bozdech, Z., Bachmann, A., & Spielmann, T. (2021b). The parasitophorous vacuole nutrient channel is critical for drug access in malaria parasites and modulates the artemisinin resistance fitness cost. *Cell Host & Microbe*, *29*(12), 1774-1787.e9. https://doi.org/10.1016/j.chom.2021.11.002

Mesén-Ramírez, P., Bergmann, B., Tran, T. T., Garten, M., Stäcker, J., Naranjo-Prado, I., Höhn, K., Zimmerberg, J., & Spielmann, T. (2019). Exp1 is critical for nutrient uptake across the parasitophorous vacuole membrane of malaria parasites. *PLoS Biology*, *17*(9), e3000473. https://doi.org/10.1371/journal.pbio.3000473

Meshnick, S. R., Taylor, T. E., & Kamchonwongpaisan, S. (1996). Artemisinin and the antimalarial endoperoxides: From herbal remedy to targeted chemotherapy. *Microbiological Reviews*, *60*(2), 301–315. https://doi.org/10.1128/mr.60.2.301-315.1996

Miguel-Blanco, C., Molina, I., Bardera, A. I., Díaz, B., las Heras, L. de, Lozano, S., González, C., Rodrigues, J., Delves, M. J., Ruecker, A., Colmenarejo, G., Viera, S., Martínez-Martínez, M. S., Fernández, E., Baum, J., Sinden, R. E., & Herreros, E. (2017). Hundreds of dual-stage antimalarial molecules discovered by a functional gametocyte screen. *Nature Communications*, *8*(1), 15160. https://doi.org/10.1038/ncomms15160

Mo, Y., Zhou, H., Xu, J., Chen, X., Li, L., & Zhang, S. (2023). Genetically encoded fluorescence lifetime biosensors: Overview, advances, and opportunities. *Analyst*, *148*(20), 4939–4953. https://doi.org/10.1039/D3AN01201H

Mohring, F., Jortzik, E., & Becker, K. (2016). Comparison of methods probing the intracellular redox milieu in Plasmodium falciparum. *Molecular and Biochemical Parasitology*, *206*(1-2), 75–83. https://doi.org/10.1016/j.molbiopara.2015.11.002

Morais, I., Medeiros, M. M., Carvalho, M., Morello, J., Teixeira, S. M., Maciel, S., Nhantumbo, J., Balau, A., Rosa, M. T. G., Nogueira, F., Rodrigues, J. A., Carvalho, F. A., Antunes, A. M. M., & Arez, A. P. (2022). Synthetic Red Blood Cell-Specific Glycolytic Intermediate 2,3-Diphosphoglycerate (2,3-DPG) Inhibits Plasmodium falciparum Development In Vitro. *Frontiers in Cellular and Infection Microbiology*, *12*, 840968. https://doi.org/10.3389/fcimb.2022.840968

Mounkoro, P., Michel, T., & Meunier, B. (2021). Revisiting the mode of action of the antimalarial proguanil using the yeast model. *Biochemical and Biophysical Research Communications*, *534*, 94–98. https://doi.org/10.1016/j.bbrc.2020.12.004

Nandal, R., Kumar, D., Aggarwal, N., Kumar, V., Narasimhan, B., Marwaha, R. K., Sharma, P. C., Kumar, S., Bansal, N., Chopra, H., & Deep, A. (2024). Recent advances, challenges and updates on the development of therapeutics for malaria. *EXCLI Journal*, *23*, 672–713. https://doi.org/10.17179/excli2023-6856

Niazi, S. K., Al-Shaqha, W. M., & Mirza, Z. (2023). Proposal of International Council for Harmonization (ICH) Guideline for the Approval of Biosimilars. *Journal of Market*

Access & Health Policy, *11*(1), 2147286. https://doi.org/10.1080/20016689.2022.2147286

Olszewski, K. L., & Llinás, M. (2011). Central carbon metabolism of Plasmodium parasites. *Molecular and Biochemical Parasitology*, *175*(2), 95–103. https://doi.org/10.1016/j.molbiopara.2010.09.001

Omara-Opyene, A. L., Moura, P. A., Sulsona, C. R., Bonilla, J. A., Yowell, C. A., Fujioka, H., Fidock, D. A., & Dame, J. B. (2004). Genetic disruption of the Plasmodium falciparum digestive vacuole plasmepsins demonstrates their functional redundancy. *Journal of Biological Chemistry*, *279*(52), 54088–54096. https://doi.org/10.1074/jbc.M409605200

Ovechkina, V. S., Zakian, S. M., Medvedev, S. P., & Valetdinova, K. R. (2021). Genetically Encoded Fluorescent Biosensors for Biomedical Applications. *Biomedicines*, *9*(11), 1528. https://doi.org/10.3390/biomedicines9111528

Painter, H. J., Morrisey, J. M., Mather, M. W., & Vaidya, A. B. (2007). Specific role of mitochondrial electron transport in blood-stage Plasmodium falciparum. *Nature*, *446*(7131), 88–91. https://doi.org/10.1038/nature05572

Painter, H. J., Morrisey, J. M., & Vaidya, A. B. (2010). Mitochondrial electron transport inhibition and viability of intraerythrocytic Plasmodium falciparum. *Antimicrobial Agents and Chemotherapy*, *54*(12), 5281–5287. https://doi.org/10.1128/AAC.00937-10

Pandey, K., Ferreira, P. E., Ishikawa, T., Nagai, T., Kaneko, O., & Yahata, K. (2016). Ca(2+) monitoring in Plasmodium falciparum using the yellow cameleon-Nano biosensor. *Scientific Reports*, *6*(1), 23454. https://doi.org/10.1038/srep23454

Patel, O. P. S., Beteck, R. M., & Legoabe, L. J. (2021). Antimalarial application of quinones: A recent update. *European Journal of Medicinal Chemistry*, *210*, 113084. https://doi.org/10.1016/j.ejmech.2020.113084

Peatey, C. L., Leroy, D., Gardiner, D. L., & Trenholme, K. R. (2012). Anti-malarial drugs: How effective are they against Plasmodium falciparum gametocytes? *Malaria Journal*, *11*, 34. https://doi.org/10.1186/1475-2875-11-34

Poole, R. C., & Halestrap, A. P. (1994). N-terminal protein sequence analysis of the rabbit erythrocyte lactate transporter suggests identity with the cloned monocarboxylate transport protein MCT1. *The Biochemical Journal*, *303 (Pt 3)*(Pt 3), 755–759. https://doi.org/10.1042/bj3030755

Possemiers, H., Vandermosten, L., & van den Steen, P. E. (2021). Etiology of lactic acidosis in malaria. *PLoS Pathogens*, *17*(1), e1009122. https://doi.org/10.1371/journal.ppat.1009122

Preuss, J., Jortzik, E., & Becker, K. (2012). Glucose-6-phosphate metabolism in Plasmodium falciparum. *IUBMB Life*, *64*(7), 603–611. https://doi.org/10.1002/iub.1047

Price, R. N., Uhlemann, A.-C., Brockman, A., McGready, R., Ashley, E., Phaipun, L., Patel, R., Laing, K., Looareesuwan, S., White, N. J., Nosten, F., & Krishna, S. (2004). Mefloquine resistance in Plasmodium falciparum and increased pfmdr1 gene copy number. *Lancet (London, England)*, *364*(9432), 438–447. https://doi.org/10.1016/S0140-6736(04)16767-6

Rahbari, M., Rahlfs, S., Jortzik, E., Bogeski, I., & Becker, K. (2017). H2o2 dynamics in the malaria parasite Plasmodium falciparum. *PloS One*, *12*(4), e0174837. https://doi.org/10.1371/journal.pone.0174837

Ravindar, L., Hasbullah, S. A., Rakesh, K. P., & Hassan, N. I. (2023). Recent developments in antimalarial activities of 4-aminoquinoline derivatives. *European Journal of Medicinal Chemistry*, *256*, 115458. https://doi.org/10.1016/j.ejmech.2023.115458

Reifenrath, M., & Boles, E. (2018). A superfolder variant of pH-sensitive pHluorin for in vivo pH measurements in the endoplasmic reticulum. *Scientific Reports*, *8*(1), 11985. https://doi.org/10.1038/s41598-018-30367-z

Roth, E. F., Raventos-Suarez, C., Perkins, M., & Nagel, R. L. (1982). Glutathione stability and oxidative stress in P. Falciparum infection in vitro: Responses of normal and G6PD

deficient cells. *Biochemical and Biophysical Research Communications*, *109*(2), 355–362. https://doi.org/10.1016/0006-291X(82)91728-4

Rudrapal, M., & Chetia, D. (2016). Endoperoxide antimalarials: Development, structural diversity and pharmacodynamic aspects with reference to 1,2,4-trioxane-based structural scaffold. *Drug Design, Development and Therapy*, *10*, 3575–3590. https://doi.org/10.2147/DDDT.S118116

Sabitzki, R., Roßmann, A.-L., Schmitt, M., Flemming, S., Guillén-Samander, A., Behrens, H. M., Jonscher, E., Höhn, K., Fröhlke, U., & Spielmann, T. (2024). Role of Rabenosyn-5 and Rab5b in host cell cytosol uptake reveals conservation of endosomal transport in malaria parasites. *PLoS Biology*, *22*(5), e3002639. https://doi.org/10.1371/journal.pbio.3002639

Saliba, K. J., Horner, H. A., & Kirk, K. (1998). Transport and metabolism of the essential vitamin pantothenic acid in human erythrocytes infected with the malaria parasite Plasmodium falciparum. *The Journal of Biological Chemistry*, *273*(17), 10190–10195. https://doi.org/10.1074/jbc.273.17.10190

Saliba, K. J., & Kirk, K. (1999). Ph regulation in the intracellular malaria parasite, Plasmodium falciparum. H(+) extrusion via a V-type H(+)-ATPase. *Journal of Biological Chemistry*, *274*(47), 33213–33219. https://doi.org/10.1074/jbc.274.47.33213

Sallam, M., Al-Khatib, A. O., Al-Mahzoum, K. S., Abdelaziz, D. H., & Sallam, M. (2025). Current Developments in Malaria Vaccination: A Concise Review on Implementation, Challenges, and Future Directions. *Clinical Pharmacology : Advances and Applications*, *17*, 29–47. https://doi.org/10.2147/CPAA.S513282

Sheridan, C. M., Garcia, V. E., Ahyong, V., & DeRisi, J. L. (2018). The Plasmodium falciparum cytoplasmic translation apparatus: A promising therapeutic target not yet exploited by clinically approved anti-malarials. *Malaria Journal*, *17*(1), 465. https://doi.org/10.1186/s12936-018-2616-7

Sherman, I. W. (1979). Biochemistry of Plasmodium (malarial parasites). *Microbiological Reviews*, *43*(4), 453–495. https://doi.org/10.1128/mr.43.4.453-495.1979

Shi, X., Wei, M., Xu, Z., Liu, Y., Zhang, M., Lv, L., & Wang, Q. (2021). Vitamin C Inhibits Blood-Stage Plasmodium Parasites via Oxidative Stress. *Frontiers in Cell and Developmental Biology*, *9*, 639944. https://doi.org/10.3389/fcell.2021.639944

Shivapurkar, R., Hingamire, T., Kulkarni, A. S., Rajamohanan, P. R., Reddy, D. S., & Shanmugam, D. (2018). Evaluating antimalarial efficacy by tracking glycolysis in Plasmodium falciparum using NMR spectroscopy. *Scientific Reports*, *8*(1), 18076. https://doi.org/10.1038/s41598-018-36197-3

Siqueira-Neto, J. L., Wicht, K. J., Chibale, K., Burrows, J. N., Fidock, D. A., & Winzeler, E. A. (2023). Antimalarial drug discovery: Progress and approaches. *Nature Reviews. Drug Discovery*, *22*(10), 807–826. https://doi.org/10.1038/s41573-023-00772-9

Siregar, J. E., Kurisu, G., Kobayashi, T., Matsuzaki, M., Sakamoto, K., Mi-ichi, F., Watanabe, Y., Hirai, M., Matsuoka, H., Syafruddin, D., Marzuki, S., & Kita, K. (2015). Direct evidence for the atovaquone action on the Plasmodium cytochrome bc1 complex. *Parasitology International*, *64*(3), 295–300. https://doi.org/10.1016/j.parint.2014.09.011

Skinner-Adams, T. S., Fisher, G. M., Riches, A. G., Hutt, O. E., Jarvis, K. E., Wilson, T., Itzstein, M. von, Chopra, P., Antonova-Koch, Y., Meister, S., Winzeler, E. A., Clarke, M., Fidock, D. A., Burrows, J. N., Ryan, J. H., & Andrews, K. T. (2019). Cyclization-blocked proguanil as a strategy to improve the antimalarial activity of atovaquone. *Communications Biology*, *2*(1), 166. https://doi.org/10.1038/s42003-019-0397-3

Šlapeta, J., Sutherland, C. J., & Fuehrer, H.-P. (2024). Calling them names: Variants of Plasmodium ovale. *Trends in Parasitology*, *40*(3), 205–206. https://doi.org/10.1016/j.pt.2023.12.010

Snounou, G., Sharp, P. M., & Culleton, R. (2024a). Appropriate naming of the two Plasmodium ovale species. *Trends in Parasitology*, *40*(3), 207–208. https://doi.org/10.1016/j.pt.2024.01.004

Snounou, G., Sharp, P. M., & Culleton, R. (2024b). The two parasite species formerly known as Plasmodium ovale. *Trends in Parasitology*, *40*(1), 21–27. https://doi.org/10.1016/j.pt.2023.11.004

Sparkes, P. C., Famodimu, M. T., Alves, E., Springer, E., Przyborski, J., & Delves, M. J. (2024). Mitochondrial ATP synthesis is essential for efficient gametogenesis in Plasmodium falciparum. *Communications Biology*, *7*(1), 1525. https://doi.org/10.1038/s42003-024-07240-z

Spielmann, T., Gras, S., Sabitzki, R., & Meissner, M. (2020). Endocytosis in Plasmodium and Toxoplasma Parasites. *Trends in Parasitology*, *36*(6), 520–532. https://doi.org/10.1016/j.pt.2020.03.010

Springer, E., Heimsch, K. C., Rahlfs, S., Becker, K., & Przyborski, J. M. (2024). Real-time measurements of ATP dynamics via ATeams in Plasmodium falciparum reveal drug-class-specific response patterns. *Antimicrobial Agents and Chemotherapy*, *68*(5), e0169023. https://doi.org/10.1128/aac.01690-23

Springer, E., Heimsch, K. C., Sidiropoulos, Niklas, Krijnse Locker, Jacomina, & Przyborski J. M. (2025). Arylmethylamino steroid compound 1o interferes with Plasmodium falciparum's hemoglobin metabolism. *Antimicrobial Agents and Chemotherapy, 69*(8), e0033225. https://doi.org/10.1128/aac.00332-25

Suryavanshi, A., Chandrashekarmath, A., Pandey, N., & Balaram, H. (2025). Metabolic Flexibility and Essentiality of the Tricarboxylic Acid Cycle in Plasmodium. *ACS Infectious Diseases*, *11*(2), 335–349. https://doi.org/10.1021/acsinfecdis.4c00788

Taylor, W. R. J., & White, N. J. (2004). Antimalarial drug toxicity: A review. *Drug Safety*, *27*(1), 25–61. https://doi.org/10.2165/00002018-200427010-00003

Terai, K., Imanishi, A., Li, C., & Matsuda, M. (2019). Two Decades of Genetically Encoded Biosensors Based on Förster Resonance Energy Transfer. *Cell Structure and Function*, *44*(2), 153–169. https://doi.org/10.1247/csf.18035

Thiele, P. J., Mela-Lopez, R., Blandin, S. A., & Klug, D. (2024). Let it glow: Genetically encoded fluorescent reporters in Plasmodium. *Malaria Journal*, *23*(1), 114. https://doi.org/10.1186/s12936-024-04936-9

Toloe, J., Mollajew, R., Kügler, S., & Mironov, S. L. (2014). Metabolic differences in hippocampal 'Rett' neurons revealed by ATP imaging. *Molecular and Cellular Neurosciences*, *59*, 47–56. https://doi.org/10.1016/j.mcn.2013.12.008

Trapotsi, M.-A., Hosseini-Gerami, L., & Bender, A. (2022). Computational analyses of mechanism of action (MoA): Data, methods and integration. *RSC Chemical Biology*, *3*(2), 170–200. https://doi.org/10.1039/d1cb00069a

Umumararungu, T., Nkuranga, J. B., Habarurema, G., Nyandwi, J. B., Mukazayire, M. J., Mukiza, J., Muganga, R., Hahirwa, I., Mpenda, M., Katembezi, A. N., Olawode, E. O., Kayitare, E., & Kayumba, P. C. (2023). Recent developments in antimalarial drug discovery. *Bioorganic & Medicinal Chemistry*, *88-89*, 117339. https://doi.org/10.1016/j.bmc.2023.117339

Valdebenito, R., Ruminot, I., Garrido-Gerter, P., Fernández-Moncada, I., Forero-Quintero, L., Alegría, K., Becker, H. M., Deitmer, J. W., & Barros, L. F. (2016). Targeting of astrocytic glucose metabolism by beta-hydroxybutyrate. *Journal of Cerebral Blood Flow and Metabolism : Official Journal of the International Society of Cerebral Blood Flow and Metabolism*, *36*(10), 1813–1822. https://doi.org/10.1177/0271678X15613955

Vale, N., Moreira, R., & Gomes, P. (2009). Primaquine revisited six decades after its discovery. *European Journal of Medicinal Chemistry*, *44*(3), 937–953. https://doi.org/10.1016/j.ejmech.2008.08.011

van Niekerk, D. D., Du Toit, F., Green, K., Palm, D., & Snoep, J. L. (2023). A detailed kinetic model of glycolysis in Plasmodium falciparum-infected red blood cells for antimalarial drug target identification. *The Journal of Biological Chemistry*, *299*(9), 105111. https://doi.org/10.1016/j.jbc.2023.105111

van Niekerk, D. D., Penkler, G. P., Du Toit, F., & Snoep, J. L. (2016). Targeting glycolysis in the malaria parasite Plasmodium falciparum. *The FEBS Journal*, *283*(4), 634–646. https://doi.org/10.1111/febs.13615

van Schalkwyk, D. A., Saliba, K. J., Biagini, G. A., Bray, P. G., & Kirk, K. (2013). Loss of pH control in Plasmodium falciparum parasites subjected to oxidative stress. *PloS One*, *8*(3), e58933. https://doi.org/10.1371/journal.pone.0058933

Villiers, K. A. de, & Egan, T. J. (2021). Heme Detoxification in the Malaria Parasite: A Target for Antimalarial Drug Development. *Accounts of Chemical Research*, *54*(11), 2649–2659. https://doi.org/10.1021/acs.accounts.1c00154

Wang, H., Webster, P., Chen, L., & Fisher, A. L. (2019). Cell-autonomous and non-autonomous roles of daf-16 in muscle function and mitochondrial capacity in aging C. Elegans. *Aging (Albany NY)*, *11*(8), 2295–2311. https://doi.org/10.18632/aging.101914

Ward, K. E., Fidock, D. A., & Bridgford, J. L. (2022). Plasmodium falciparum resistance to artemisinin-based combination therapies. *Current Opinion in Microbiology*, *69*, 102193. https://doi.org/10.1016/j.mib.2022.102193

White, N. J., Pukrittayakamee, S., Hien, T. T., Faiz, M. A., Mokuolu, O. A., & Dondorp, A. M. (2014). Malaria. *Lancet (London, England)*, *383*(9918), 723–735. https://doi.org/10.1016/S0140-6736(13)60024-0

WHO (2023, November 30). World malaria report 2023. *World Health Organization*. https://www.who.int/publications/i/item/9789240086173

WHO (2024a, November 30). WHO guidelines for malaria. *World Health Organization*. https://www.who.int/publications/i/item/guidelines-for-malaria

WHO (2024b, December 11). World malaria report 2024. *World Health Organization*. https://www.who.int/publications/i/item/9789240104440

Wiser, M. F. (2024). The Digestive Vacuole of the Malaria Parasite: A Specialized Lysosome. *Pathogens*, *13*(3), 182. https://doi.org/10.3390/pathogens13030182

Wong, W., Bai, X.-C., Sleebs, B. E., Triglia, T., Brown, A., Thompson, J. K., Jackson, K. E., Hanssen, E., Marapana, D. S., Fernandez, I. S., Ralph, S. A., Cowman, A. F., Scheres, S. H. W., & Baum, J. (2017). Mefloquine targets the Plasmodium falciparum 80S ribosome to inhibit protein synthesis. *Nature Microbiology*, *2*(6), 17031. https://doi.org/10.1038/nmicrobiol.2017.31

Woodrow, C. J., Penny, J. I., & Krishna, S. (1999). Intraerythrocytic Plasmodium falciparum expresses a high affinity facilitative hexose transporter. *The Journal of Biological Chemistry*, *274*(11), 7272–7277. https://doi.org/10.1074/jbc.274.11.7272

Wu, B., Rambow, J., Bock, S., Holm-Bertelsen, J., Wiechert, M., Soares, A. B., Spielmann, T., & Beitz, E. (2015). Identity of a Plasmodium lactate/H(+) symporter structurally unrelated to human transporters. *Nature Communications*, *6*(1), 6284. https://doi.org/10.1038/ncomms7284

Yeh, E., & DeRisi, J. L. (2011). Chemical rescue of malaria parasites lacking an apicoplast defines organelle function in blood-stage Plasmodium falciparum. *PLoS Biology*, *9*(8), e1001138. https://doi.org/10.1371/journal.pbio.1001138

Young, J. A., Fivelman, Q. L., Blair, P. L., La Vega, P. de, Le Roch, K. G., Zhou, Y., Carucci, D. J., Baker, D. A., & Winzeler, E. A. (2005). The Plasmodium falciparum sexual development transcriptome: A microarray analysis using ontology-based pattern identification. *Molecular and Biochemical Parasitology*, *143*(1), 67–79. https://doi.org/10.1016/j.molbiopara.2005.05.007

Zhao, F.-Q., & Keating, A. F. (2007). Functional properties and genomics of glucose transporters. *Current Genomics*, *8*(2), 113–128. https://doi.org/10.2174/138920207780368187

Acknowledgements / Danksagung

Zuallererst möchte ich mich besonders bei **Prof. Dr. Jude M. Przyborski** für die Hauptbetreuung meiner Doktorarbeit bedanken. Als er 2020 die Leitung der Arbeitsgruppe von Prof. Dr. Katja Becker übernommen und mich als Doktorand gewissermaßen adoptiert hatte, ermöglichte er es mir, mich in einem breiten Methodenspektrum ganz neu auszuprobieren. Ich danke ihm besonders für das vom ihm vorgebrachte Vertrauen, das mir die Möglichkeit gab das Projekt ganz nach meinen Vorstellungen lenken zu können. Zudem schätze ich besonders unsere fruchtbaren *high energy discussions*, die dazu beitrugen das Beste aus dem Projekt herauszuholen.

An dieser Stelle möchte ich auch nochmal ganz herzlichst **Prof. Dr. Katja Becker** danken, die mir im Zuge meiner Masterarbeit noch etwas von ihrem wissenschaftlichen Spirit mit auf den Weg meiner Promotionsreise mitgegeben hat.

Ich bedanke mich außerdem herzlichst bei **Prof. Dr. Uwe Wenzel** für die Übernahme des Zweitgutachtens sowie für die Betreuung meiner Bachelorarbeit in seinen Laboren. Er ermöglichte es mir, damals in noch jungen Jahren, in die Welt der Wissenschaft reinzuschnuppern und ein Bewusstsein in mir zu schaffen, in welche Richtung meine Reise noch führen würde.

Zudem möchte ich auch allen weiteren **Mitgliedern der Prüfungskommission**, für ihr Interesse an meiner Arbeit danken. Ich möchte mich desweiteren bei **Prof. Dr. Jacomina Krijnse Locker** für die Unterstützung im Bereich der Elektronenmikroskopie bedanken. **Dr. Stefan Rahlfs** danke ich besonders für seine Unterstützung im Bereich der Proteinexpression und seine sonstigen Tipps zu jeder Lebenslage.

Ich danke ganz besonders auch **Dr. Kim Heimsch** für unsere Zusammenarbeit im Büro und Labor, für ihre Sonden- und Parasitenkulturexpertise, sowie ihre Gesellschaft während der vielen Wochenenden und späten Abende in der Zellkultur.

Zudem danke ich meiner **Familie**, meinen **Freunden** und allen **Kollegen**, die mich während dieser Arbeit unterstützt oder begleitet haben.

Zu guter Letzt möchte ich all denen gedenken, denen ich nicht mehr danken kann und die das Ende meiner Promotionszeit nicht mehr miterleben konnten – meinen Großeltern **Marieluise, Willi, Ursel** und **Alfons**.

Ganz besonders widme ich diese Arbeit aber **Philipp Korn**, der einfach viel zu früh gegangen ist.

Explorative Gang 4ever